Alexey Kazarnikov

STATISTICAL PARAMETER IDENTIFICATION OF REACTION-DIFFUSION SYSTEMS BY TURING PATTERNS

ACTA UNIVERSITATIS LAPPEENRANTAENSIS 941

Alexey Kazarnikov

STATISTICAL PARAMETER IDENTIFICATION OF REACTION-DIFFUSION SYSTEMS BY TURING PATTERNS

Dissertation for the degree of Doctor of Science (Technology) to be presented with due permission for public examination and criticism at Lappeenranta-Lahti University of Technology LUT, Lappeenranta, Finland on the 14th of December, 2020, at 10:00 a.m.

Acta Universitatis
Lappeenrantaensis 941

Supervisor Professor Heikki Haario
LUT School of Engineering Science
Lappeenranta-Lahti University of Technology LUT
Finland

Reviewers Professor Pekka Neittaanmäki
Faculty of Information Technology
University of Jyväskylä
Finland

Assistant Professor Frits Veerman
Mathematical Institute
Leiden University
Netherlands

Opponent Assistant Professor Antti Hannukainen
Department of Mathematics and Systems Analysis
Aalto University
Finland

ISBN 978-952-335-602-3
ISBN 978-952-335-603-0 (PDF)
ISSN-L 1456-4491
ISSN 1456-4491

Lappeenranta-Lahti University of Technology LUT
LUT University Press 2020

Abstract

Alexey Kazarnikov
Statistical parameter identification of reaction-diffusion systems by Turing patterns
Lappeenranta 2020
84 pages
Acta Universitatis Lappeenrantaensis 941
Diss. Lappeenranta-Lahti University of Technology LUT
ISBN 978-952-335-602-3, 978-952-335-603-0 (PDF), ISSN-L 1456-4491, ISSN 1456-4491

Mathematical models allow a connection to be made between a pattern observed on a macroscopic scale and a hypothetical underlying mechanism. Different mechanisms, however, can result in similar patterns. In developmental biology, for example, *de novo* formation of periodic structures similar to purely chemical Turing patterns can also be obtained using mechano-chemical models with only one diffusing morphogen. In addition, patterns obtained with a fixed model and fixed parameter values but with small random perturbations of initial data, will significantly differ in shape, while being nominally of the same type. With randomised inital data, each model parameter value corresponds to a family of patterns rather than a fixed solution. Consequently, standard residual-based methods such as least squares cannot be used for parameter estimation. A computational approach allowing model calibration to certain patterns will enable not only model identification based on experimental pattern data but also comparison of different mechanisms by indicating how well a specific model can be fitted to the data produced by models based on another mechanism.

The aim of the current thesis is to present a solution for such problems. The situation is analogous to the identification of chaotic systems, as in both cases different initial values lead to different solutions which, however, belong to the same family of solutions. In this work, a recently developed statistical approach for parameter studies of chaotic dynamical systems is modified for application with non-chaotic reaction-diffusion systems used as test examples of pattern formation processes. A statistical algorithm for parameter identification of reaction-diffusion systems is suggested that needs steady-state pattern data only, without knowledge of initial values or transient data. Bayesian sampling methods are able to quantify "all" the model variants that are able to fit given pattern data well enough. The developed approach provides a tool for robust discrimination of competing mechanisms proposed to explain experimental data.

Three classical reaction-diffusion models of pattern formation are considered: the FitzHugh-Nagumo model, Gierer-Meinhardt system and Brusselator reaction-diffusion system. The accuracy of model identification achieved by different amounts of training data is quantified by MCMC algorithms. The performance of the method is satisfactory in all cases, as verified by Bayesian sampling methods: a large amount of data leads to an extremely accurate detection of changes in model parameters, practically impossible to detect visu-

ally, while a modest amount of training patterns leads to the same level of detection as, roughly speaking, might be observed with the naked eye. Finally, parameter identification is demonstrated, i.e. convergence of the method when starting with initial parameter values far away from the correct ones. The identification is done by minimizing of a stochastic cost function, solved by an evolutionary optimization algorithm.

The construction of a posterior parameter distribution by Bayesian sampling methods and running the stochastic optimization algorithm requires a large number of model simulations. Therefore, the efficiency of the numerical code is crucial for successful application of the approach. An optimized parallel algorithm is implemented for the numerical solutions of the equations under study. The calculations are done in graphical processing units (GPUs) using the Nvidia CUDA parallel computing platform. Significant improvement in performance is achieved, making the proposed approach suitable for numerical applications.

Keywords: reaction-diffusion equations, pattern formation, parameter identification, MCMC, correlation integral likelihood

Acknowledgements

This study is the result of a Double Degree PhD project between Lappeenranta-Lahti University of Technology (LUT) and Southern Federal University (SFedU). One part of the research was carried out at the LUT School of Engineering Science between 2015 and 2020, another one at the Department of Computational Mathematics and Mathematical Physics (SFedU) between 2013 and 2018.

First of all, I am extremely grateful to my supervisor, Professor Heikki Haario for his guidance, support, patience and inspiration during my research journey. My deepest gratitude goes as well to Svetlana V. Revina, whose competence, responsiveness and friendliness supported me to move forward in my studies. In addition, my sincere thanks go to Prof. Dr. Anna Marciniak-Czochra for her valuable advices and insightful comments on the dissertation manuscript.

I would like to express my sincere gratitude to my preliminary examiners, Professor Pekka Neittaanmäki and Assistant Professor Frits Veerman for providing valuable feedback which has helped me to improve the quality of the thesis.

Next, I would like to thank my colleague Alexander Bibov for many fruitful and insightful discussions on various scientific topics. My warmest gratitude goes to my colleagues from LUT: Sebastian Springer, Ramona Maraia and Vladimir Shemyakin. In addition, I would like to especially thank the very recent member of LUT community, Angelina Senchukova for her moral support during the final year of my research journey.

I would like to express my hearty gratitude to my family: my mother Anna V. Kazarnikova, my father Vladimir A. Kazarnikov, my grandmother Elena V. Shestakovskaya and (especially!) my "famous" grandfather Vladimir E. Shestakovsky. While being geographically far away from you, I always feel an emotional contact. I am very grateful to you for teaching me to never give up, always believing in me and supporting me in all plans and beginnings. In addition, I would like to warmly thank Professor Valentina V. Zotova for her encouragement, support, wisdom and sincere friendship during my whole life.

Finally, I would like to express my hearty gratitude to my friends: Sergey Klimov and Kseniya Klimova, Oleg Turchenko and Lyubov Alpeeva, Mikhail Novikov and Kristina Vetlitsyina-Novikova, Anatoliy Ryabov and Tatyana Migulina, Fyodor Pevnev and Kseniya Pevneva. Naturally, special thanks go to Mr. Stepan S. Apetrii for his constant moral support.

Alexey Kazarnikov
December 2020
Lappeenranta, Finland

To all of you:
use freely

Sincerely Yours, Alexey!

Contents

1 Introduction

A general two-component reaction-diffusion system can be written in the form

$$v_t = \nu_1 \Delta v + f(v, w); \quad w_t = \nu_2 \Delta w + g(v, w), \tag{1.1}$$

with Neumann boundary conditions

$$\frac{\partial v}{\partial n}|_{\partial\Omega} = 0, \quad \frac{\partial w}{\partial n}|_{\partial\Omega} = 0, \tag{1.2}$$

where variables $v = v(\boldsymbol{x}, t)$ and $w = w(\boldsymbol{x}, t)$ describe spatio-temporal dynamics of unknown chemical concentrations, Δ is the Laplace operator, and $\nu_1,\ \nu_2 > 0$ are fixed diffusion coefficients. The non-linear functions $f(v, w)$ and $g(v, w)$ represent local chemical reactions and $t \geq 0$. Here $\boldsymbol{x} \in \Omega$, where $\Omega \subset \mathbb{R}^m$, $m = 1, 2, 3$ is a bounded domain with smooth boundary $\partial\Omega$.

Real chemical systems, modelled by equations (1.1) eventually evolve to a spatially homogeneous steady state called chemical equilibrium. The process of decay, however, may exhibit a simple exponential decay or more complicated spatio-temporal transient behaviour (see Glansdorff and Prigogine (1971a) for details). A detailed experimental investigation of these transient processes can be carried out by employing open reactors, whereby the fresh reagents are constantly pumped into the reactor and used products are constantly removed (Cross and Greenside (2009)). As a result, the experimental observation of rich non-equilibrium phenomena, known as spatio-temporal patterns, becomes possible. In important special case, when diffusion constants of the interacting species have a sufficiently large ratio, the reaction between the chemicals may cause the destabilisation of chemical equilibrium, thus leading to the formation of inhomogeneous spatial structures, called Turing patterns. This mechanism has a wide range of applications in theoretical biology (see Murray (1993) for detailed information), for example explaining the production of patterns in animal skin (Suzuki (2011)).

1.1 Pattern formation in reaction-diffusion systems

The formation of spatio-temporal patterns is observed in various natural phenomena, such as chemical reactions, and environmental, physical and biological processes (see the review by Cross and Hohenberg (1993)). Reaction-diffusion systems form an important class of mathematical models that describe self-organisation processes (Perthame (2015); Koch and Meinhardt (1994); Maini et al. (1997); Murray (1993); Kondo and Miura (2010a)). For the first time, one-component reaction-diffusion equations were used to model population processes by A.N. Kolmogorov, I.G. Petrovsky and N.S. Piskunov (see the original paper, Kolmogorov et al. (1937) and English translation, Kolmogorov et al. (1991)) and later by Fisher (1937). In 1952, A. Turing for the first time considered a two-component reaction-diffusion system as a qualitative model for describing the process of biological morphogenesis. The model assumed that two different signalling molecules exist, called morphogens, whose non-linear interaction combined with dif-

ferent diffusion rates lead to destabilisation of a well-mixed equilibrium state and the formation of spatially heterogeneous concentration patterns. Consequently, these chemical pre-patterns determine the development of morphological patterns. By studying the reaction-diffusion system (1.1) with linear reaction terms, Turing (1952) derived the conditions of a diffusion-driven instability (called also Turing instability). According to some authors (see the review by Bailleul et al. (2020)), this theory explains the formation of spatially heterogeneous stationary structures in the early stages of morphogenesis. Turing instability was further investigated by Prigogine and Nicolis (1967) and Erneux et al. (1978). The idea was applied in the chemical and biological contexts (Gmitro and Scriven (1966); Segel and Jackson (1972)) and was extended to other problems of mathematical modelling.

In 1951, B.P. Belousov experimentally discovered an oscillatory chemical reaction (Belousov (1959)), demonstrating time-dependent patterns. Subsequently A.M. Zhabotinsky et al. continued the experimental study of this reaction and proposed the first mathematical model of the phenomenon (Field and Burger (1985); Zhabotinsky (1974)). In particular, it was found by Zaikin and Zhabotinsky (1970) that when the mixture is placed in a thin layer, spatio-temporal patterns, such as propagating fronts (Zaikin and Zhabotinsky (1970)), spiral waves (Welsh et al. (1983); Müller et al. (1985, 1987); Welsh and Gomatam (1990)) and toroidal scrolls (Winfree (1973)) can appear. These regimes are successfully reproduced, for example, in the spatially distributed Brusselator model proposed by Glansdorff and Prigogine (1971b), which is now one of the classical reaction-diffusion systems. Numerical simulations of the Brusselator model predict the formation of Turing patterns when diffusion coefficients differ by at least one order of magnitude (Rovinskii (1987)). At the same time, experimentally obtained diffusion coefficients show much less variation (Glansdorff and Prigogine (1971a)). Nevertheless, it was shown by Pearson and Horsthemke (1989) that a diffusion-driven instability may occur in the Brusselator reaction-diffusion system with nearly equal diffusion coefficients under very special conditions. Chemical nonequilibrium regimes, however, are necessarily transient as thermodynamically closed systems must eventually approach spatially homogeneous chemical equilibrium.

In 1972, A. Gierer and H. Meinhardt applied a reaction-diffusion mechanism to describe the formation of new tentacles on the head of freshwater polyp *Hydra Linnaeus*. In their model pattern formation is explained by the interaction of activator and inhibitor molecules (Gierer and Meinhardt (1972)). The slowly diffusing activator enhances its own production, amplifying any small peaks in the initial distribution. This causes the production of concentration peaks of the rapidly diffusing inhibitor, which limits the growth of the activator and prevents the formation of new activator peaks near existing ones due to a larger diffusion coefficient.

A necessary condition for the emergence of diffusion-driven instability was the requirement that one of the components of the reaction diffuses much faster than the other (Maini et al. (1997)). This, in particular, can explain the difficulty of experimentally obtaining Turing patterns (Vanag (2004)). The experimental observation of these stationary regimes was reported first by Castets et al. (1990) and later Agladze et al. (1992). The experiment examined the chlorite-iodine-malonic acid (CIMA) reaction in an open reactor system, by

continuously supplying the reaction layer with new reagents. The reactor consisted of a hydrogel block with two continuous-flow stirred tank reactors on opposite sides. This allowed reactant concentrations to remain uniform and constant during the experiment and achieve the necessary difference in the diffusion rates of the reagents. The experiment allowed stable non-equilibrium chemical patterns to be produced, corresponding to the predictions of Turing's theory. A mathematical model of this reaction was proposed by Lengyel and Epstein (1991).
Subsequently, the formation of spatially inhomogeneous stationary and spatio-temporal patterns was discovered numerically and experimentally in other chemical and biological systems. For example, in the work of Pearson (1993), the Gray-Scott reaction-diffusion model (see Gray and Scott (1983, 1984, 1985)), which is a generalisation of Selkov's glycolysis model (Selkov (1968)), was numerically studied. For some values of the model parameters, stable spatial and spatio-temporal patterns were discovered. In Lee et al. (1993a), results similar to Pearson (1993) were obtained experimentally. Other chemical and biological systems whose spatially distributed analogues demonstrate structural formation include the Gierer-Meinhardt system and the Schnakenberg system (see Schnakenberg (1979)), which is a modified model of the Brusselator.
Kondo and Asai (1995) proposed a mathematical model for the formation of pigment structures on the skin of sea angel fish *Pomacanthus*, based on the reaction-diffusion mechanism. In this work, the system was first considered in the spatial domain expanding with time. Subsequently, these ideas were employed for other biological problems (see the review in Kondo and Miura (2010b)), including development of skin pigment patterns in zebrafish (Asai et al. (1999)), sea shells (Meinhardt (1995)) and other marine organisms, feather follicle formation (Jung et al. (1998)) and tooth development (Salazar-Ciudad and Jernvall (2002)). At present, the Turing mechanism has found a wide range of applications in the modelling of chemical systems (Facchini et al. (2009); Szalai and De Kepper (2008)), explaining the growth and development of biological populations (Xu et al. (2015); Tang et al. (2016); Owen and Lewis (2001); Upadhyay et al. (2014)), studying the behaviour of microorganism colonies (Lee et al. (1993b); Vilas et al. (2012)), explaining animal skin pattern formation (Kondo and Asai (1995); Madzvamuse et al. (2002)), designing neural networks (Zhao and Huang (2014); Dong et al. (2017)) and image processing (Nomura et al. (2011); Ebihara et al. (2003)).

1.2 Motivation and objective of the research

In general, the right-hand side of the reaction-diffusion system (1.1) depends on some control parameters (which could be either kinetic parameters in reaction terms or diffusion coefficients). For some values of these control parameters (called critical values), the trivial (homogeneous) solutions of the respective equations might lose their stability properties and in the neighbourhood of these points the system could evolve to a new regime exhibiting a spatial or spatio-temporal order. The examples of such branching solutions are shown in Fig. 1.1 and Fig. 1.2. Bifurcation theory allows us to describe the branching behaviour of solutions to reaction-diffusion equations as a function of dimensionless parameters. It leads to determining mathematical principles governing the exchange of

stability of intersecting solution branches and allows the construction of analytic and convergent expressions for branched out (or secondary) solutions emerging at the bifurcation points.

The rigorous analysis of the bifurcation behaviour of solutions to reaction-diffusion systems is important for understanding the processes of self-organisation and pattern formation. Analytical approaches are able to provide a deeper understanding of the qualitative features of the behaviour of non-linear systems, and new exact and approximate solutions can be used for testing the correctness and reliability of computational schemes and algorithms. Away from the critical values, however, reaction-diffusion systems can support spatio-temporal patterns of remarkable diversity and complexity. These regimes can be successfully studied analytically by the methods of geometric singular perturbation theory, when the problem has a clear separation of time scales (see Hek (2009); Kaper (1999) and Kuehn (2015) for general information). For example, Wei (1999, 2001); Wei and Winter (2003) studied the existence and stability of spot patterns in the Brusselator model by geometrical methods, Doelman et al. (2009) examined the existence of stationary and travelling pulse solutions in three-component reaction-diffusion system and Doelman and Veerman (2015) developed an explicit theory for existence, stability and bifurcation of pulses in the general class of two-component reaction-diffusion equations in one-dimensional domain. At the same time, modern numerical methods allow us to effectively study the processes of pattern formation in reaction-diffusion systems, regardless of the complexity of the region geometry and the values of the control parameters.

Mathematical models allow a connection between a pattern observed on a macroscopic scale and a hypothetical underlying mechanism to be established. But different mechanisms may result in a similar pattern. For example, in developmental biology *de novo* formation of periodic structures similar to purely chemical Turing patterns can be obtained in a mechano-chemical model with only one diffusing morphogen (Mercker et al. (2015); Brinkmann et al. (2018); Mercker et al. (2013)). Another example concerns comparison of the classical Turing patterns (close-to-equilibrium patterns) with far-from-equilibrium patterns obtained due to hysteresis in the structure of model non-linearities (Härting et al. (2017)). These mechanisms are often not amenable to direct experimental verification. A computational approach allowing model calibration to a certain pattern will enable not only model identification based on experimental data but also comparison of divergent models (and mechanisms) by checking how well a specific model can be fitted to the data produced by models based on another mechanism.

However, identification of model parameters based on stationary patterns is a challenging task. Patterns obtained with fixed model parameter values but small random perturbations of the initial values can significantly differ in location and shape (Zhang and Tian (2014); Murray (1993)), while being of the "same" type. In this sense, for unknown or randomised initial values, each model parameter corresponds to a family of patterns rather than a fixed solution. On the other hand, changes to model parameters affect pattern formation as well. But it is difficult to quantify exactly how much the parameters should vary in order to cause a statistically significant deviation from the change in dynamics caused by perturbation of initial values. Also, it is difficult to create a cost function that would allow reliable quantification of the model parameters that correspond to given pattern data. Most

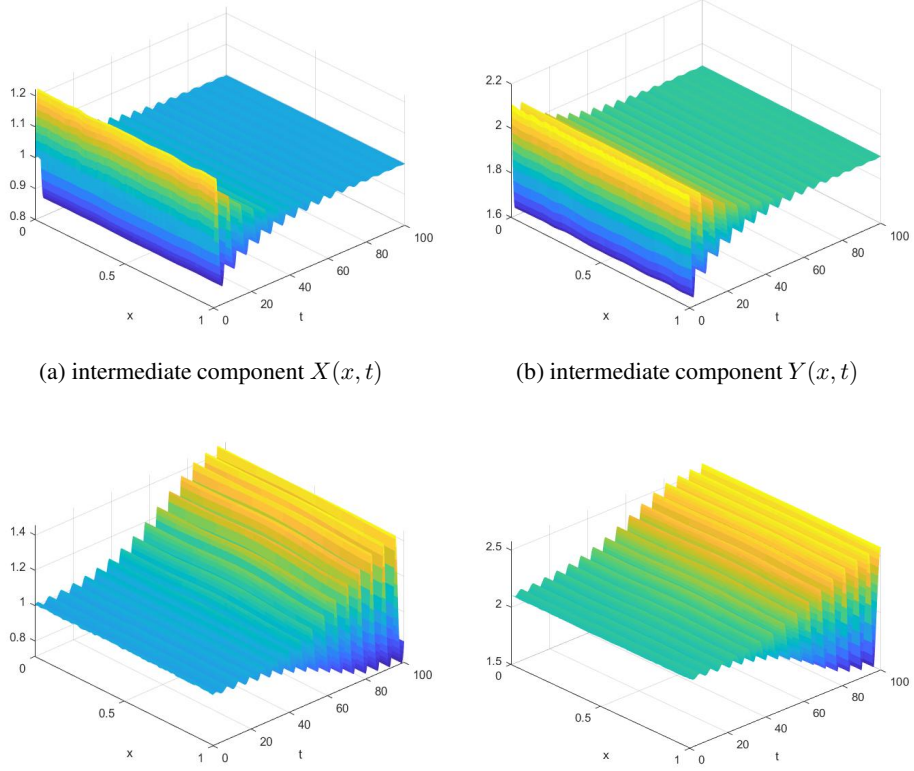

(a) intermediate component $X(x,t)$

(b) intermediate component $Y(x,t)$

(c) intermediate component $X(x,t)$

(d) intermediate component $Y(x,t)$

Figure 1.1: The branching out of a spatially homogeneous limit cycle in the Brusselator reaction-diffusion system. Parameter values: $A = 1$, $L = 1$, $\nu_1 = 1$, $\nu_2 = 1$, $B = B_{cr} + \varepsilon$, $B_{cr} = 1 + A^2$. Initial conditions are taken as small random perturbations of the homogeneous steady state. When the parameter B is less than the critical value B_{cr} the solution of the system decays to the stable homogeneous steady state (see (a) and (b)). The branching out of the new secondary solution occurs for $B = B_{cr}$ and a stable homogeneous oscillatory regime is observed in the system for $B > B_{cr}$ (see (c) and (d)). This oscillatory behaviour of the model corresponds to volume concentration oscillations in the Belousov-Zhabotinsky chemical reaction (Glansdorff and Prigogine (1971a)).

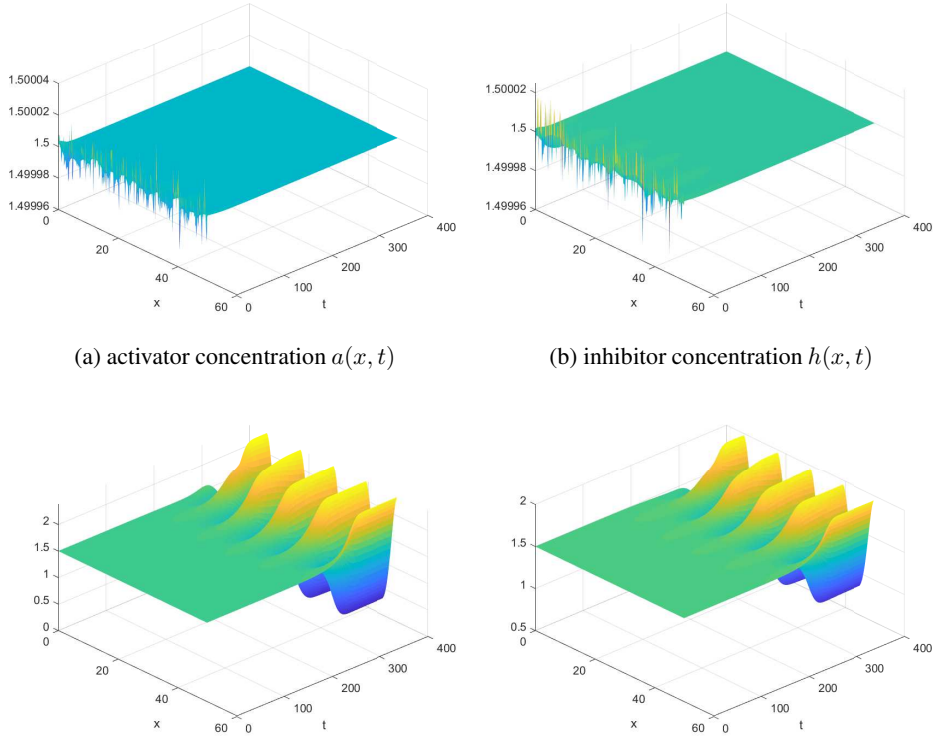

(a) activator concentration $a(x,t)$

(b) inhibitor concentration $h(x,t)$

(c) activator concentration $a(x,t)$

(d) inhibitor concentration $h(x,t)$

Figure 1.2: The branching out of a spike patterns in the Gierer-Meinhardt activator-inhibitor model. Parameter values: $L = 50$, $\rho_0 = 0$, $\rho = 1$, $c = 1$, $\mu = 1$, $c' = 1$, $\rho' = 1$, $\nu = 1.5$, $D_a = 1$, $D_h = d_{cr} + \varepsilon$, $d_{cr} \approx 8.7564$. Initial conditions are taken as small random perturbations of the homogeneous steady state. When the diffusion coefficient D_h is less than the critical value d_{cr}, the perturbations of the homogeneous steady state decay (see (a) and (b)). The loss of stability occurs for $D_h = d_{cr}$ and the formation of stable spatially inhomogeneous steady states (Turing patterns) is observed in the system for $D_h > d_{cr}$ (see (c) and (d)). This behaviour corresponds to the formation of new tentacles on the head of Hydra freshwater polyp, where peaks of activator concentration correspond to the regions where the formation of new tentacles takes place (Gierer and Meinhardt (1972)).

typically, one has to resort to tedious and subjective hand-tuning.
The aim of the current thesis is to present a solution for such problems. The situation is analogous to the identification of chaotic systems, as in both cases different initial values lead to different solutions which, however, belong to the same family of solutions. So we modify the recently developed statistical approach for parameter studies of chaotic ODE systems (Haario et al. (2015)) to the non-chaotic reaction-diffusion systems studied here. The method is tested with the FitzHugh-Nagumo, Gierer-Meinhardt and Brusselator models, that exhibit the formation of Turing patterns. We introduce a cost function that enables a statistically sound identification of the model parameters by steady-state pattern data only. A remarkable feature of the presented approach is a strong sensitivity with respect to even small but systematic changes in model behaviour, practically impossible to detect by the naked eye.
Quantitative issues, related to comparing theoretical and experimental data for the case of reaction-diffusion systems and reconstructing system dynamics from observational data, are intensively studied in literature at the present time. One may recall, for example, the detection of structural changes in Turing patterns by recurrence plots (Facchini et al. (2009); Mocenni et al. (2010)), analysis of correlation between pattern formation and theoretical models (Miura et al. (2000)), numerical and experimental approaches to the design and control of pattern formation (Vilas et al. (2012); Escala et al. (2015); Ghorai and Poria (2016); Vanag and Epstein (2008); Horváth et al. (1999); Chakravarti et al. (1995)), quantitative analysis of noise impact on patterns (Barrass et al. (2006); Li (2011)) and parameter estimation for reaction-diffusion systems (Kramer and Bollt (2013); Garvie et al. (2010); Campillo-Funollet et al. (2019)). However, these approaches assume either known initial values or transient data. To the best of our knowledge, the approach discussed here is unique in that model parameters are identified by steady-state pattern data only, with unknown initial values. This is the situation often faced in experimental work.
Generalised recurrence plots are also successfully employed for identifying the dynamics of reaction-diffusion systems. For example, in Facchini et al. (2009) generalised recurrence plot concept is used to detect different regimes in the formation of spot patterns in the Belousov-Zhabotinsky reaction. In Mocenni et al. (2010) the same approach is used to detect structural changes of Turing patterns in the Schnakenberg model and study stability properties of spiral waves in the complex Ginzburg-Landau equation. However, it should be pointed out that our focus is different: while the mentioned works aim at the detection of domains with characteristically different behaviour, our aim is to distinguish local changes within a given domain of behaviour. More exactly, we identify the distribution of parameters that produce solutions undistinguishable from those of a given data set.

1.3 Research questions

Based on the research problem and the objective, this thesis will address the following research questions:

1. How can a statistical approach to the identification of parameters with steady state data be introduced without using information on transient or initial data?

2. How can a likelihood allowing the model parameters to be distinguished that correspond to given patterns be constructed?

3. How can an efficient numerical algorithm for running the approach be implemented?

The method of statistical parameter identification being discussed in the present work can be applied to the general case of pattern formation process (1.1). In the current thesis, however, we limit our discussion to three well-known reaction-diffusion systems. The general information about these models is given below.

1.4 Equations under study

In the current work we consider three classical reaction-diffusion systems: the FitzHugh-Nagumo model, the Gierer-Meinhardt activator-inhibitor system and the Brusselator reaction-diffusion system.

1.4.1 FitzHugh-Nagumo model

The FitzHugh-Nagumo model is a spatially distributed analogue of the generalised Rayleigh-Van der Pol equation. The model was first proposed by FitzHugh (1961) as a model for propagation of a nerve impulse.
In 1883 Strutt (Lord Rayleigh) proposed the equation for describing the dynamics of sound vibrations in a clarinet reed:

$$\dot{y_1} = y_2; \qquad \dot{y_2} = -y_1 + \mu y_2 - y_2^3, \tag{1.3}$$

where y_1 is the dimensionless clarinet reed displacement, y_2 is the velocity of the reed, and μ is the dimensionless damping coefficient. Model (1.3) has found many applications in the description of physical processes of various nature (see the review by Cveticanin (2015)): oscillatory processes in various musical instruments (Strutt (Lord Rayleigh,L)), electrical oscillations (Inaba and Mori (1992)), dynamics of artificial biological systems (Filho et al. (2005)), etc.
Van der Pol (1920) proposed a model for describing electrical oscillations in a positive feedback generator. The equation has the form:

$$\ddot{u} - \epsilon(1 - u^2)\dot{u} + u = 0, \tag{1.4}$$

or can be written as an ODE system:

$$\dot{u_1} = u_2; \qquad \dot{u_2} = -u_1 + \epsilon(u_2 - {u_1}^2 u_2), \tag{1.5}$$

where u is the voltage in a dimensionless form and ϵ is a dimensionless feedback coefficient. The Van der Pol equation is an idealised model of a tube generator that allows periodic electrical oscillations to be modelled. The generator consists of an oscillating circuit (such as a capacitor-inductive coil circuit) and an amplifier. It is assumed that the current-voltage characteristic of the amplifier $i(u)$ is a cubic polynomial, i.e. $i(u) = g_0 u - g_2 u^3$,

where $g_0, g_2 > 0$. The Van der Pol equation can be derived by applying the second Kirchhoff law to the oscillating circuit (see Van der Pol (1920) for details). The transition to the dimensionless form of the equation is carried out by performing time change: $t = \omega\tilde{t}, \omega = \dfrac{1}{\sqrt{LC}}$ and introducing the notation $\epsilon = \dfrac{Mg_0 - RC}{\sqrt{LC}}$.
One of the subsequent works by Van der Pol (1926) was devoted to the study of relaxation oscillations in this equation. Further, Van der Pol and Van der Mark (1927) studied the dynamics of the oscillator under the action of a periodic driving force $F(t) = bk\lambda\sin(\lambda t)$, $k > 0$. During experiments with the generator, it was noted that an unusual noise was observed in the system at some frequency ranges λ, which was one of the first experimental observations of deterministic chaos (see the memorial paper by Cartwright (1960)). This problem was considered in more detail by Cartwright and Littlewood (1945), where, in particular, the presence of an infinite number of unstable periodic orbits in the system with a sufficiently large external force F was discovered.

The Rayleigh and Van der Pol equations are classical models for the analysis of periodic self-oscillations. It is known that there is no fundamental difference between the equations and a change of variables can lead to one another (Hasegawa (2011)). There are many works in the literature devoted to the numerical study of the dynamics of coupled Rayleigh oscillators (1.3), Van der Pol (1.4) and Duffing (see Han et al. (2017); Zhang and Li (2017); Chunbiao et al. (1999); Kuznetsov et al. (2007)).

Hodgkin and Huxley (1952) proposed a model for the propagation of a nerve impulse in the giant axon of the squid. In this model, the cell membrane is presented as an electrical circuit, each of the components of which has its own biological analogue (Gerstner and Kistler (2002)). A semi-permeable cell membrane that separates the inside of the cell from extracellular fluid plays the role of capacity (capacitor) C. It is assumed that the external current $I(t)$ can either increase the charge of the capacitor or penetrate into the cell through ion channels in the cell membrane. Three types of channels are considered in the model: the calcium channel K, the sodium channel Na and the membrane pore channel L, which is responsible for passive conductivity. It is assumed that the conductivity of each channel is a function of membrane potential. Membrane potential acts as a battery. Thus, the Hodgkin-Huxley model has the form:

$$\begin{aligned} &C\dot{v} = I(t) - g_{Na}m^3h(v - E_{Na}) - g_Kn^4(v - E_K) - g_L(v - E_L);\\ &\dot{m} = \alpha_m(v)(1 - m) - \beta_m(v)m;\\ &\dot{n} = \alpha_n(v)(1 - n) - \beta_n(v)n;\\ &\dot{h} = \alpha_h(v)(1 - h) - \beta_h(v)h, \end{aligned} \tag{1.6}$$

where $v(t)$ is the membrane potential, $I(t)$ is the external current, $m(t), n(t), h(t)$ are the dimensionless quantities responsible for activation ion channels, $\alpha_m(v)$, $\alpha_n(v)$, $\alpha_h(v)$, $\beta_m(v)$, $\beta_n(v)$, $\beta_h(v)$ are non-linear functions characterising the conductivity of ion channels, $g_{Na}, g_K, g_L \in \mathbb{R}$ are maximum channel conductivities, and E_{Na}, E_K, E_L are the equilibrium Nerst potentials.

At present, two-dimensional reductions of the system (1.6) have been obtained by applying simplifying assumptions based on the experimental data (Gerstner and Kistler (2002);

FitzHugh (1955)). It is assumed that $m(t)$ changes much faster than $v(t)$, $n(t)$ and $h(t)$, then $v \equiv const$, $m(t) = m_0(v)$, $m_0(v) = \lim_{t\to+\infty} m(t)$. By introducing the approximation $n(t) \approx 1 - h(t)$, and the new variable $w(t) = b - h(t) = an(t)$, where $a, b > 0$, the system (1.6) reduces to a system of two equations:

$$\dot{v} = F(v, w) + I(t); \qquad \dot{w} = \frac{1}{\tau} G(v, w). \tag{1.7}$$

where $I(t)$ is the external current, the variable $w(t)$ is called the recovery variable, and it is assumed that $w(t)$ is a slow variable compared to $v(t)$, which is achieved by selecting the parameter $\tau > 0$. Specific reductions of the Hodgkin-Huxley model are obtained from (1.7) by various approximations of the functions $F(v, w)$ and $G(v, w)$ (see Gerstner and Kistler (2002); Jaeger and Jung (2015)). One of the most common reductions of this model was proposed by FitzHugh (1961):

$$\dot{v} = -w + \mu v - v^3 + I(t); \qquad \dot{w} = \epsilon(v - \alpha w - \beta), \tag{1.8}$$

where the parameters α and β are assumed to be non-negative. The system of ordinary differential equations (1.8) is a generalisation of the Rayleigh (1.3) and Van der Pol (1.4) equations. Currently, there are several varieties of equations (1.8) in the literature, which can be explained by the adaptation of the model to specific physiological objects (Gerstner and Kistler (2002)).

Later, Nagumo et al. (1962) analysed the dynamics of the electric circuit corresponding to the given model and investigated the spatially distributed analogue of a system (1.8)

$$v_t = \nu_1 \Delta v + \mu v - v^3 + I(t); \qquad w_t = \epsilon(v - \alpha w - \beta).$$

In the initial physiological formulation considered by Nagumo et al. (1962), the model was considered under the assumption of one spatial variable $x \in (0, \ell)$ and restriction on diffusion coefficients $\nu_1 << \nu_2$, assuming the case $\nu_1 = 0$. The case $\nu_1 \geq \nu_2$ is also of interest in studying the formation of Turing patterns (Cross and Greenside (2009)).

The existence and stability of the spatio-temporal patterns in the FitzHugh-Nagumo model (1.8) has been intensively studied in literature from analytical point of view. For example, Carpenter (1977) used a geometric approach to singular perturbation problems to find travelling wave solutions of (1.8); Hastings (1974, 1976) showed the existence of "single pulse" waves by analysing homoclinic and periodic orbits of the model; Jones (1984) analysed the stability of travelling wave solutions with respect to the full system of partial differential equations; Krupa et al. (1997) studied the dynamics of fast and slow waves in (1.8); Sandstede (1998) examined the behaviour of the N-front solutions, bifurcating from a twisted heteroclinic loop in the underlying ordinary differential equation describing travelling-wave solutions and Li et al. (2019) constructed semi-stable spatially heterogeneous steady states of the equation (1.8) and various types of stable steady states with jump discontinuities.

1.4.2 Gierer-Meinhardt activator-inhibitor system

In 1972 A. Gierer and H. Meinhardt proposed a simple model explaining *de novo* formation of spatial tissue patterns. The model assumes that there are two diffusing chemicals on the tissue surface (called morphogens): a short-range activator and a long-range inhibitor. Their interaction and diffusion result in the formation of a chemical pre-pattern (primary pattern), which determines the consecutive formation of a morphological pattern. Morphogens are released by certain cell types, called morphogen sources, whose densities are assumed to be independent of the concentrations of morphogens. This assumption arises from the empirical evidence that the establishment of a chemical pre-pattern occurs much faster than the change of the source densities (for example, due to cell differentiation).
In the theory developed by A. Gierer and H. Meinhardt, a tissue is represented as a one-dimensional interval $x \in (0, L)$, supplied with suitable boundary conditions. The concentrations of activator and inhibitor are denoted by $a(x,t)$ and $h(x,t)$ respectively, and $\rho(x)$ and $\rho'(x)$ describe the respective source densities. It is assumed that the synthesis or release of inhibitor depends on local activator concentration and that the inhibitor diffuses and equilibrates much faster than the activator. As a result, the inhibitor concentration is considered as a function of mean activator concentration $\bar{a}(t) = \int_0^L a(x,t)dx$, measured over the surface area. Next, it is postulated that the change of activator concentration is determined as a difference between production and destruction rates, which are proportional to the powers of morphogen concentrations and the following approximative equation is proposed:

$$\frac{\partial a}{\partial t} \approx \gamma\rho\frac{a^k}{\bar{a}^l}(1 - \frac{\beta}{\rho}\frac{\bar{a}^n}{a^m}), \tag{1.9}$$

where $k, l, m, n \in \mathbb{N}$ are reaction rate parameters, and $\gamma > 0$ and $\beta > 0$ describe the influence of inhibitor source density. In addition, it is assumed that $k > m$ to avoid the negative values of $a(x,t)$ and as well $m > n > 0$.
By considering the spatially homogeneous (well-mixed) case, when:

$$\rho(x) \equiv \bar{\rho} \equiv const, \quad a(x,t) \equiv a(t) \equiv \bar{a}(t),$$

it is possible to write equation (1.9) as follows:

$$\frac{\partial \bar{a}}{\partial t} \approx \gamma\bar{\rho}\bar{a}^{k-l}(1 - \frac{\beta}{\bar{\rho}}\bar{a}^{n-m}). \tag{1.10}$$

The solution of equation (1.10) tends to the equilibrium given by formula:

$$\bar{a} = a_0 = \sqrt[n-m]{\frac{\bar{\rho}}{\beta}}, \tag{1.11}$$

for any non-zero initial concentration of activator. Let us next consider the spatially distributed equation (1.9) and linearise it around the steady state (1.11) by considering small

perturbations of the activator concentration $a(x,t)$ and the source density $\rho(x)$:

$$\rho = \bar{\rho} + \Delta\rho, \quad a = \bar{a} + \Delta a.$$

This leads to the following equation:

$$\frac{\partial a}{\partial t} \approx \gamma\bar{\rho}\bar{a}^{k-l}\left(\frac{\Delta\rho}{\bar{\rho}} + m\frac{\Delta a}{\bar{a}}\right) \tag{1.12}$$

From equation (1.12) Gierer and Meinhardt (1972) derive an assumption that even initial source distribution $\Delta\rho = 0$ results in the formation of activator peaks in the regions, where initial concentration of activator $a(x,0)$ is higher than the average value $\int_0^L a(x,0)dx$. In the regions where $a(x,t)$ is below average, however, the activator concentration will decay. The same behaviour can occur in a situation when the initial concentration of activator is evenly distributed ($a(x,0) \equiv \bar{a}$), but the distribution of sources is inhomogeneous. In this case, the regions with high source concentrations will determine the polarity of activator peaks.

It should be pointed out that the concentration of activator will grow infinitely, unless some limiting factor is introduced. Gierer and Meinhardt (1972) suggested two possible mechanisms to limit the growth: activator-substrate (depletion) and activator-inhibitor models. The activator-substrate model is constructed by assuming that activator sources are activated by $a(x,t)$ and as well by some substance of concentration $s(x,t)$, which is consumed by activator. This leads to the following model:

$$\frac{\partial a}{\partial t} = \rho_0\rho + c\rho a^k f(s) - \mu a + D_a\frac{\partial^2 a}{\partial x^2}; \quad \frac{\partial s}{\partial t} = c_0 - c'\rho a^k f(s) - \nu s + D_s\frac{\partial^2 s}{\partial x^2},$$

where $\rho_0 > 0$ and $c_0 > 0$ denote the rates of activator and substrate production, $c > 0$ and $c' > 0$ are reaction rates, $f(s)$ is a monotonically growing function, μ and ν are activator and substrate decay rates and D_a, D_s are diffusion coefficients. In addition, it is assumed that ρ_0, D_a and ν are small and $D_s >> D_a$. If the source density distribution forms a shallow gradient ($\rho(x) \approx \bar{\rho}$), then taking into account the fast propagation speed of substrate the following approximation is obtained:

$$f(s) \approx \frac{c_0}{c'\bar{\rho}\bar{a}^k},$$

which leads to the following approximative equation:

$$\frac{\partial a}{\partial t} \approx \frac{\rho c c_0 a^k}{\bar{\rho}c'\bar{a}^k}\left(1 - \frac{c'\mu\bar{\rho}\bar{a}^k}{cc_0\rho a^{k-1}}\right),$$

which behaves similarly to (1.9) if $k \geq 2$. The simplest version of activator-substrate

model is given by the following system:

$$\frac{\partial a}{\partial t} = \rho_0\rho + c\rho a^2 s - \mu a + D_a\frac{\partial^2 a}{\partial x^2}; \quad \frac{\partial s}{\partial t} = c_0 - c'\rho a^2 s - \nu s + D_s\frac{\partial^2 s}{\partial x^2}.$$

The activator-inhibitor model is obtained under the assumption that there are two substances: activator $a(x,t)$ and inhibitor $h(x,t)$ acting on morphogen sources. It is assumed that reaction rates are proportional to some powers of $a(x,t)$ and $h(x,t)$. In addition it is assumed that reagents are removed by first-order kinetics and that there is a basal production of activator, proportional to $\rho(x)$. These assumptions lead to the following system of equations:

$$\frac{\partial a}{\partial t} = \rho_0\rho + c\rho\frac{a^r}{h^s} - \mu a + D_a\frac{\partial^2 a}{\partial x^2}; \quad \frac{\partial h}{\partial t} = c'\rho'\frac{a^t}{h^u} - \nu h + D_h\frac{\partial^2 h}{\partial x^2}, \tag{1.13}$$

where $\rho_0 << 1$ is activator basal production rate, $c > 0$ and $c' > 0$ are reaction rates and $\mu, \nu > 0$ are morphogen decay rates. Diffusion coefficients are assumed to satisfy the condition $D_a << D_h$. From the model (1.13), Gierer and Meinhardt (1972) derive the following approximative equation:

$$\frac{\partial a}{\partial t} \approx \rho\frac{a^r}{\bar{a}^{\frac{st}{u+1}}}\left(1 - \frac{\beta}{\rho}\frac{\bar{a}^{\frac{st}{u+1}}}{a^{r-1}}\right),$$

which demonstrates the pattern formation if the condition:

$$\frac{st}{u+1} > r - 1 > 0,$$

is satisfied. A commonly used special case of the general Gierer-Meinhardt activator-inhibitor system (1.13), which is used in the current work, is named the activator-inhibitor model with different sources and is obtained from (1.13) by setting $r = t = 2$, $s = 1$, which leads to the following system of equations:

$$\frac{\partial a}{\partial t} = \rho_0\rho + c\rho\frac{a^2}{h} - \mu a + D_a\frac{\partial^2 a}{\partial x^2}; \quad \frac{\partial h}{\partial t} = c'\rho' a^2 - \nu h + D_h\frac{\partial^2 h}{\partial x^2}. \tag{1.14}$$

Doelman et al. (2001a) studied the existence and stability of asymptotically large N-pulse patterns in one-dimensional Gierer-Meinhardt system by applying techniques of geometric singular perturbation theory and non-local eigenvalue problem method. Ward and Wei (2003) examined the Hopf bifurcation of spike solutions and Doelman et al. (2001b) studied the existence problem for stationary multi-pulse solutions. Doelman et al. (2007) analytically studied the asymptotic stability of two strongly interacting pulses in a regularised model. Veerman and Doelman (2013) considered a problem of the existence and stability of localised pulses in the Gierer-Meinhardt system with additional "slow" nonlinear term.

For the two-dimensional Gierer-Meinhardt system Wei and Winter (1999) constructed solutions with a single interior condensation points in the case of strong coupling, when

the diffusion rate of the activator is very small and the diffusion rate of inhibitor is finite. Wei and Winter (2001) rigorously proved the existence and stability of multi-peaked solutions (spikes) in a two-dimensional domain with strong coupling case, and Wei and Winter (2002) considered weak coupling case, when diffusion coefficients of activator and inhibitor tend to zero and infinity respectively.

1.4.3 Brusselator reaction-diffusion system

The Brusselator reaction-diffusion system was proposed by Glansdorff and Prigogine (1971b) as a model of hypothetical chemical reaction that could reproduce the non-equilibrium phenomena (for example, uniform oscillations and travelling waves) observed in the Belousov-Zhabotinsky reaction. The scheme of hypothetical reaction is described as follows:

$$\begin{aligned} &A \to X, \\ &2X + Y \to 3X, \\ &B + X \to Y + D, \\ &X \to E. \end{aligned} \tag{1.15}$$

and the overall reaction is:

$$A + B \to E + D.$$

It should be pointed out that reaction scheme (1.15) was not intended to describe a specific chemical experiment. It contains a trimolecular step and as a result could be considered as physically unrealistic (Glansdorff and Prigogine (1971b,a)). The scheme involves, however, only two intermediate components X and Y, which significantly simplifies the analysis of such a system. Next we consider as constants the concentrations of the initial and final products (A, B, D, E) and arrive at the model with only two intermediate components X and Y. The corresponding kinetic equations are:

$$\begin{aligned} \frac{\partial X}{\partial t} &= k_1 A + k_2 X^2 Y - k_3 B X - k_4 X + D_X \frac{\partial^2 X}{\partial x^2}; \\ \frac{\partial Y}{\partial t} &= k_3 B X - k_2 X^2 Y + D_Y \frac{\partial^2 Y}{\partial x^2}, \end{aligned} \tag{1.16}$$

where $x \in (0, L)$ and Neumann boundary conditions are set at the boundary.
The Brusselator reaction-diffusion system is obtained from system (1.16) by setting all kinetic constants k_1, k_2, k_3, and k_4 equal to one, thus arriving at the following system of equations:

$$\frac{\partial X}{\partial t} = A + X^2 Y - (B+1)X + D_X \frac{\partial^2 X}{\partial x^2}; \quad \frac{\partial Y}{\partial t} = BX - X^2 Y + D_Y \frac{\partial^2 Y}{\partial x^2}. \tag{1.17}$$

Doelman et al. (1997a,b) showed the existence of single-pulse and multi-pulse stationary patterns in the system (1.17) by using the techniques of geometric singular perturbation theory and performed the stability analysis of these solutions. Doelman et al. (2000, 2001c) proved the existence of two symmetric pulses moving apart from each other with slowly varying velocities, analysed their stability by applying the non-local eigenvalue

problem method and studied the pulse-splitting bifurcations. Later, Morgan and Kaper (2004) constructed the axisymmetric ring solutions for the 2D version of the model (1.17) and studied the splitting of these regimes into spot patterns.

1.5 Author's contribution

The candidate implemented the numerical code for the problem under study, performed the numerical analysis, wrote the literature review and the original draft of the thesis. The general supervision of the ongoing research and experiments being carried out, text correction and proofreading were done by the candidate's supervisor, Professor Heikki Haario. The main results of the thesis were published in Kazarnikov and Haario (2020).

1.6 Structure of the thesis

The current thesis was completed according to the Double Degree agreement between LUT University and Southern Federal University (Rostov-on-Don, Russia). Current research can be divided into two parts. In the first part, completed under the supervision by Svetlana V. Revina and defended in 2018 (see Kazarnikov (2018)) the analytical investigation of the bifurcational behaviour of the FitzHugh-Nagumo reaction-diffusion system and its limit cases was performed. In the second part, completed under the supervision by Heikki Haario, the statistical parameter identification of reaction-diffusion systems by Turing patterns was studied.
The dissertation consists of five chapters. Chapter 1 provides the background and presents the relevance of the study. Chapter 2 summarises the previous analytical results obtained under the supervision by Svetlana V. Revina. Chapter 3 contains the general overview of the Correlation Integral Likelihood (CIL) approach to the parameter estimation of reaction-diffusion systems and provides general information about the implementation of the numerical part in MATLAB and CUDA. Chapter 4 presents the findings of numerical experiments. Finally, Chapter 5 concludes the thesis by summarising the main results of the current research.

2 Bifurcational behaviour of the FitzHugh-Nagumo reaction-diffusion system

2.1 Introduction

This section contains the summary of the results included in the Ph.D. thesis (Kazarnikov (2018)), which was completed by the author at Southern Federal University (Rostov-on-Don, Russia) under the supervision of Svetlana V. Revina and defended in 2018. The main aim of this thesis is to investigate by analytical methods the formation of spatially inhomogeneous time-periodic and stationary patterns in the FitzHugh-Nagumo reaction-diffusion system and its limit cases, as well as determine the stability properties of branched-out solutions and numerically analyse the evolution of the respective regimes for the values of the bifurcation parameter far away from the threshold of instability.
The thesis considers the FitzHugh-Nagumo reaction-diffusion system, which can be written in the form:

$$v_t = \nu_1 \Delta v + \epsilon(w - \alpha v - \beta); \quad w_t = \nu_2 \Delta w - v + \mu w - w^3, \tag{2.1}$$

where $v = v(x,t)$, $w = w(x,t)$, $x \in \Omega$, $t > 0$ denotes time; $\mu \in \mathbb{R}$, α, $\beta \geq 0$, $\epsilon > 0$ are reaction parameters, and $\nu_1 > 0$, $\nu_2 > 0$ are diffusion coefficients. It is assumed that $\Omega \subset \mathbb{R}^{\mathrm{m}}$, $m = 1, 2, 3$, is either a bounded domain with boundary $\partial\Omega$ of class C^2 or a rectangular parallelepiped. In the thesis we focus on the Rayleigh reaction-diffusion system, which is obtained from (2.1) by setting $\alpha = 0$, $\beta = 0$ and $\epsilon = 1$:

$$v_t = \nu_1 \Delta v + w; \quad w_t = \nu_2 \Delta w - v + \mu w - w^3. \tag{2.2}$$

In addition to Neumann boundary conditions (1.2), we consider Dirichlet boundary conditions:

$$v|_{\partial\Omega} = w|_{\partial\Omega} = 0, \tag{2.3}$$

and mixed boundary conditions, when some part of boundary is supplied with Diriclet boundary conditions while the remaining part is supplied with Neumann boundary conditions:

$$v|_{S_1} = w|_{S_1} = 0, \; \frac{\partial v}{\partial n}|_{S_2} = \frac{\partial w}{\partial n}|_{S_2} = 0, \; S_1 \cup S_2 = \partial\Omega. \tag{2.4}$$

In this work we provide analytical conditions for spatially inhomogeneous time-periodic and stationary regimes branching out of the trivial (zero) solution. To this end, we apply the Liapunov-Schmidt method in the form, developed by V.I. Yudovich (Yudovich (1971, 1972)). First, the bifurcations in the Rayleigh-reaction-diffusion system (2.2) are studied under the assumption that the diffusion coefficients $0 < \nu_1 \leq \nu_2$ are fixed and the boundary $\partial\Omega$ is supplied with Dirichlet boundary conditions (2.3) or mixed boundary conditions (2.4). Next, for the special case of system (2.2) when spatial variable belongs to one-dimensional interval $x \in (0, 1)$:

$$v_t = \nu_1 v_{xx} + w; \quad w_t = \nu_2 w_{xx} - v + \mu w - w^3, \tag{2.5}$$

with Neumann boundary conditions:

$$\frac{\partial v}{\partial x}|_{x=0,1} = \frac{\partial w}{\partial x}|_{x=0,1} = 0,$$

we show the existence of a countable set of infinite-dimensional invariant subspaces and study the bifurcational behaviour of the solutions on the respective subspaces. Finally we extend the results to the more general model (2.1) assuming that reaction parameters are set to the values $\epsilon = 1$ and $\beta = 0$. Here, boundary $\partial\Omega$ is supplied with Dirichlet boundary conditions (2.3), mixed boundary conditions (2.4) or Neumann boundary conditions (1.2). Parameter $\alpha \geq 0$ and diffusion coefficients ν_1, ν_2 are fixed, but no relation between ν_1 and ν_2 is assumed.
The detailed proofs can be found in Kazarnikov and Revina (2016b,a, 2017, 2018).

2.2 Bifurcational behaviour of the Rayleigh reaction-diffusion system

Let us write the Rayleigh reaction-diffusion system (2.2) as an ordinary differential equation in Hilbert space H of vector functions $\boldsymbol{u} = (v, w)$, whose components belong to $L_2(\Omega)$. It is assumed that $\Omega \subset \mathbb{R}^{\mathrm{m}}$, $m = 1, 2, 3$ is a rectangular parallelepiped or a bounded domain such that $\partial\Omega \in C^2$. Let us introduce linear operator $A(\mu) : H \to H$ on the assumption that for every vector function $\boldsymbol{u} = (v, w)$, $v, w \in W_2^2(\Omega)$

$$\mathrm{A}(\mu)\mathbf{u} = -A_0\boldsymbol{u} + \mathrm{B}\boldsymbol{u} + \mu\mathrm{C}\boldsymbol{u}. \tag{2.6}$$

Here, operator $A_0 = -\mathrm{D}\Delta$, where Δ is the vector Laplace operator. It is a self-adjoint, positively defined operator in H, while operators $B, C, D : \mathbb{R}^2 \to \mathbb{R}^2$ are defined by matrices

$$\mathrm{B} = \begin{pmatrix} 0 & 1 \\ -1 & 0 \end{pmatrix}, \mathrm{C} = \begin{pmatrix} 0 & 0 \\ 0 & 1 \end{pmatrix}, \mathrm{D} = \begin{pmatrix} \nu_1 & 0 \\ 0 & \nu_2 \end{pmatrix}. \tag{2.7}$$

It is assumed that the domain of definition of operator $A(\mu)$ is the set $\mathcal{D}(A_0)$ of vector functions $\boldsymbol{u} = (v, w)$, $v, w \in W_2^2(\Omega)$, satisfying boundary conditions (2.3) or (2.4) correspondingly. Diffusion coefficients ν_1 and ν_2 are fixed and satisfy the condition $0 < \nu_1 \leq \nu_2$.
Let us introduce tri-linear operator $K(\boldsymbol{a}, \boldsymbol{b}, \boldsymbol{c}) : H \times H \times H \to H$ on the assumption that

$$K(\boldsymbol{a}, \boldsymbol{b}, \boldsymbol{c}) = (0, a_2 b_2 c_2)\,, \tag{2.8}$$

for any $\boldsymbol{a} = (a_1(x,t), a_2(x,t))$, $\boldsymbol{b} = (b_1(x,t), b_2(x,t))$, and $\boldsymbol{c} = (c_1(x,t), c_2(x,t))$ from the set $\mathcal{D}(A_0)$.
By applying the Hölder inequality to operator $K(\boldsymbol{a}, \boldsymbol{b}, \boldsymbol{c})$ the following estimate is obtained:

$$||K(\boldsymbol{a}, \boldsymbol{b}, \boldsymbol{c})||_{L_2} \leq ||a_2(x,t)||_{L_6}||b_2(x,t)||_{L_6}||c_2(x,t)||_{L_6}, \tag{2.9}$$

and from the Sobolev embedding theorems it follows that $W_2^2(\Omega) \subset C(\bar{\Omega})$ for $m < 4$;

$W_2^2(\Omega) \subset L_q(\Omega)$, where $q \in [1, +\infty)$ for $m = 4$ and $q \in [1, 10)$ for $m = 5$ correspondingly, moreover the embedding is compact. Therefore, for $m = 1, \ldots, 5$ the following estimate holds:

$$||K(\boldsymbol{a}, \boldsymbol{b}, \boldsymbol{c})||_{L_2} \leq M||a_2(x,t)||_{W_2^2}||b_2(x,t)||_{W_2^2}||c_2(x,t)||_{W_2^2}. \tag{2.10}$$

Then, system (2.2) can be written in operator form:

$$\dot{\boldsymbol{u}} = \mathrm{A}(\mu)\boldsymbol{u} - K(\boldsymbol{u}, \boldsymbol{u}, \boldsymbol{u}); \quad \boldsymbol{u} \in H. \tag{2.11}$$

Let us define as λ_k eigenvalues of the scalar Laplace operator $-\Delta$, whose domain of definition is Ω with corresponding boundary conditions imposed on $\partial\Omega$:

$$-\Delta\psi_k = \lambda_k\psi_k, \tag{2.12}$$

assuming that λ_k are arranged in ascending order and each eigenvalue is counted according to its multiplicity and denoting as ψ_k the respective ordered orthonormal system of eigenfunctions.
To analyse the linear stability of the Rayleigh reaction-diffusion system (2.11) around the trivial (zero) solution, the linear spectral problem is considered:

$$\mathrm{A}(\mu)\boldsymbol{u} = \sigma\boldsymbol{u}, \quad \boldsymbol{u} \neq 0, \tag{2.13}$$

where $\boldsymbol{u} \in H$.

Definition 1 *We say that the value μ_{cr} is the critical value of the control parameter μ if the spectrum of linear operator $A(\mu_{cr})$ lies in the closed left half-plane of the complex plane and there exists at least one eigenvalue σ laying on the imaginary axis and satisfying $\frac{dRe(\sigma)}{d\mu}|_{\mu=\mu_{cr}} \neq 0$. If only zero eigenvalue lies in the imaginary axis for $\mu = \mu_{cr}$, we say that a monotonous instability occurs. If there exists a pair of purely imaginary eigenvalues $\pm i\omega_0$ ($\omega_0 \neq 0$) for $\mu = \mu_{cr}$, we say that an oscillatory instability occurs.*

Next, the critical values of control parameter μ, corresponding to monotonous and oscillatory instabilities, are found. Let $\nu_1\lambda_1 < 1$. Then, lemma 1 is proved by expanding the vector function $\boldsymbol{u}$ into a Fourier series (Kazarnikov (2018)).

Lemma 1 *Let $\nu_1 \leq \nu_2$ and $\nu_1\lambda_1 < 1$. Then, an oscillatory instability of the zero solution to system* (2.11) *occurs and the critical value of the control parameter μ is given by formula:*

$$\mu_{cr} = (\nu_1 + \nu_2)\lambda_1. \tag{2.14}$$

Operator $A(\mu_{cr})$ has a pair of simple purely imaginary eigenvalues:

$$\sigma_{1,2}(\mu_{cr}) = \pm i\omega_0, \qquad \omega_0 = \sqrt{1 - \nu_1^2\lambda_1^2}. \tag{2.15}$$

By following the scheme of the Liapunov-Schmidt method, the eigenfunction $\boldsymbol{\varphi} \in H$ of the linear spectral problem and the eigenfunction $\boldsymbol{\Phi} \in H$ of the linear conjugated problem

are sought:

$$A(\mu_{cr})\boldsymbol{\varphi} - i\omega_0\boldsymbol{\varphi} = 0, \quad A^*(\mu_{cr})\boldsymbol{\Phi} + i\omega_0\boldsymbol{\Phi} = 0,$$

assuming $(\boldsymbol{\varphi}, \boldsymbol{\Phi}) = 1$. The eigenfunctions are expressed by:

$$\boldsymbol{\varphi} = \frac{i}{2\omega_0}\begin{pmatrix} 1 \\ \nu_1\lambda_1 + i\omega_0 \end{pmatrix}\psi_1(x),\ \boldsymbol{\Phi} = \frac{1}{(\nu_1\lambda_1 - i\omega_0)}\begin{pmatrix} 1 \\ -(\nu_1\lambda_1 - i\omega_0) \end{pmatrix}\psi_1(x). \tag{2.16}$$

Let $\nu_1\lambda_1 > 1$. Then, lemma 2 is proved similarly to lemma 1 (Kazarnikov (2018)).

Lemma 2 *Let $\nu_1 \leq \nu_2$ and $\nu_1\lambda_1 > 1$. Then, a monotonous instability of the zero solution to system* (2.11) *occurs and the critical value of the control parameter μ is given by formula:*

$$\mu_{cr} = \frac{1}{\nu_1\lambda_1} + \nu_2\lambda_1. \tag{2.17}$$

Here, zero eigenvalue $\sigma = 0$ of the operator $A(\mu_{cr})$ is simple.

The case when $\nu_1\lambda_1 = 1$ is a degenerate case (adjoined vector exists). In what follows, only non-degenerate cases are considered. For $\nu_1\lambda_1 > 1$ eigenfunctions $\boldsymbol{\varphi} \in H$ and $\boldsymbol{\Phi} \in H$ of the linear spectral problem and linear conjugated problem are defined as non-trivial solutions of the equations:

$$A(\mu_{cr})\boldsymbol{\varphi} = 0, \quad A^*(\mu_{cr})\boldsymbol{\Phi} = 0, \quad (\boldsymbol{\varphi}, \boldsymbol{\Phi}) = 1$$

and are expressed by:

$$\boldsymbol{\varphi} = \frac{1}{1 + \nu_1\lambda_1}\begin{pmatrix} 1 \\ \nu_1\lambda_1 \end{pmatrix}\psi_1(x), \qquad \boldsymbol{\Phi} = \frac{1}{1 - \nu_1\lambda_1}\begin{pmatrix} 1 \\ -\nu_1\lambda_1 \end{pmatrix}\psi_1(x). \tag{2.18}$$

Next, the Liapunov-Schmidt method is applied to find the $\frac{2\pi}{\omega}$-periodic in time solution of equation (2.11), where ω is unknown cyclic frequency. A change of time in equation (2.11) is performed by setting $\tau = \omega t$ and defining $\varepsilon^2 = \mu - \mu_{cr}$ and the following equation is obtained:

$$\omega\dot{\boldsymbol{u}} - A(\mu_{cr})\boldsymbol{u} = \varepsilon^2\mathrm{C}\boldsymbol{u} - K(\boldsymbol{u}, \boldsymbol{u}, \boldsymbol{u}), \tag{2.19}$$

where the dot denotes the differentiation by τ. An unknown solution $\boldsymbol{u}$, 2π-periodic in τ and unknown cyclic frequency ω are sought in the form of a series expansion in powers of ε:

$$\boldsymbol{u} = \sum_{i=1}^{\infty}\varepsilon^i\boldsymbol{u}_i, \qquad \omega = \sum_{i=0}^{\infty}\varepsilon^i\omega_i, \tag{2.20}$$

where $\omega_0 = \sqrt{1 - \nu_1^2\lambda_1^2}$. By substituting (2.20) into (2.19) and equating the coefficients of like powers of ε, the sequence of equations is obtained. By analysing the first five equations in the sequence, the following theorem is proved (Kazarnikov and Revina (2016b)).

Theorem 1 *Let $\nu_1 \leq \nu_2$ and $\nu_1\lambda_1 < 1$. Then, there exists $\mu_{cr} = (\nu_1 + \nu_2)\lambda_1$ such that the zero solution of the Rayleigh reaction-diffusion system (2.2) is asymptotically stable*

for $\mu < \mu_{cr}$. The soft oscillatory instability of the zero solution occurs for $\mu = \mu_{cr}$ and for small values of $\varepsilon = \sqrt{\mu - \mu_{cr}} > 0$, there exists a stable limit cycle of the system (2.2). When $\mu = \mu_{cr}$ the soft oscillatory loss of stability of the zero solution takes place and there exists a stable limit cycle of the system (2.2) for small values of $\varepsilon = \sqrt{\mu - \mu_{cr}} > 0$. The first terms of the power series expansion of auto-oscillation mode are given by:

$$\begin{aligned} &\boldsymbol{u} = \varepsilon\alpha_1(e^{i\omega t}\boldsymbol{\varphi} + e^{-i\omega t}\boldsymbol{\varphi}^*) + \varepsilon^3(\alpha_3(e^{i\omega t}\boldsymbol{\varphi} + e^{-i\omega t}\boldsymbol{\varphi}^*) + \boldsymbol{u}_3^p(\omega t)) + O(\varepsilon^4) \\ &\omega = \sqrt{1 - \nu_1^2\lambda_1^2} + \varepsilon^4\omega_4 + O(\varepsilon^5), \end{aligned}$$

where $\boldsymbol{\varphi}$ is defined in (2.16)*, values α_1, α_3, ω_4 and $\boldsymbol{u}_3^p$ are found explicitly.*

For $n \geq 5$, the equation for finding the n-th term of the power series expansion can be written in the form:

$$\omega_0\dot{\boldsymbol{u}}_n - A(\mu_{cr})\boldsymbol{u}_n = C\boldsymbol{u}_{n-2} - \sum_{i=1}^{n-1}\omega_{n-i}\dot{\boldsymbol{u}}_n - \sum_{i_1+i_2+i_3=n} 3K(\boldsymbol{u}_{i_1}, \boldsymbol{u}_{i_2}, \boldsymbol{u}_{i_3}) \equiv \boldsymbol{f}_n, \tag{2.21}$$

where $\boldsymbol{u}_n \in H$. The following two theorems can be proved by induction.

Theorem 2 *Let $\nu_1\lambda_1 < 1$. Then, even terms of the power series expansion of auto-oscillation mode and even terms of the cyclic frequency ω are equal to zero: for every $k \in \mathbb{N}$ $\boldsymbol{u}_{2k} = 0, \omega_{2k-1} = 0$.*

Theorem 3 *Let $\nu_1\lambda_1 < 1$. Then, the right-hand side of the equation* (2.21) *for finding the n-th term of the power series expansion of auto-oscillation mode is an odd trigonometric polynomial of the degree n with respect to time:*

$$\omega_0\dot{\boldsymbol{u}}_n - A(\mu_{cr})\boldsymbol{u}_n = \boldsymbol{f}_{1n}(x)e^{i\tau} + \boldsymbol{f}_{3n}(x)e^{3i\tau} + \cdots + \boldsymbol{f}_{nn}(x)e^{in\tau} + c.c., \quad \boldsymbol{f}_{kn}(x) \in H$$

and its solution, 2π-periodic in time has the form:

$$u_n = \alpha_n\boldsymbol{\varphi}e^{i\tau} + \boldsymbol{w}_{1n}(x)e^{i\tau} + \cdots + \boldsymbol{w}_{nn}(x)e^{in\tau} + c.c., \quad \boldsymbol{w}_{kn}(x) = -(A(\mu_{cr}) - ik\omega_0 I)^{-1}\boldsymbol{f}_{kn}(x)$$

By setting in (2.19) $\omega = 0$, the equation for finding stationary solutions of system (2.11) is obtained:

$$-A(\mu_{cr})\boldsymbol{u} = \varepsilon^2 \mathrm{C}\boldsymbol{u} - K(\boldsymbol{u}, \boldsymbol{u}, \boldsymbol{u}). \tag{2.22}$$

The stationary solution $\boldsymbol{u}$ is sought in the form of a series expansion in powers of ε (2.20). By applying the Liapunov-Schmidt method, the following theorems are proved (Kazarnikov and Revina (2016a)):

Theorem 4 *Let $\nu_1 \leq \nu_2$ and $\nu_1\lambda_1 > 1$. Then, there exists $\mu_{cr} = \frac{1}{\nu_1\lambda_1} + \nu_2\lambda_1$ such that the zero solution of the Rayleigh reaction-diffusion system (2.2) is asymptotically stable for $\mu < \mu_{cr}$. A soft monotonous loss of stability of the zero solution occurs for $\mu = \mu_{cr}$*

and there exists a pair of stable stationary solutions of the system (2.2) for small values of $\varepsilon = \sqrt{\mu - \mu_{cr}} > 0$*:*

$$\boldsymbol{u} = \pm\varepsilon\alpha_1\boldsymbol{\varphi} \pm \varepsilon^3(\alpha_3\boldsymbol{\varphi} + \boldsymbol{u}_3^p) + O(\varepsilon^4)$$

where $\boldsymbol{\varphi}$ *is defined in* (2.18)*, values* α_1*,* α_3 *and* $\boldsymbol{u}_3^p$ *are found explicitly.*

Theorem 5 *Let* $\nu_1\lambda_1 > 1$*. Then, even terms of the series expansion in powers of* ε *of the stationary solution are equal to zero: for every* $k \in \mathbb{N}$ $\boldsymbol{u}_{2k} = 0$*.*

2.3 Invariant subspaces

Let us consider the Rayleigh reaction-diffusion system in one-dimensional interval $x \in (0, 1)$ supplied with Neumann boundary conditions (1.2). As before, it is assumed that diffusion coefficients are fixed and satisfy the condition $0 < \nu_1 \leq \nu_2$.
Assume that number $k \in N$ is fixed. Let us denote as Γ_k the set:

$$\Gamma_k = \{k(2j-1), j \in N\}.$$

As H_k we denote the subspace of H with basis:

$$\{\boldsymbol{e_1}\psi_i(x)\,,\ \boldsymbol{e_2}\psi_i(x)\},\ i \in \Gamma_k, \tag{2.23}$$

where $\boldsymbol{e_1} = (1, 0)$, $\boldsymbol{e_2} = (0, 1)$ and ψ_k are defined in (2.12). In addition, we define $H_0 = H$. Then, the following theorem holds (Kazarnikov and Revina (2017)):

Theorem 6 *Subspaces* H_k*,* $k \in \mathbb{N}$ *are invariant with respect to the Rayleigh reaction-diffusion system* (2.5) *with Neumann boundary conditions* (1.2)*.*

By studying the linear spectral problem (2.13), we find that a spatially homogeneous auto-oscillation mode branches out from the zero solution for $\mu_{cr}^{(0)} = 0$ when $\boldsymbol{u} \in H_0 \equiv H$. Next, by considering (2.13) for $\boldsymbol{u} \in H_k$, $k \in \mathbb{N}$, we arrive at a countable set of critical values of the control parameter μ for which the branching out of spatially inhomogeneous oscillatory and stationary solutions occurs. Taking into account that all λ_k are simple in a one-dimensional case, the following analogues of lemmas 1 and 2 are proved (Kazarnikov (2018)):

Lemma 3 *Let* $\nu_1\lambda_k < 1$*. Then, an oscillatory instability of the zero solution to the Rayleigh reaction-diffusion system* (2.5) *occurs on the invariant subspace* H_k *and the critical value of the control parameter* μ *is:*

$$\mu_{cr}^{(k)} = (\nu_1 + \nu_2)\lambda_k. \tag{2.24}$$

Operator $A(\mu_{cr}^{(k)})$ *has a pair of simple purely imaginary eigenvalues:*

$$\sigma_{1,2}(\mu_{cr}^{(k)}) = \pm i\omega_0, \qquad \omega_{0k} = \sqrt{1 - \nu_1^2\lambda_k^2}. \tag{2.25}$$

As before, let us find the eigenfunction $\boldsymbol{\varphi}$ of the linear spectral problem and the eigenfunction $\boldsymbol{\Phi}$ of the linear conjugated problem:

$$A(\mu_{cr}^{(k)})\boldsymbol{\varphi} - i\omega_{0k}\boldsymbol{\varphi} = 0, \quad A^*(\mu_{cr}^{(k)})\boldsymbol{\Phi} + i\omega_{0k}\boldsymbol{\Phi} = 0, \quad (\boldsymbol{\varphi}, \boldsymbol{\Phi}) = 1.$$

They are expressed by:

$$\boldsymbol{\varphi} = \frac{i}{2\omega_{0k}} \begin{pmatrix} 1 \\ \nu_1\lambda_k + i\omega_{0k} \end{pmatrix} \psi_k(x), \; \boldsymbol{\Phi} = \frac{1}{(\nu_1\lambda_1 - i\omega_{0k})} \begin{pmatrix} 1 \\ -\nu_1\lambda_k + i\,\omega_{0k} \end{pmatrix} \psi_k\,(x)\,. \tag{2.26}$$

Lemma 4 *Let $k \neq 0$ and $\nu_1\lambda_k > 1$. Then, a monotonous loss instability of the zero solution to the Rayleigh reaction-diffusion system* (2.5) *occurs on the invariant subspace H_k and the critical value of the control parameter μ is:*

$$\mu_{cr}^{(k)} = \frac{1}{\nu_1\lambda_k} + \nu_2\lambda_k. \tag{2.27}$$

Here, zero eigenvalue $\sigma = 0$ of operator $A(\mu_{cr}^{(k)})$ is simple.

Eigenfunctions $\boldsymbol{\varphi}$ and $\boldsymbol{\Phi}$ of operator $A(\mu_{cr}^{(k)})$ are expressed by:

$$\boldsymbol{\varphi} = \frac{1}{1 + \nu_1\lambda_k} \begin{pmatrix} 1 \\ \nu_1\lambda_k \end{pmatrix} \psi_k(x), \quad \boldsymbol{\Phi} = \frac{1}{1 - \nu_1\lambda_k} \begin{pmatrix} 1 \\ -\nu_1\lambda_k \end{pmatrix} \psi_k\,(x)\,. \tag{2.28}$$

Let $k \in \mathbb{N}$ and $\nu_1\lambda_k < 1$. Let us consider the Rayleigh reaction-diffusion system on the invariant subspace H_k. Then, the following theorem holds (Kazarnikov and Revina (2017)):

Theorem 7 *Consider the Rayleigh reaction-diffusion system* (2.5) *on the invariant subspace H_k, $k \geq 0$ and let $\nu_1\lambda_k < 1$. Then, there exists $\mu_{cr}^{(k)} = (\nu_1 + \nu_2)\lambda_k$ such that the zero solution to the Rayleigh reaction-diffusion system* (2.2) *is asymptotically stable in H_k for $\mu < \mu_{cr}^{(k)}$. The soft oscillatory instability of the zero solution occurs when $\mu = \mu_{cr}^{(k)}$ and for small values of $\varepsilon = \sqrt{\mu - \mu_{cr}^{(k)}} > 0$ there exists a limit cycle of the system* (2.2)*, stable in H_k. The first terms of the power series expansion of auto-oscillation mode are given by:*

$$\begin{aligned} &\boldsymbol{u} = \varepsilon\alpha_1(e^{i\omega t}\boldsymbol{\varphi} + e^{-i\omega t}\boldsymbol{\varphi}^*) + \varepsilon^3(\alpha_3(e^{i\omega t}\boldsymbol{\varphi} + e^{-i\omega t}\boldsymbol{\varphi}^*) + \boldsymbol{u}_3^p(\omega t)) + O(\varepsilon^4), \\ &\omega = \omega_0 + \varepsilon^4\omega_4 + O(\varepsilon^5). \end{aligned}$$

where $\boldsymbol{\varphi}$ is defined in (2.26)*, values α_1, α_3, ω_4 and $\boldsymbol{u}_3^p$ are found explicitly.*

For $n \geq 5$, the equation for finding the n-th term of the power series expansion of auto-oscillation mode can be written in the form (2.21), where $\boldsymbol{u}_n \in H$. The following theorems can be proved by induction (Kazarnikov and Revina (2017)):

Theorem 8 *Consider the Rayleigh reaction-diffusion system on the invariant subspace H_k, $k \geq 0$ and let $\nu_1\lambda_k < 1$. Then, even terms of the power series expansion of auto-oscillation mode and even terms of the power series expansion of cyclic frequency ω are equal to zero: for every $k \in \mathbb{N}$ $\boldsymbol{u}_{2k} = 0$, $\omega_{2k-1} = 0$.*

Theorem 9 *Consider the Rayleigh reaction-diffusion system on the invariant subspace H_k, $k \in \mathbb{N}$ and let $\nu_1\lambda_k < 1$. Then, the right-hand side of the equation for finding the n-th term of the power series expansion of auto-oscillation mode* (2.21) *is the even trigonometric polynomial of the degree n with respect to τ:*

$$\omega_0\dot{\boldsymbol{u}}_n - A(\mu_{cr})\boldsymbol{u}_n = \boldsymbol{f}_{1n}(x)e^{i\tau} + \boldsymbol{f}_{3n}(x)e^{3i\tau} + \ldots + \boldsymbol{f}_{nn}(x)e^{in\tau} + \text{c.c.},$$

where $\boldsymbol{f}_{sn}(x) \in H_k$, and functions $\boldsymbol{f}_{sn}(x)$ are linear combinations of the basis functions ψ_j with indexes $j \in \Gamma_{k,n} = \{j \in \Gamma_k : j \leq kn\}$. The general solution of this equation can be expressed in the form:

$$u_n = \alpha_n\boldsymbol{\varphi}e^{i\tau} + \boldsymbol{w}_{1n}(x)e^{i\tau} + \ldots + \boldsymbol{w}_{nn}(x)e^{in\tau} + \text{c.c.},$$

where $\boldsymbol{w}_{sn}(x) = -(A - is\omega_0 I)^{-1}\boldsymbol{f}_{sn}(x)$, and functions $\boldsymbol{w}_{sn}(x)$ are linear combinations of basis functions ψ_j with indexes $j \in \Gamma_{k,n}$.

Considering the subspace H_0, the results for the n-th term of the power series expansion of volume oscillations are obtained (Kazarnikov and Revina (2017)).

Theorem 10 *Consider the Rayleigh reaction-diffusion system on the invariant subspace H_0. Let us introduce set $\mathcal{A}_1 = \{m = 2s - 1,\ s \geq 3\} \subset \Gamma_1$. Note that $n \in \mathcal{A}_1$. Consider equation* (2.21)*. Then, the following holds:*

1. *The right-hand side of equation* (2.21) *is an odd trigonometric polynomial of the degree n with respect to time*
2. *The solution of equation* (2.21)*, 2π-periodic in time is an odd trigonometric polynomial of the degree n with respect to time*
3. *Numbers α_{n-2} and ω_{n-1} are equal to zero in rotation on the elements $n \in \mathcal{A}_1$, which means that the following holds:*
   - *$\boldsymbol{f}_{sn} = (iR^1_{ns},\ R^2_{ns})$ for $n = 5, 9, 13, \ldots$, where $R^{1,2}_{ns} \in \mathbb{R}$ and $\alpha_{n-2} = 0$;*
   - *$\boldsymbol{f}_{kn} = (R^1_{ns},\ iR^2_{ns})$ for $n = 7, 11, 15, \ldots$, where $R^{1,2}_{ns} \in \mathbb{R}$ and $\omega_{n-1} = 0$.*

Next we consider the Rayleigh reaction-diffusion system on the invariant subspace H_k and assume that $\nu_1\lambda_k > 1$. By applying the Liapunov-Schmidt method, the following theorem is proved (Kazarnikov and Revina (2017)):

Theorem 11 *Consider the Rayleigh reaction-diffusion system on the invariant subspace H_k, $k \in \mathbb{N}$ and let $\nu_1\lambda_k > 1$. Then, there exists $\mu^{(k)}_{cr} = \frac{1}{\nu_1\lambda_k} + \nu_2\lambda_k$ such that the zero*

solution to the Rayleigh reaction-diffusion system (2.2) *is asymptotically stable in* H_k *for* $\mu < \mu_{cr}^{(k)}$. *The soft monotonous instability to the zero solution occurs for* $\mu = \mu_{cr}^{(k)}$ *and for small values of* $\varepsilon = \sqrt{\mu - \mu_{cr}^{(k)}} > 0$ *there exists a pair of stable stationary solutions to the system. The first terms of the power series expansions of the secondary solutions are given by:*

$$\boldsymbol{u} = \pm\varepsilon \boldsymbol{a_1} \cos(\pi k x) \pm \varepsilon^3 (\boldsymbol{a_3} \cos(\pi k x) + \boldsymbol{b_3} \cos(3\pi k x)) + O(\varepsilon^4)$$

where the values $\boldsymbol{a_1}$, $\boldsymbol{a_3}$ *and* $\boldsymbol{b_3}$ *are found explicitly.*

For $n \geq 5$, the equation for finding the n-th term of power series expansion can be written in the form (2.21) for $\omega_i = 0$ and $\boldsymbol{u}_n \in H$:

$$-A(\mu_{cr})\boldsymbol{u}_n = C\boldsymbol{u}_{n-2} - \sum_{i_1 + i_2 + i_3 = n} 3K(\boldsymbol{u}_{i_1}, \boldsymbol{u}_{i_2}, \boldsymbol{u}_{i_3}) \equiv \boldsymbol{f}_n. \tag{2.29}$$

The following theorems can be proved by induction:

Theorem 12 *Consider the Rayleigh reaction-diffusion system on the invariant subspace* H_k, $k \in \mathbb{N}$ *and let* $\nu_1\lambda_k > 1$. *Then, even components of the power series expansion are equal to zero: for every* $m \in \mathbb{N}$ $\boldsymbol{u}_{2m} = 0$.

Theorem 13 *Consider the Rayleigh reaction-diffusion system on the invariant subspace* H_k, $k \in \mathbb{N}$ *and let* $\nu_1\lambda_k > 1$. *Then, the right-hand side* $\boldsymbol{f}_n(x)$ *of the equation* (2.29) *and partial solution* $\boldsymbol{u}_n^p(x)$ *of this equation,* 2π*-periodic in time are linear combinations of basis functions* ψ_j *with indexes* $j \in \Gamma_{k,n}$.

In summary, the general character of the bifurcation behaviour of the Rayleigh reaction-diffusion system (2.5) on the subspaces H_k can be described as follows. The zero solution of the Rayleigh reaction-diffusion system is stable in the whole space $H = H_0$ for $\mu < \mu_{cr}^{(0)} = 0$. For $\mu = \mu_{cr}^{(0)}$ it loses stability and enters a stable spatially uniform self-oscillating regime. For $\mu \leqslant \mu_{cr}^{(1)}$, the zero solution of system (2.5) is stable in H_1. For small $\mu > \mu_{cr}^{(1)}$ there is a stable secondary solution in H_1. If $\nu_1\lambda_1 < 1$, then $\mu_{cr}^{(1)} = 2\nu_1\lambda_1$ and the branching out of the limit cycle occurs; if $\nu_1\lambda_1 \geqslant 1$, then $\mu_{cr}^{(1)} = \dfrac{1}{\nu_1\lambda_1} + \nu_1\lambda_1$ and non-trivial stationary solution arises.
For $\mu \leqslant \mu_{cr}^{(2)}$, the zero solution (2.5) is stable in H_2. For small $\mu > \mu_{cr}^{(2)}$ there exists a stable secondary solution in H_2 that is a non-trivial stationary solution or a cycle, depending on whether the inequality $\nu_1\lambda_2 > 1$ is satisfied.
Continuing this process, we conclude that on each of the invariant subspaces H_k, $k = 1, 2, 3, \ldots$, when the control parameter μ passes through the critical value $\mu_{cr}^{(k)}$, there is a branching out of secondary solutions that are stable in H_k for small $\mu > \mu_{cr}^{k}$, but are unstable in H. Among them, there can only be a finite number of cycles. Starting from some k_*, which is specified by the condition $\nu_1\lambda_{k_*} \geqslant 1$, only non-trivial stationary modes branch out from the zero solution.

The process of destruction of secondary solutions on the subspaces H_k, $k = 1, 2$ with increasing values of μ was investigated in numerical experiments. The diffusion coefficients were fixed equal to $\nu_1 = \nu_2 = 0.1$. In this case, an oscillatory instability occurs on the subspace H_1, and monotonic instability occurs on H_2.

The numerical solution of the system (2.2) was constructed using the Galerkin method for increasing values of $\mu = \mu_{cr}^k + \varepsilon^2$, $k = 1, 2$. The initial conditions were specified by the formulas for the first terms of the expansion of the secondary time-periodic and stationary solutions in the form of power series. For $\varepsilon < 0.18$, a spatially inhomogeneous self-oscillating regime was observed on H_1, being in good agreement with the formulas obtained, which gradually changed to a stationary solution for $\varepsilon \in (0.2, 0.3)$. With a further increase in ε, the profile of the first component of the solution $v(x,t)$ remained sinusoidal, while $w(x,t)$ asymptotically tended to meander mode, with $\max_{x\in[0,l]} |w(x,t)| \sim \varepsilon$. A spatially inhomogeneous stationary solution was observed on the subspace H_2 for $\mu > \mu_{cr}^{(2)}$. As μ increased, the profile of the first component of the solution $v(x,t)$ remained sinusoidal, while $w(x,t)$ asymptotically tended to meander mode, and $\max_{x\in[0,1]} |w(x,t)| \sim \varepsilon$.

The results of the analysis can be extended to other types of boundary conditions considered here. Invariant subspaces are introduced in a similar way in the case of the Dirichlet boundary conditions (2.3). Further, an analysis of formulas for secondary solutions leads to the conclusion that secondary stationary or time-periodic solutions satisfying the Neumann conditions (1.2) on the interval $[0, 1]$ also satisfy mixed boundary conditions on the segment $[0, \frac{1}{2}]$: Neumann conditions at $x = 0$ and Dirichlet conditions at $x = \frac{1}{2}$. A similar statement holds for the case of the Dirichlet boundary conditions (2.3).

The results for invariant subspaces can be generalised to the case of an m-dimensional parallelepiped with incommensurate squares of sides.

2.4 Bifurcational behaviour of the FitzHugh-Nagumo reaction-diffusion system

Let us consider the FitzHugh-Nagumo reaction-diffusion system (2.1) under assumption that $\Omega \subset \mathbb{R}^m$, $m = 1, 2, 3$, is a bounded domain with boundary $\partial\Omega \in C^2$ or rectangular parallelepiped and as well $\epsilon = 1$ and $\beta = 0$. Parameter $\alpha \geq 0$ and diffusion coefficients ν_1, ν_2 are assumed to be fixed. It is assumed that the boundary $\partial\Omega$ is supplied with Dirichlet boundary conditions (2.3), or mixed boundary conditions (2.4) or Neumann boundary conditions (1.2).

Let us write the system (2.1) as the ordinary differential equation in the Hilbert space H. As before, we introduce a linear operator $A_\alpha(\mu) : H \to H$ on the assumption that for every $\boldsymbol{u} = (v, w)$, $v, w \in W_2^2(\Omega)$

$$\mathrm{A}_\alpha(\mu)\mathbf{u} = \mathrm{D}\Delta\boldsymbol{u} + \mathrm{B}_\alpha\boldsymbol{u} + \mu\mathrm{C}\boldsymbol{u}. \tag{2.30}$$

Here, operators B_α, C and D are defined by matrices:

$$\mathrm{B}_\alpha = \begin{pmatrix} -\alpha & 1 \\ -1 & 0 \end{pmatrix}, \mathrm{C} = \begin{pmatrix} 0 & 0 \\ 0 & 1 \end{pmatrix}, \mathrm{D} = \begin{pmatrix} \nu_1 & 0 \\ 0 & \nu_2 \end{pmatrix} \tag{2.31}$$

and in the limit case $\alpha = 0$ expressions (2.31) and (2.30) transform into (2.7) and (2.6) correspondingly.

As before, boundary conditions are taken into account by properly choosing the domain of the definition of the operator $A_\alpha(\mu)$. Operator $A_\alpha(\mu)$ is defined either on the set $\mathcal{D}(A_0)$ of vector functions $\boldsymbol{u} = (v, w)$, $v, w \in W_2^2(\Omega)$, satisfying Dirichlet boundary conditions (2.3) or mixed boundary conditions (2.4) or on the set $\mathcal{D}(\widetilde{A_0})$, $\widetilde{A_0} = A_0 + I$ of vector functions $\boldsymbol{u} = (v, w)$, $v, w \in W_2^2(\Omega)$, satisfying Neumann boundary conditions (1.2).

For the tri-linear operator $K(\boldsymbol{a}, \boldsymbol{b}, \boldsymbol{c})$ the estimates (2.9) and (2.10) hold. Then, the FitzHugh-Nagumo reaction-diffusion system (2.1) can be written in operator form:

$$\dot{\boldsymbol{u}} = \mathrm{A}_\alpha(\mu)\boldsymbol{u} - K(\boldsymbol{u}, \boldsymbol{u}, \boldsymbol{u}); \quad \boldsymbol{u} \in H. \tag{2.32}$$

Let us introduce function $F(\lambda) = \min(f_1(\lambda), f_2(\lambda))$, where:

$$f_1(\lambda) = \lambda(\nu_1 + \nu_2) + \alpha;\ f_2(\lambda) = \lambda\nu_2 + \frac{1}{\lambda\nu_1 + \alpha}.$$

Then, the critical value of the control parameter μ is defined by formula:

$$\mu_{cr} = \min_{\lambda \in \{\lambda_k\}_{k=0}^{+\infty}} F(\lambda).$$

Function $F(\lambda)$ is a monotonically increasing function and is bounded from below when $\nu_1 \le \nu_2$. Then, $\mu_{cr} = F(\lambda_0)$ and the results for this case are analogical to those obtained earlier for the Rayleigh reaction-diffusion system. For studying the case $\nu_1 > \nu_2$ let us consider the values $\gamma_i(\alpha)$, $i = 1, \ldots, 4$:

$$\gamma_1(\alpha) = -\frac{\alpha}{\nu_1} + \frac{2\sqrt{\nu_2}}{(\nu_1 + \nu_2)\sqrt{\nu_1}}, \quad \gamma_2(\alpha) = \lambda_{eq} = -\frac{\alpha}{\nu_1} + \frac{1}{\nu_1},$$

$$\gamma_3(\alpha) = \lambda_{min} = -\frac{\alpha}{\nu_1} + \frac{1}{\sqrt{\nu_1\nu_2}}, \quad \gamma_4(\alpha) = -\frac{\alpha}{\nu_1} + \frac{1}{\nu_2}$$

and corresponding wave numbers $k_i = k_i(\gamma_i)$, $i = 1, \ldots, 4$. In addition, let us introduce the values α_1, α_2, α_3 and α_4:

$$\alpha_1 = \frac{2\sqrt{\nu_1}\sqrt{\nu_2}}{\nu_1 + \nu_2}, \quad \alpha_2 = 1, \quad \alpha_3 = \sqrt{\frac{\nu_1}{\nu_2}}, \quad \alpha_4 = \frac{\nu_1}{\nu_2}, \tag{2.33}$$

The values γ_i, $i = 1, 2, 3, 4$ are positive when $\alpha < \alpha_1$, but successively change the sign as α grows (see Table 2.1).

Let us study the dependence of μ_{cr} on diffusion coefficients ν_1, ν_2 and parameter α.

Table 2.1: The sign of γ_i, $i = 1, 2, 3, 4$ for different values of α

The range of α	The sign of γ_k
$\alpha \in [0, \alpha_1]$	$\gamma_k \geq 0$
$\alpha \in (\alpha_1, \alpha_2]$	$\gamma_1 < 0$, $\gamma_2, \gamma_3, \gamma_4 \geq 0$
$\alpha \in (\alpha_2, \alpha_3]$	$\gamma_1, \gamma_2 < 0$, $\gamma_3, \gamma_4 \geq 0$
$\alpha \in (\alpha_3, \alpha_4]$	$\gamma_1, \gamma_2, \gamma_3 < 0$, $\gamma_4 \geq 0$
$\alpha > \alpha_4$	$\gamma_1, \gamma_2, \gamma_3, \gamma_4 < 0$

We have $\gamma_k > 0$, $k = 1, 2, 3, 4$ for small $\alpha \in (0, \alpha_1)$. Then, $F(\lambda) = f_1(\lambda)$ for $\lambda < \gamma_2(\alpha)$ and $F(\lambda) = f_2(\lambda)$ for $\lambda \geq \gamma_2(\alpha)$. As a result, either monotonous or oscillatory instability of the zero solution to the FitzHugh-Nagumo reaction-diffusion system (2.1) occurs depending on the values of diffusion coefficients ν_1 and ν_2. The formulas for μ_{cr} and the classification of instability types for $\alpha \in (0, \alpha_1)$ and $\lambda_0 > 0$ are given in Table 2.2. If $\lambda_0 = 0$, then $\mu_{cr} = \alpha$ and oscillatory instability of the zero solution to the FitzHugh-Nagumo reaction-diffusion system (2.1) always occurs.

The oscillatory instability cannot occur for the values of $\alpha \geq \alpha_2$ (see Table 2.3). Let $\alpha \in [\alpha_2, \alpha_3)$. Then, $\gamma_1 < 0, \gamma_2 \leq 0$ and $\gamma_3, \gamma_4 > 0$ and as a result $F(\lambda) \equiv f_2(\lambda)$. However, $F_2(\lambda)$ is a non-monotonic function. In this case, monotonous instability always occurs, but k_0 depends on the values of model parameters. The results for $\alpha \in [\alpha_2, \alpha_3)$ and $\lambda_0 > 0$ are summarised in Table 2.3. When $\lambda_0 = 0$ we get that $\mu_{cr} = \frac{1}{\alpha}$ if $\nexists k_0 : f_2(\lambda_{k_0}) < f_2(0)$ and $\mu_{cr} = \lambda_0\nu_2 + \frac{1}{\lambda_0\nu_1+\alpha}$ otherwise.

The scheme of the Lyapunov-Schmidt method is applicable to the case of bounded domain Ω, if λ_{k_0} is a simple eigenvalue. Next we consider the one-dimensional case when $x \in (0, l)$ and as a result all λ_k are simple. Then, a monotonous instability of the zero solution to the FitzHugh-Nagumo reaction-diffusion system (2.1) may occur for $\alpha > 0$ and Neumann boundary conditions (1.2), which is impossible in the limit case of the Rayleigh reaction-diffusion system (2.5) when $\alpha = 0$. If it occurs, then a pair of spatially homogeneous stationary solutions branches out, spatially homogeneous for $k_0 = 0$ and spatially inhomogeneous otherwise. Let us next consider the case $k_0 > 0$. For the FitzHugh-Nagumo reaction-diffusion system (2.1) holds the analogue of lemma 1 (Kazarnikov and Revina (2018)).

Lemma 5 *Consider the natural number k_0 satisfying $F(\lambda_{k_0}) = \min\limits_{\lambda \in \{\lambda_k\}_{k=0}^{+\infty}} F(\lambda)$. Let $\lambda_{k_0} > \gamma_2(\alpha)$ and let the following inequality holds:*

$$\nu_2 \neq \frac{1}{(\lambda_{k_0} + \frac{\alpha}{\nu_1})(\lambda_{k_0+1} + \frac{\alpha}{\nu_1})\nu_1}. \tag{2.34}$$

Then, a monotonous instability of the zero solution to the FitzHugh-Nagumo reaction-

Table 2.2: Critical value of the parameter μ_{cr} for the FitzHugh-Nagumo reaction-diffusion system (2.1). The case $\alpha \in (0, \alpha_1)$ and $\lambda_0 > 0$.

	Condition	μ_{cr}	Instability
$\nu_1 \leq \nu_2$	$\lambda_0 < \gamma_2(\alpha)$	$\mu_{cr} = \lambda_0 (\nu_1 + \nu_2) + \alpha$	osc.
	$\lambda_0 \geq \gamma_2(\alpha)$	$\mu_{cr} = \lambda_0 \nu_2 + \frac{1}{\lambda_0 \nu_1 + \alpha}$	mon.
$\nu_1 > \nu_2$	$\lambda_0 < \gamma_1(\alpha)$	$\mu_{cr} = \lambda_0 (\nu_1 + \nu_2) + \alpha$	osc.
	$\lambda_0 = \gamma_1, \nexists k : \lambda_k = \gamma_3(\alpha)$	$\mu_{cr} = \lambda_0 (\nu_1 + \nu_2) + \alpha$	osc.
	$\gamma_1(\alpha) < \lambda_0 < \gamma_2(\alpha)$, $\forall k \in [k_2, k_4]\ f_2(\lambda_k) > f_1(\lambda_0)$	$\mu_{cr} = \lambda_0 (\nu_1 + \nu_2) + \alpha$	osc.
	$\gamma_1(\alpha) < \lambda_0 < \gamma_2(\alpha)$, $\nexists k \in [k_2, k_4] : \lambda_k \in (\gamma_2(\alpha), \gamma_4(\alpha))$	$\mu_{cr} = \lambda_0 (\nu_1 + \nu_2) + \alpha$	osc.
	$\gamma_1(\alpha) < \lambda_0 < \gamma_2(\alpha)$, $\exists k_0 : f_2(\lambda_{k_0}) < f_1(\lambda_0)$	$\mu_{cr} = \lambda_{k_0} \nu_2 + \frac{1}{\lambda_{k_0} \nu_1 + \alpha}$	mon.
	$\gamma_2(\alpha) < \lambda_0 < \gamma_3(\alpha)$, $\forall k \in [k_2, k_4] : f_2(\lambda_k) > f_2(\lambda_0)$	$\mu_{cr} = \lambda_0 \nu_2 + \frac{1}{\lambda_0 \nu_1 + \alpha}$	mon.
	$\gamma_2(\alpha) < \lambda_0 < \gamma_3(\alpha)$, $\nexists k \in [k_2, k_4] : \lambda_k \in (\gamma_2(\alpha), \gamma_4(\alpha))$	$\mu_{cr} = \lambda_0 \nu_2 + \frac{1}{\lambda_0 \nu_1 + \alpha}$	mon.
	$\gamma_2(\alpha) < \lambda_0 < \gamma_3(\alpha)$, $\exists k_0 \in [k_2, k_4] : f_2(\lambda_{k_0}) < f_2(\lambda_0)$	$\mu_{cr} = \lambda_{k_0} \nu_2 + \frac{1}{\lambda_{k_0} \nu_1 + \alpha}$	mon.
	$\lambda_0 \geq \gamma_3(\alpha)$	$\mu_{cr} = \lambda_0 \nu_2 + \frac{1}{\lambda_0 \nu_1 + \alpha}$	mon.

Table 2.3: Critical value of the parameter μ_{cr} for the FitzHugh-Nagumo reaction-diffusion system (2.1). The case $\alpha \in [\alpha_2, \alpha_3)$ and $\lambda_0 > 0$

	Condition	μ_{cr}	Instability
$\nu_1 \leq \nu_2$	—	$\mu_{cr} = \lambda_0 \nu_2 + \frac{1}{\lambda_0 \nu_1 + \alpha}$	mon.
$\nu_1 > \nu_2$	$\lambda_0 < \gamma_3(\alpha)$, $\forall k \in [k_2, k_4] : f_2(\lambda_k) > f_2(\lambda_0)$	$\mu_{cr} = \lambda_0 \nu_2 + \frac{1}{\lambda_0 \nu_1 + \alpha}$	mon.
	$\lambda_0 < \gamma_3(\alpha)$, $\nexists k \in [k_2, k_4] : \lambda_k \in (\gamma_2(\alpha), \gamma_4(\alpha))$	$\mu_{cr} = \lambda_0 \nu_2 + \frac{1}{\lambda_0 \nu_1 + \alpha}$	mon.
	$\lambda_0 < \gamma_3(\alpha)$, $\exists k_0 \in [k_2, k_4] : f_2(k_0) \leq f_2(\lambda_0)$	$\mu_{cr} = \lambda_{k_0} \nu_2 + \frac{1}{\lambda_{k_0} \nu_1 + \alpha}$	mon.
	$\lambda_0 \geq \gamma_3(\alpha)$	$\mu_{cr} = \lambda_0 \nu_2 + \frac{1}{\lambda_0 \nu_1 + \alpha}$	mon.

diffusion system (2.1) *occurs and the critical value of the control parameter* μ *is:*

$$\mu_{cr} = \lambda_{k_0}\nu_2 + \frac{1}{\lambda_{k_0}\nu_1 + \alpha}. \tag{2.35}$$

Here, zero eigenvalue $\sigma = 0$ *of operator* $A_\alpha(\mu_{cr})$ *is simple.*

The following theorem is proved by applying the Liapunov-Schmidt method (Kazarnikov and Revina (2018)):

Theorem 14 *Let us assume that the requirements of lemma 5 are satisfied. Then, there exist* $\mu_{cr} = \lambda_{k_0}\nu_2 + \frac{1}{\lambda_{k_0}\nu_1+\alpha}$ *such that the zero solution to the FitzHugh-Nagumo reaction-diffusion system* (2.1) *is asymptotically stable for* $\mu < \mu_{cr}$*. The soft monotonous instability of the zero solution occurs for At* $\mu = \mu_{cr}$ *and for small values of* $\varepsilon = \sqrt{\mu - \mu_{cr}} > 0$ *there exists a pair of stable stationary solutions to the system. The first terms of a power series expansions of stationary solutions are given by:*

$$\boldsymbol{u} = \pm\varepsilon\boldsymbol{a_1}\cos\left(\frac{\pi k_0 x}{l}\right) \pm \varepsilon^3(\boldsymbol{a_3}\cos\left(\frac{\pi k_0 x}{l}\right) + \boldsymbol{b_3}\cos\left(3\frac{\pi k_0 x}{l}\right)) + O(\varepsilon^4)$$

where the values $\boldsymbol{a_1}$*,* $\boldsymbol{a_3}$ *and* $\boldsymbol{b_3}$ *are found explicitly.*

The following two theorems can be proved by induction:

Theorem 15 *Even components of the power series expansion of stationary solutions are equal to zero: for every* $k \in \mathbb{N}$ $\boldsymbol{u}_{2k} = 0$*.*

Theorem 16 *Vector functions* $\boldsymbol{f}_n(x)$ *on the right-hand side of the equation for finding the* n*-th term of the power series expansion are linear combinations of the basis functions* ψ_k*, where* k *is an odd number satisfying the condition* $k_0 \le k \le nk_0$*.*

The evolution of secondary stationary solutions of the system (2.1) as values of μ grow has been studied numerically. The experiments were carried out for the parameter values $\alpha = 1$, $\nu_1 = 1$, $\nu_2 = 10^{-2}, 10^{-4}, 10^{-5}$, $\mu = \mu_{cr} + \varepsilon^2$. The initial data was set up by the formulas for the first terms of the asymptotics for the secondary stationary solution, the equation (2.1) was approximated by the Method of Lines on the equidistant grid and numerical integration of the ODE system was done using the Dormand-Prince method. It was found that for the values $\varepsilon << 1$ the secondary solutions keep their form. As the values of ε grow, the secondary solutions are replaced by the Turing patterns. When $\varepsilon > 10$ the spatially homogeneous stationary regime is observed in the system.
Function $F(\lambda)$ is a bounded-from-below and monotonically-growing function for $\nu_1 \le \nu_2$. Then, there exists a unique value $\lambda = \lambda_0 = 0 : \mu_{cr} = F(\lambda_0)$. Thus, an oscillatory instability of the zero solution occurs if $\alpha < \alpha_2$ and monotonous instability occurs otherwise. The case $\alpha = \alpha_2$ is a degenerate case. Because $\mu_{cr} = F(\lambda_0)$, the branched-out secondary solutions are spatially homogeneous. Let us consider system (2.1) on subspaces H_k (2.23), defined earlier for the Rayleigh reaction-diffusion system (2.5). Then, theorem 17 holds.

Theorem 17 *Let $x \in (0, l)$ and $\nu_1 \leq \nu_2$. Then, subspaces H_k, $k \in \mathbb{N}$ are invariant with respect to the FitzHugh-Nagumo reaction-diffusion system* (2.1) *with Neumann boundary conditions* (1.2)*.*

By considering linear spectral problem (2.1) for $\boldsymbol{u} \in H_k$, $k \in \mathbb{N}$ we arrive at the countable set of critical values $\mu_{cr}^{(k)}$, for which occurs the branching out of new spatially inhomogeneous oscillatory and stationary regimes on H_k. Let us consider the FitzHugh-Nagumo reaction-diffusion system (2.1) on the invariant subspace H_k for $k \in \mathbb{N}$. By applying the Lyapunov-Schmidt method, the following theorems can be proved:

Theorem 18 *Let us consider the FitzHugh-Nagumo reaction-diffusion system* (2.1) *on the invariant subspace H_k, $k \in \mathbb{N}$ and assume that the condition $\nu_1\lambda_k + \alpha < 1$ is satisfied. Then, there exists $\mu_{cr}^{(k)} = (\nu_1 + \nu_2)\lambda_k + \alpha$ such that the zero solution to the FitzHugh-Nagumo reaction-diffusion system* (2.1) *is asymptotically stable in H_k for $\mu < \mu_{cr}^{(k)}$. The soft oscillatory instability of the zero solution occurs for $\mu = \mu_{cr}^{(k)}$ and for small values of $\varepsilon = \sqrt{\mu - \mu_{cr}^{(k)}} > 0$ there exists a limit cycle of system* (2.1)*, stable in H_k.*

Theorem 19 *Let us consider the FitzHugh-Nagumo reaction-diffusion system* (2.1) *on the invariant subspace H_k, $k \in \mathbb{N}$ and assume that the condition $\nu_1\lambda_k + \alpha > 1$ is satisfied. Then, there exists $\mu_{cr}^{(k)} = \frac{1}{\nu_1\lambda_k+\alpha} + \nu_2\lambda_k$ such that the zero solution to the FitzHugh-Nagumo reaction-diffusion system* (2.1) *is asymptotically stable in H_k for $\mu < \mu_{cr}^{(k)}$. The soft monotonous instability of the zero solution occurs for $\mu = \mu_{cr}^{(k)}$ and for small values of $\varepsilon = \sqrt{\mu - \mu_{cr}^{(k)}} > 0$ there exists a pair of stationary solutions to system* (2.1)*, stable in H_k.*

2.5 Summary

The main results of the thesis (Kazarnikov (2018)) can be summarised as follows:

1. Exact power series representations for spatio-temporal and stationary patterns branching out from the zero solution to the Rayleigh reaction-diffusion system due to monotonous or oscillatory instability were obtained for the case when $\Omega \subset \mathbb{R}^m$, $m = 1, 2, 3$ is a bounded domain with $\partial\Omega \in C^2$ or rectangular parallelepiped supplied with Diriclet or mixed boundary conditions. By constructing an abstract scheme and applying the Liapunov-Schmidt method, formulas for the n-th term of a power series expansions were obtained. The evolution of the branched-out regimes was studied numerically for the special cases of interval and rectangular spatial domains.

2. The bifurcational behaviour of the solutions to the Rayleigh reaction-diffusion system was studied on the infinite-dimensional subspaces of the phase space in the case of one spatial variable and Neumann boundary conditions. It was shown that there exists a countable set of critical values of the control parameter for which the branching out of spatially inhomogeneous stationary and auto-oscillation modes

occurs. The first terms of power series expansions of secondary solutions were found explicitly and the formulas for the n-th term of the power series expansion were analysed. By conducting the numerical experiments, it was found out that the transformation of secondary auto-oscillation modes into stationary regimes occurred as the control parameter value passes away from the threshold of instability.

3. The partial case of the FitzHugh-Nagumo reaction-diffusion system (2.1) was considered in $\Omega \subset \mathbb{R}^m$, $m = 1, 2, 3$, where Ω is a bounded domain with $\partial\Omega \in C^2$ or rectangular parallelepiped for $\varepsilon = 1$ and different diffusion coefficients ν_1 and ν_2. The critical values of the control parameter μ were found, the dependence of instability type on the values of diffusion coefficients ν_1 and ν_2 was studied. For the case of one spatial variable $x \in (0, \ell)$ and Neumann boundary conditions the first terms of power series expansions of spatially inhomogeneous stationary solutions were found explicitly and the evolution of the branched-out solutions was studied numerically.

In (Kazarnikov (2018)), reaction parameter μ played the role of bifurcational parameter. It is naturally possible, however, to apply the same scheme to other model parameters, such as diffusion coefficients. For example, considering $d = \frac{\nu_1}{\nu_2}$ as a varying control parameter allows us to perform the analytical investigation of the branching out of stationary solutions, known as Turing patterns. It should be pointed out that those analytical approaches discussed in the current chapter, can be applied only in the situation when the bifurcational parameter is close to the onset of instability. The analysis of far-from-equilibrium patterns can be carried out analytically as well, by using the techniques of geometric singular perturbation theory. However, parameter identification of the equations under study usually require numerical simulation of the model to be performed. This situation is discussed in the next section.

3 Correlation Integral Likelihood

3.1 Introduction

This section contains general information about Correlation Integral Likelihood and its numerical implementation for parameter identification of reaction-diffusion systems by Turing patterns. CIL can be considered as a method allowing quantification of the "sameness" of patterns that are created by a given pattern formation process. In a more formal sense, the task is to create a statistical likelihood that quantifies the variability of a given data set of patterns. Having CIL allows the identification of the parameters of the model employed. After the identification step, the posterior distribution of the parameters can be constructed by finding "all" parameter values for which the model matches the likelihood function. The likelihood is naturally conditional on data. A large data set provides more accurate information than a limited one.

In the remainder of this section we consider a reaction-diffusion system (1.1) in a squared unit domain $\Omega = (0,1) \times (0,1)$ supplied with homogeneous Neumann (zero-flux) boundary conditions (1.2). We focus on three well-known types of kinetics: the FitzHugh-Nagumo model, the Gierer-Meinhardt activator-inhibitor system, and the Brusselator reaction-diffusion system. For each model, we assume that all parameters are fixed except the pair of varying control parameters. Recall that the FitzHugh-Nagumo model involves the following reaction terms:

$$f(v,w) = \varepsilon(w - \alpha v); \quad g(v,w) = -v + \mu w - w^3, \tag{3.1}$$

where $\mu \in \mathbb{R}$ and $\varepsilon > 0$ are varying control parameters, $\alpha \geq 0$ is the fixed reaction term. The kinetics of the Gierer-Meinhardt activator-inhibitor system are given by equations:

$$f(v,w) = -\mu_v v + \frac{v^2}{w}; \quad g(v,w) = -\mu_w w + v^2, \tag{3.2}$$

where activator and inhibitor decay rates $\mu_v, \mu_w > 0$ are chosen as control parameters. Finally, the Brusselator reaction-diffusion system is given by the following kinetics:

$$f(v,w) = A - (B+1)v + v^2 w; \quad g(v,w) = Bv - v^2 w, \tag{3.3}$$

where constant concentrations of reagents A and B are varying control parameters.

As initial conditions, we take spatially homogeneous steady states (v_0, w_0) of the system (1.1), given by the following condition:

$$f(v_0, w_0) = g(v_0, w_0) = 0, \tag{3.4}$$

perturbed with a small uniform random noise:

$$v(\boldsymbol{x}, 0) = v_0 + U(0, \delta),\ w(\boldsymbol{x}, 0) = w_0 + U(0, \delta),\ \delta < 1,$$

where $U(0,\delta)$ is a uniformly distributed random variable, $(v_0, w_0) = (0,0)$ for model

(3.1), $(v_0, w_0) = (\frac{\mu_w}{\mu_v}, \frac{\mu_w}{\mu_v^2})$ for system (3.2) and $(v_0, w_0) = (A, \frac{B}{A})$ for equations (3.3) respectively.
Turing (1952) discovered that the reaction between two chemicals in system (1.1) with different diffusion rates may cause the destabilisation of the homogeneous steady state (3.4), and lead to the formation of non-homogeneous spatial structures. This mechanism is called the diffusion-driven instability. It has inspired a vast number of mathematical models, providing explanations of symmetry breaking, animal coat markings formation (Murray (1993)), oscillating chemical reactions (Glansdorff and Prigogine (1971a)) and other phenomena. The conditions for Turing bifurcation can be obtained by analysing the linear stability of system (1.1) around the spatially homogeneous steady state (3.4). This analysis was first performed by Turing (1952) for a reaction-diffusion system with linear reaction terms and then extended by Prigogine and Nicolis (1967) to non-linear systems.
For fixed parameters, satisfying diffusion-driven instability conditions, the models (1.1) with kinetics (3.1), (3.2) and (3.3) exhibit the formation of spatially inhomogeneous patterns (Turing patterns). The patterns, observed in numerical simulations, differ for different random initial perturbations of the homogeneous steady state (see Fig. 3.1). These patterns, however, can be considered as belonging to one type with respect to model parameters. At the same time, changes in model parameters naturally affect the final shape, appearance and type of patterns being observed in the system (see Fig. 3.2).

3.2 Finite difference approximation

To project an infinite-dimensional system onto a finite-dimensional system we apply the Method of Lines (MOL). We create the decomposition of domain Ω by equidistant grid with fixed step size $h = 1/(M_{dim} - 1)$, $M_{dim} \in \mathbb{N}$ and arrive at a finite set of points:

$$\{(x_1^i, x_2^j) : \, x_1^i = ih, \, x_2^j = jh, \, i, j = 0, \ldots, M_{dim} - 1\}.$$

Next, the Laplace operator is discretised by the five-point stencil (Grossmann et al. (2007); Hupkes and Van Vleck (2016)):

$$\Delta u \approx \frac{u_{i+1,j} + u_{i-1,j} + u_{i,j+1} + u_{i,j-1} - 4u_{i,j}}{h^2} = \nabla_5^2 u_{i,j},$$

and an infinite-dimensional reaction-diffusion system (1.1) is reduced to a finite set of $2M_{dim}^2$ ordinary differential equations (ODE), which is expressed by the system:

$$\begin{aligned} \dot{v}_{i,j}(t) &= \nu_1 \nabla_5^2 v_{i,j}(t) + f(v_{i,j}(t), w_{i,j}(t)), \\ \dot{w}_{i,j}(t) &= \nu_2 \nabla_5^2 w_{i,j}(t) + g(v_{i,j}(t), w_{i,j}(t)), \end{aligned} \tag{3.5}$$

where $i, j = 0, 1, \ldots, M_{dim} - 1$ and Neumann boundary conditions are taken into account by applying a central difference scheme (Grossmann et al. (2007)). In all numerical experiments we use $M_{dim} = 64$ (with the exception of a sparse grid case with $M_{dim} = 32$, which is discussed in Sec. 4.3).
When the control parameters of a reaction-diffusion model are fixed and belong to Turing

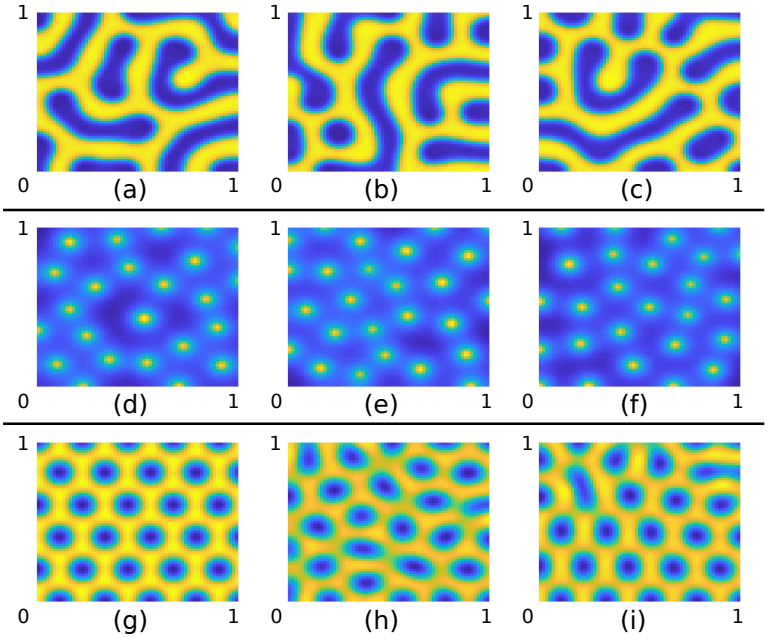

Figure 3.1: Turing patterns obtained from direct simulations with fixed parameter values and different initial conditions, taken as small random perturbations of the homogeneous steady state: (a)-(c) labyrinthine-type patterns (variable w) in the FitzHugh-Nagumo model ($\nu_1 = 0.05$, $\nu_2 = 0.00028$, $\alpha = 1$, $\varepsilon = 10$, $\mu = 1$), (d)-(f) isolated spot peaks (variable w) in the Gierer-Meinhardt system ($\nu_1 = 0.00025$, $\nu_2 = 0.01$, $\mu_v = 0.5$, $\mu_w = 1$) and (g)-(i) hexagons (variable v) in the Brusselator reaction diffusion-system ($\nu_1 = 0.0016$, $\nu_2 = 0.0131$, $A = 4.5$, $B = 6.96$).

domain, patterns are obtained from numerical simulations as steady states of the MOL ODE system (3.5). Perturbations of initial conditions result in convergence of numerical solution to different steady states.

3.3 Correlation Integral Likelihood

In this section we recall the distance concept introduced by Haario et al. (2015) for chaotic dynamical systems, and adapt its use to quantify pattern formation in reaction-diffusion systems. Individual trajectories of chaotic systems are unpredictable with respect to small perturbations of initial values. Turing patterns are stationary solutions of the reaction-diffusion system and naturally depend on the initial state. In most real experimental situations the initial values cannot be assumed to be exactly known, so this rules out the use of usual likelihood functions for parameter estimation, based on residuals between model and data. Instead, we create a likelihood that characterises a family of solutions, given either by real data or, as in the examples here, by model simulations.

The general idea of the approach is as follows. We assume to have a training set of data

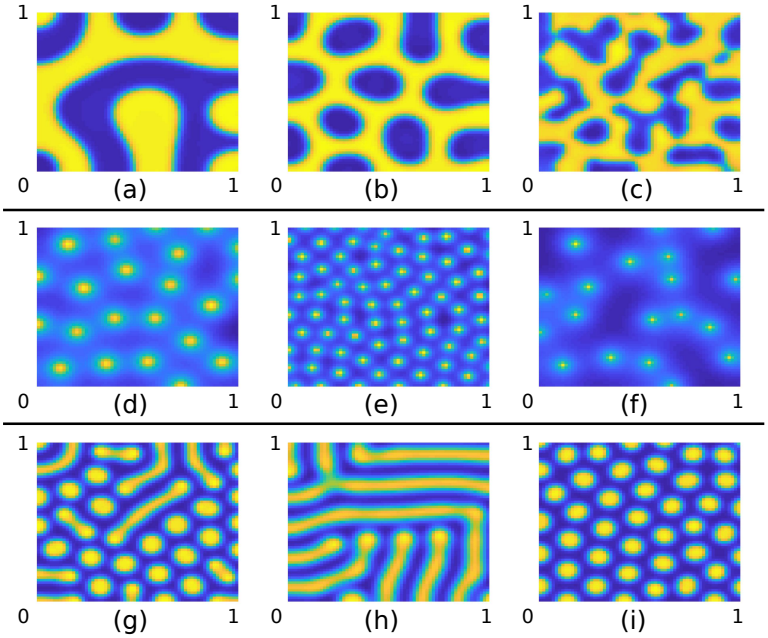

Figure 3.2: Turing patterns obtained from direct simulations with different parameter values and fixed initial conditions. Diffusion coefficients and plotted system variables are the same as in Fig. 3.1. The FitzHugh-Nagumo model: (a) $\alpha = 1$, $\varepsilon = 1, \mu = 1$, (b) $\alpha = 1.25$, $\varepsilon = 5.5$, $\mu = 1$, (c) $\alpha = 1.02$, $\varepsilon = 6.45$, $\mu = 1.8$. The Gierer-Meinhardt system: (d) $\mu_v = 0.35$, $\mu_w = 1.0$, (e) $\mu_v = 0.75$, $\mu_w = 4.0$, (f) $\mu_v = 1.0$, $\mu_w = 0.75$. The Brusselator reaction-diffusion system: (g) $A = 5$, $B = 13$, (h) $A = 4.5$, $B = 8.72$, (i) $A = 4.5$, $B = 13.29$.

consisting of an ensemble of n_{ens} subsets, each consisting of N vectors. For any given ensemble pair we compute the N^2 distances between all their vectors, and construct the empirical cumulative distribution function (eCDF, see, e.g., van der Vaart (1998)) of the distances. It turns out that these eCDF vectors are normally distributed. To empirically estimate the distribution, the eCDF vectors are computed between all the $n_{ens}(n_{ens}-1)/2$ pairs of the ensemble subsets. The mean and covariance of the ensuing set of eCDF vectors can then be calculated. So we arrive at a Gaussian likelihood for the 'feature vector', the eCDF of distances between vectors from two data sets of length N.

The original motivation for such a likelihood construction comes from the literature on fractal dimensions. We briefly recall this background of the method, and proceed then to the modifications needed when applying the approach to Turing type patterns.

Consider a chaotic ODE system, defined by the following equation:

$$\frac{d\boldsymbol{s}}{dt} = \boldsymbol{F}(\boldsymbol{s}, \boldsymbol{\theta}),\ \boldsymbol{s}(t)|_{t=0} = \boldsymbol{x}, \tag{3.6}$$

where $\boldsymbol{s} \in \mathbb{R}^n$ is a system state, $\boldsymbol{x}$ is a vector of initial conditions and $\boldsymbol{\theta} \in \mathbb{R}^d$ is a

parameter vector. Such systems (for example, the classical Lorenz system) are highly sensitive to initial conditions and model parameters; small changes in these values lead to widely diverging trajectories, which makes long-term predictions impossible in general. Haario et al. (2015) deal with the following question: how can a practically computable distance concept for chaotic trajectories be defined; i.e. how can the distribution of model parameters be defined for which the variability due to the differences in parameter values is indistinguishable from the chaotic variability of the system, as quantified by a given amount of training data?

The distance concept is based on the notion of correlation integral vector. In the following, we use the notation $\boldsymbol{s} = \boldsymbol{s}(\boldsymbol{\theta}, \boldsymbol{x}, t)$ for a trajectory $\boldsymbol{s}$ of chaotic system (3.6) that depends on a model parameter vector $\boldsymbol{\theta}$, input values $\boldsymbol{x}$ and time t. Generally, $\boldsymbol{x}$ may include any variables whose small changes lead to chaotic unpredictability, e.g., the tolerances of the numerical solver. In the current paper, however, we denote the initial values of an ODE system by $\boldsymbol{x}$ only.

Denoted by $\boldsymbol{s_i} \in \mathbb{R}^n$, $i = 1, 2, \ldots, N$ the points of the trajectory $\boldsymbol{s} = \boldsymbol{s}(\boldsymbol{\theta}, \boldsymbol{x}, t)$, evaluated for consecutive time points $t = t_i$. For a fixed $R > 0$ set

$$C(R, N) = \frac{1}{N^2} \sum_{1 \le i,j \le N} \#(||\boldsymbol{s}_i - \boldsymbol{s}_j|| < R).$$

Above, $||.||$ denotes the Euclidean distance. So $C(R, N)$ gives the fraction of pairs of points with a distance less than R. As the radius R tends to zero, $C(R, N) \sim R^\gamma$, where γ is the classical *correlation dimension*, given by the formula (see Cencini et al. (2009)):

$$\gamma = \lim_{R \to 0} \frac{\log C(R, N)}{\log R}. \tag{3.7}$$

We are, however, not interested in the intrinsic fractal dimension of a given trajectory as given by the limit $R \to 0$, but want to characterise the distance between different trajectories, using all relevant scales R.

Suppose we have an ensemble of different trajectories $\boldsymbol{s}^k = \boldsymbol{s}^k(\boldsymbol{\theta}, \boldsymbol{x})$, $k = 1, ..., n_{ens}$, each evaluated at time points t_i, $i = 1, ..., N$. For fixed $R > 0$ and k, l set:

$$C(R, N, \boldsymbol{s}^k, \boldsymbol{s}^l) = \frac{1}{N^2} \sum_{1 \le i,j \le N} \#(||\boldsymbol{s}_i^k - \boldsymbol{s}_j^l|| < R). \tag{3.8}$$

We assume furthermore that the state $\boldsymbol{s}$ remains bounded, and all the trajectory vectors $\boldsymbol{s}_i^k$ are samples from the same underlying fixed attractor (i.e., they are measurements given by a stationary time series, or obtained by integrating a fixed chaotic system with perturbed initial values x). Choose $R_0 > 0$ such that $||\boldsymbol{s}_i^k - \boldsymbol{s}_j^l|| < R_0$ for all $k, l = 1, ..., n_{ens}$, $i, j = 1, \ldots, N$. For a given integer M, the *generalised correlation integral vector* $\boldsymbol{y^{k,l}}$ of the pair $\boldsymbol{s}^k, \boldsymbol{s}^l$ is given by the components:

$$y_m^{k,l} = C(R_m, N, \boldsymbol{s}^k, \boldsymbol{s}^l),\ m = 1, 2, \ldots, M, \tag{3.9}$$

where $R_m = b^{-m}R_0$ with $b > 1$ (for the numerical evaluations we follow the usual settings found in literature (Cencini et al. (2009), see also the examples below).
The correlation integral vector $\boldsymbol{y}$ is stochastic, as the evaluations are done by randomised initial conditions $\boldsymbol{x}$. It turns out that the distribution of the correlation integral vector is Gaussian. Intuitively, as the expression (3.8) consists of averages, the Central Limit Theorem might be expected to hold. More exactly, the expression $\boldsymbol{y} = (y_m)_{m=1}^M$ defines the empirical cumulative distribution function of the respective set of distances, evaluated at bin values R_m. The basic form of Donsker's theorem states that empirical cumulative distribution functions of i.i.d scalar random numbers asymptotically tend to a Brownian bridge (Donsker (1951, 1952)). In more general settings that cover our situation, the Gaussianity is established by theorems of the so-called U-statistics; see Borovkova et al. (2001); Neumeyer (2004). In Borovkova et al. (2001), especially, the Gaussianity of the numerical construction used to estimate the correlation dimension (3.7) of the classical Lorenz attractor is discussed.
The *Correlation Integral Likelihood (CIL)* is defined as the Gaussian distribution $N(\boldsymbol{\mu}_0, \boldsymbol{\Sigma}_0)$, where $\boldsymbol{\mu}_0$ and $\boldsymbol{\Sigma}_0$ are the mean and covariance of the vector $\boldsymbol{y}$. Numerically, $\boldsymbol{\mu}_0$ and $\boldsymbol{\Sigma}_0$ are estimated as discussed in the beginning of this section using the vectors (3.9) given by the training set using all the pairs $k, l = 1, 2, ..., n_{ens}$.
In this paper we use the generalised correlation integral in order to create a statistical distribution that quantifies the variability of Turing patterns within a given reaction-diffusion system (1.1). Certain modifications to the approach in Haario et al. (2015) are necessary. First, by applying the Method of Lines we reduce an infinite-dimensional reaction-diffusion system (1.1) to a finite ODE system (3.5), which makes it possible to apply the CIL concept.
Next, we modify the concept of trajectory $\boldsymbol{s} = \boldsymbol{s}(\boldsymbol{\theta}, \boldsymbol{x})$. In Haario et al. (2015), the samples $\boldsymbol{s}_i$ are vectors from a numerically computed trajectory $\boldsymbol{s}$, evaluated at time points t_i. So in the case of chaotic ODE system, they actually are samples from the global chaotic attractor in the phase space. In the case of the reaction-diffusion system (1.1), when model parameters belong to a pure Turing domain, numerical simulations converge to stable stationary states. These stationary states belong to a global attracting set of the system considered. Therefore, we choose inhomogeneous steady states of the reaction-diffusion systems to be the samples $\boldsymbol{s}_i$. Each ensemble of N patterns is obtained by solving the equation (1.1) N times with a fixed model parameter vector $\boldsymbol{\theta}$ but randomised initial values $\boldsymbol{x}$.
Finally, we choose the distance appropriately. For $\boldsymbol{s}_i$, $\boldsymbol{s}_j$ we define the distance by L_2-norm formula:

$$||\boldsymbol{s}_i - \boldsymbol{s}_j||^2 = \int_\Omega [(v_i - v_j)^2 + (w_i - w_j)^2] dx_1 dx_2.$$

In numerical experiments this integral is approximated by the trapezoidal rule.
Numerically, the mean and covariance of the Gaussian distribution of the correlation integral vector $\boldsymbol{y}$ can be empirically estimated by an ensemble of vectors $\boldsymbol{y}^l$, $l = 1, ..., n_{ens}$. After this we can employ the usual MCMC (Markov Chain Monte Carlo) sampling methods to find out the distribution of model parameters for which the variability due to the

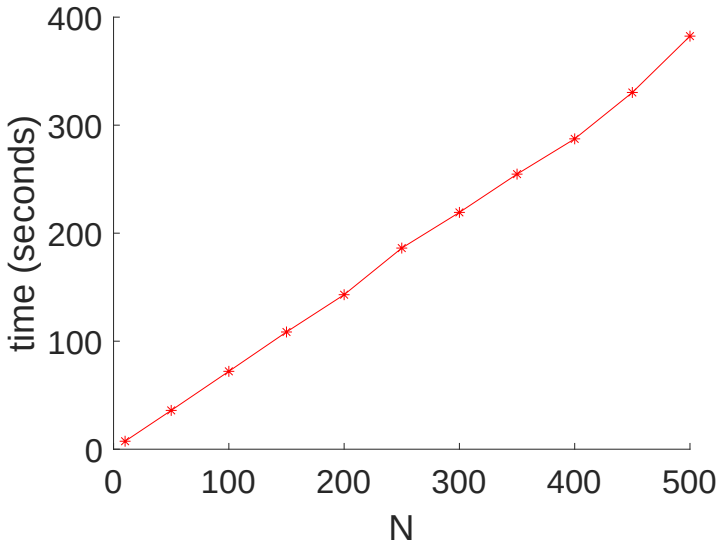

Figure 3.3: Time taken by consecutive integration of N MOL systems (3.5) by the explicit Runge-Kutta method "RK4" in C++ (host code) for the case of sparse spatial grid (32×32 nodes).

differences in parameter values is indistinguishable from the variability of the training set. Equally well, a given set of empirical data, such as patterns in the present case, can be used to construct the likelihood, which enables the identification of unknown model parameters.

Numerical experiments are discussed in detail in Section 4. The code was written in MATLAB language, while the most time-consuming parts were implemented in C++/CUDA and integrated into MATLAB via MEX interface. For running the MCMC sampling methods the MCMC toolbox for MATLAB was used (see Haario et al. (2006) for details). The rest of the current section is devoted to the details of numerical implementation of the CIL approach.

3.4 Numerical implementation of the approach

The construction of a parameter posterior distribution using the Metropolis-Hastings algorithm requires a long enough MCMC chain to be computed. In general situations, one chain contains at least 4000 elements. Evaluating one element of the chain requires computing N repeated solutions of the underlying reaction-diffusion model (1.1). In the experiments, discussed in current thesis, $N \leq 500$ (see Section 4). As a result, computing one MCMC chain in the most difficult case $N = 500$ requires approximately $500 \times 4000 = 2 \times 10^6$ model integrations.

Implementing an efficient algorithm for a numerical solution of the equations under study is crucial for the successful use of the CIL algorithm. As a result, some commonly

used approaches cannot be applied to this problem. For example, the numerical integration of the MOL system (3.5) in MATLAB (`ode45` routine, Dormand-Prince method, sparse spatial grid) requires approximately 13.43 seconds. Hereinafter we consider the FitzHugh-Nagumo model (3.1) as an example, because integrating other equations under study (3.2) and (3.3) takes approximately the same time. Therefore, time taken by computation of one MCMC chain will require around 310 days, which is not acceptable for any practical applications.

It should be pointed out that interpreted code (such as MATLAB code) is usually slower than compiled code. It is possible to increase the performance of numerical integration by implementing the algorithms in some compiled language (like C++ or Fortran) and then accessing the corresponding routines from MATLAB via MEX API. This results in a significant performance increase: one numerical integration of the MOL system (3.5) performed with C++ implementation of the Runge-Kutta method ("RK4") takes approximately 0.8 seconds (which is 37 times faster than in MATLAB). In this case, however, the computational time for one chain will be approximately 18 days, which is still not enough for the effective use of the CIL approach. In addition, Central Processing Unit (CPU) is most effective while working with a moderate amount of parallel threads; therefore it is not possible to effectively perform the parallel integration of several systems. As a result, the computation time grows linearly with the number of independent simulations N (see Fig. 3.3).

In this situation one solution is to employ several computers, organised in a cluster (for example, it was succesfully performed by Campillo-Funollet et al. (2019)) by using Message Passing Interface (MPI). Another approach is conducting the computations on Graphics Processing Units (GPUs), which allow an efficient computation of a large number of solutions in parallel. Model simulations, required for computing MCMC chains, are done with the same values of model parameters and similar values of initial data, taken as small perturbations of the homogeneous steady state (3.4). As a result, these simulations can be effectively batched and executed on GPU. This enables a significant improvement in performance, making the proposed approach more suitable for numerical applications. In addition, it is possible to run all the computations by using only one machine equipped with a suitable GPU device.

3.5 General overview of CUDA

Modern GPUs are very effective at processing a large number of independent tasks in parallel if each single task is relatively simple. CUDA (Compute Unified Device Architecture) is a parallel computing platform and application programming interface (API) developed by Nvidia. The platform makes it possible to use GPU devices for general processing computing, usually termed GPGPU (General-Purpose computing on Graphics Processing Units). The CUDA platform allows the programmer to access the GPU instruction set and execute kernels, which are subroutines, designated to run on GPU and scheduled for execution from the host side. Kernel code may be written using the CUDA dialect of C++ or Fortran languages and compiled using the specialised Nvidia compiler NVCC. It is possible, however, to work with CUDA from other programming languages

as well, by using third-party wrapper libraries, such as PyCUDA.
In the CUDA programming model, each computational task (represented as kernel) is executed multiple times in parallel by different CUDA threads, which may be considered as normal CPU threads with much lighter context. All CUDA threads are grouped into blocks and blocks are packed into a grid. Grids and blocks can be defined as one-dimensional, two-dimensional or three-dimensional arrays. Each block can be considered as a Single Instruction Multiple Thread (SIMT) machine. Not all threads in the block, however, are necessarily executed in parallel. The subset of threads, which is executed physically in parallel, is called a warp. On modern machines one warp always contains 32 threads and the maximum number of threads per block is usually equal to 1024.
The NVIDIA GPU architecture is built around a scalable array of multithreaded streaming multiprocessors (SM). When the host invokes a kernel, the blocks of the kernel grid are enumerated and distributed to available multiprocessors. The threads of each block execute concurrently on one multiprocessor, and multiple thread blocks can execute concurrently on one multiprocessor. As thread blocks terminate, new blocks are launched on the vacated multiprocessors. The multiprocessor creates, manages, schedules and executes threads in groups of 32 parallel threads (warps). Individual threads composing a warp start together at the same program address, but they have their own instruction address counter and register state and are therefore free to branch and execute independently.
When a multiprocessor is given one or more thread blocks to execute, it partitions them into warps and each warp gets scheduled by a warp scheduler for execution. The way a block is partitioned into warps is always the same. A warp executes one common instruction at a time, so full efficiency is realised when all 32 threads of a warp agree on their execution path. If threads of a warp diverge via a data-dependent conditional branch, the warp executes each branch path taken, disabling threads that are not on that path. Branch divergence occurs only within a warp; different warps execute independently regardless of whether they are executing common or disjoint code paths.
The execution context (program counters, registers, etc.) for each warp processed by a multiprocessor is maintained on-chip during the entire lifetime of the warp. Therefore, switching from one execution context to another incurs no cost, and at every instruction issue time, a warp scheduler selects a warp that has threads ready to execute its next instruction (the active threads of the warp) and issues the instruction to those threads. Each multiprocessor has a set of 32-bit registers that are partitioned among the warps, and a parallel L1/L2 data cache (called shared memory, usually 96 KB) that is partitioned among the thread blocks.

3.6 Implementation of the numerical algorithms

In general, modern libraries for numerical solutions of ODEs (for example SUNDIALS suite or ODEINT library) support GPGPU computing. This functionality is either embedded into the library from the beginning or can be added to existing numerical solvers by providing new used-defined data structures. This approach allows the incorporation of required GPGPU functionality into the existing code. However, library architecture suited

Algorithm 1: Computing the numerical solution of the MOL system (3.5) for the case of sparse spatial grid

Input : $\boldsymbol{w}_0$, batch of N arrays containing initial data with 2048 elements in each (global memory)
Input : T, time interval length (scalar)
Input : dt, time integration step (scalar)
Input : $\boldsymbol{s}$, batch of N temporary arrays with 2048 elements in each (shared memory)
Input : $\boldsymbol{z}$, batch of N temporary arrays with 2048 elements in each (shared memory)
Output: $\boldsymbol{w}_T$, batch of N arrays containing computed patterns with 2048 elements in each (global memory)

begin
- $\boldsymbol{s} \leftarrow \boldsymbol{w}_0$
- __syncthreads()
- $\mathrm{N}_{dim} \leftarrow 1024$, $\mathrm{n}_0 \leftarrow$ `blockIdx.x`, $\mathrm{k} =$ `threadIdx.x`
- **for** $(t = 0; t \leq T; t+ = dt)$ **do**
  - $dv = 0, dw = 0$
  - $\boldsymbol{z}_{n_0}[k] \leftarrow \nabla_5^2 \boldsymbol{s}_{n_0}[k] + f(\boldsymbol{s}_{n_0}[k], \boldsymbol{s}_{n_0}[k + N_{dim}])$
  - $\boldsymbol{z}_{n_0}[k + N_{dim}] \leftarrow \nabla_5^2 \boldsymbol{s}_{n_0}[k + N_{dim}] + g(\boldsymbol{s}_{n_0}[k], \boldsymbol{s}_{n_0}[k + N_{dim}])$
  - __syncthreads()
  - $du+ = (1/6) * \boldsymbol{z}_{n_0}[k], dv+ = (1/6) * \boldsymbol{z}_{n_0}[k + N_{dim}]$
  - $\boldsymbol{z}_{n_0}[k] \leftarrow \boldsymbol{s}_{n_0}[k] + (1/2) * dt * \boldsymbol{z}_{n_0}[k]$
  - $\boldsymbol{z}_{n_0}[k + N_{dim}] \leftarrow \boldsymbol{s}_{n_0}[k + N_{dim}] + (1/2) * dt * \boldsymbol{z}_{n_0}[k + N_{dim}]$
  - __syncthreads()
  - $\boldsymbol{z}_{n_0}[k] \leftarrow \nabla_5^2 \boldsymbol{z}_{n_0}[k] + f(\boldsymbol{z}_{n_0}[k], \boldsymbol{z}_{n_0}[k + N_{dim}])$
  - $\boldsymbol{z}_{n_0}[k + N_{dim}] \leftarrow \nabla_5^2 \boldsymbol{z}_{n_0}[k + N_{dim}] + g(\boldsymbol{z}_{n_0}[k], \boldsymbol{z}_{n_0}[k + N_{dim}])$
  - __syncthreads()
  - $du+ = (1/3) * \boldsymbol{z}_{n_0}[k], dv+ = (1/3) * \boldsymbol{z}_{n_0}[k + N_{dim}]$
  - $\boldsymbol{z}_{n_0}[k] \leftarrow \boldsymbol{s}_{n_0}[k] + (1/2) * dt * \boldsymbol{z}_{n_0}[k]$
  - $\boldsymbol{z}_{n_0}[k + N_{dim}] \leftarrow \boldsymbol{s}_{n_0}[k + N_{dim}] + (1/2) * dt * \boldsymbol{z}_{n_0}[k + N_{dim}]$
  - __syncthreads()
  - $\boldsymbol{z}_{n_0}[k] \leftarrow \nabla_5^2 \boldsymbol{z}_{n_0}[k] + f(\boldsymbol{z}_{n_0}[k], \boldsymbol{z}_{n_0}[k + N_{dim}])$
  - $\boldsymbol{z}_{n_0}[k + N_{dim}] \leftarrow \nabla_5^2 \boldsymbol{z}_{n_0}[k + N_{dim}] + g(\boldsymbol{z}_{n_0}[k], \boldsymbol{z}_{n_0}[k + N_{dim}])$
  - __syncthreads()
  - $du+ = (1/3) * \boldsymbol{z}_{n_0}[k], dv+ = (1/3) * \boldsymbol{z}_{n_0}[k + N_{dim}]$
  - $\boldsymbol{z}_{n_0}[k] \leftarrow \boldsymbol{s}_{n_0}[k] + dt * \boldsymbol{z}_{n_0}[k]$
  - $\boldsymbol{z}_{n_0}[k + N_{dim}] \leftarrow \boldsymbol{s}_{n_0}[k + N_{dim}] + dt * \boldsymbol{z}_{n_0}[k + N_{dim}]$
  - __syncthreads()
  - $\boldsymbol{z}_{n_0}[k] \leftarrow \nabla_5^2 \boldsymbol{z}_{n_0}[k] + f(\boldsymbol{z}_{n_0}[k], \boldsymbol{z}_{n_0}[k + N_{dim}])$
  - $\boldsymbol{z}_{n_0}[k + N_{dim}] \leftarrow \nabla_5^2 \boldsymbol{z}_{n_0}[k + N_{dim}] + g(\boldsymbol{z}_{n_0}[k], \boldsymbol{z}_{n_0}[k + N_{dim}])$
  - __syncthreads()
  - $du+ = (1/6) * \boldsymbol{z}_{n_0}[k], dv+ = (1/6) * \boldsymbol{z}_{n_0}[k + N_{dim}]$
  - $\boldsymbol{s}_{n_0}[k]+ = dt * du$
  - $\boldsymbol{s}_{n_0}[k + N_{dim}]+ = dt * dv$
  - __syncthreads()
- $\boldsymbol{w}_0 \leftarrow \boldsymbol{s}$

Algorithm 2: Computing the numerical solution of the MOL system (3.5) for the case of dense spatial grid

Input : $\boldsymbol{w}_0$, batch of N arrays containing initial data with 8192 elements in each (global memory)
Input : T, time interval length (scalar)
Input : dt, time integration step (scalar)
Input : $\boldsymbol{s}$, batch of N temporary arrays with 8192 elements in each (shared memory)
Input : $\boldsymbol{z}$, batch of N temporary arrays with 8192 elements in each (shared memory)
Output: $\boldsymbol{w}_T$, batch of N arrays containing computed patterns with 8192 elements in each (global memory)

begin
- $\boldsymbol{s} \leftarrow \boldsymbol{w}_0$
- __syncthreads()
- $\mathrm{N}_{dim} \leftarrow 4096$, $\mathrm{n}_0 \leftarrow$ `blockIdx.x`, $\mathrm{k}_0 =$ `threadIdx.x`
- **for** $(t = 0; t \leq T; t+ = dt)$ **do**
  - **for** $k \in [k_0, k_0 + 1024, k_0 + 2048, k_0 + 3072]$ **do**
    - $dv = 0, dw = 0$
    - $\boldsymbol{z}_{n_0}[k] \leftarrow \nabla_5^2 \boldsymbol{s}_{n_0}[k] + f(\boldsymbol{s}_{n_0}[k], \boldsymbol{s}_{n_0}[k + N_{dim}])$
    - $\boldsymbol{z}_{n_0}[k + N_{dim}] \leftarrow \nabla_5^2 \boldsymbol{s}_{n_0}[k + N_{dim}] + g(\boldsymbol{s}_{n_0}[k], \boldsymbol{s}_{n_0}[k + N_{dim}])$
    - __syncthreads()
    - $du+ = (1/6) * \boldsymbol{z}_{n_0}[k], dv+ = (1/6) * \boldsymbol{z}_{n_0}[k + N_{dim}]$
    - $\boldsymbol{z}_{n_0}[k] \leftarrow \boldsymbol{s}_{n_0}[k] + (1/2) * dt * \boldsymbol{z}_{n_0}[k]$
    - $\boldsymbol{z}_{n_0}[k + N_{dim}] \leftarrow \boldsymbol{s}_{n_0}[k + N_{dim}] + (1/2) * dt * \boldsymbol{z}_{n_0}[k + N_{dim}]$
    - __syncthreads()
    - $\boldsymbol{z}_{n_0}[k] \leftarrow \nabla_5^2 \boldsymbol{z}_{n_0}[k] + f(\boldsymbol{z}_{n_0}[k], \boldsymbol{z}_{n_0}[k + N_{dim}])$
    - $\boldsymbol{z}_{n_0}[k + N_{dim}] \leftarrow \nabla_5^2 \boldsymbol{z}_{n_0}[k + N_{dim}] + g(\boldsymbol{z}_{n_0}[k], \boldsymbol{z}_{n_0}[k + N_{dim}])$
    - __syncthreads()
    - $du+ = (1/3) * \boldsymbol{z}_{n_0}[k], dv+ = (1/3) * \boldsymbol{z}_{n_0}[k + N_{dim}]$
    - $\boldsymbol{z}_{n_0}[k] \leftarrow \boldsymbol{s}_{n_0}[k] + (1/2) * dt * \boldsymbol{z}_{n_0}[k]$
    - $\boldsymbol{z}_{n_0}[k + N_{dim}] \leftarrow \boldsymbol{s}_{n_0}[k + N_{dim}] + (1/2) * dt * \boldsymbol{z}_{n_0}[k + N_{dim}]$
    - __syncthreads()
    - $\boldsymbol{z}_{n_0}[k] \leftarrow \nabla_5^2 \boldsymbol{z}_{n_0}[k] + f(\boldsymbol{z}_{n_0}[k], \boldsymbol{z}_{n_0}[k + N_{dim}])$
    - $\boldsymbol{z}_{n_0}[k + N_{dim}] \leftarrow \nabla_5^2 \boldsymbol{z}_{n_0}[k + N_{dim}] + g(\boldsymbol{z}_{n_0}[k], \boldsymbol{z}_{n_0}[k + N_{dim}])$
    - __syncthreads()
    - $du+ = (1/3) * \boldsymbol{z}_{n_0}[k], dv+ = (1/3) * \boldsymbol{z}_{n_0}[k + N_{dim}]$
    - $\boldsymbol{z}_{n_0}[k] \leftarrow \boldsymbol{s}_{n_0}[k] + dt * \boldsymbol{z}_{n_0}[k]$
    - $\boldsymbol{z}_{n_0}[k + N_{dim}] \leftarrow \boldsymbol{s}_{n_0}[k + N_{dim}] + dt * \boldsymbol{z}_{n_0}[k + N_{dim}]$
    - __syncthreads()
    - $\boldsymbol{z}_{n_0}[k] \leftarrow \nabla_5^2 \boldsymbol{z}_{n_0}[k] + f(\boldsymbol{z}_{n_0}[k], \boldsymbol{z}_{n_0}[k + N_{dim}])$
    - $\boldsymbol{z}_{n_0}[k + N_{dim}] \leftarrow \nabla_5^2 \boldsymbol{z}_{n_0}[k + N_{dim}] + g(\boldsymbol{z}_{n_0}[k], \boldsymbol{z}_{n_0}[k + N_{dim}])$
    - __syncthreads()
    - $du+ = (1/6) * \boldsymbol{z}_{n_0}[k], dv+ = (1/6) * \boldsymbol{z}_{n_0}[k + N_{dim}]$
    - $\boldsymbol{s}_{n_0}[k]+ = dt * du$
    - $\boldsymbol{s}_{n_0}[k + N_{dim}]+ = dt * dv$
    - __syncthreads()
- $\boldsymbol{w}_0 \leftarrow \boldsymbol{s}$

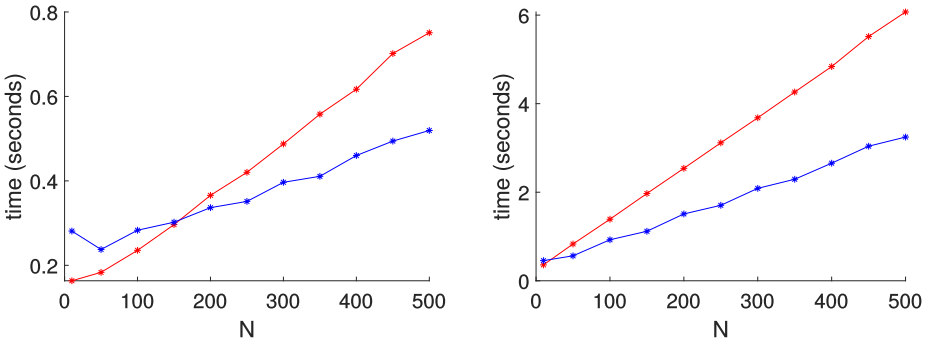

(a) (b)

Figure 3.4: Time taken by batched integration of N MOL systems (3.5) by the explicit Runge-Kutta method "RK4" for the case of sparse spatial grid (a) and dense spatial grid (b). Red line: Nvidia GTX 980 (one device), blue line: Nvidia GTX 980 SLI (two devices)

for a wide range of problems necessarily introduces an overhead, as a result sometimes significantly limiting the performance of available device for a specific problem. In addition, it limits the possibility of employing the shared memory, available in Nvidia devices, which could significantly increase the performance for such moderate-sized problems, which are discussed in the current work.

Taking all these considerations into account, the algorithm for computing the numerical solution of the MOL system (3.5) was implemented from scratch on C++/CUDA. The system was integrated with the classic Runge-Kutta method "RK4" (see Butcher (1987)). All computations were conducted in a single kernel call using the shared memory of the device to handle the intermediate data for computations. There are two separate implementations for the sparse spatial grid (32×32 nodes) and dense spatial grid (64×64 nodes), which result from the hardware limitations. In the sparse spatial grid case, the spatial resolution is equal to 1024 nodes, which is at the same time the maximal allowed number of threads in one CUDA block. In this case each block processes one simulation, which means that each thread of the block computes both components of the solution for a single pixel (see Algorithm 1). In the case of a dense spatial grid, one thread processes four spatial nodes (see Algorithm 2), which lowers the parallelism level, but at the same time it allows us to keep the computations in the shared memory of the device, thus enabling the achievement of a significant impact for memory reading and writing operations.

Implementing the numerics in CUDA allowed us to lower the time taken by integrating 500 independent systems to 0.78 seconds in the case of a sparse spatial grid and to 6.14 seconds in the case of a dense spatial grid. As a result, computing one MCMC chain takes approximately 50 minutes and 7 hours respectively. This performance level is reached by employing the hardware-level efficiency of GPU to perform batched computations. In addition, the code can be trivially parallelised between multiple devices. If the number of

simulations N is large enough, this results in a linear increase in performance, see Fig. 3.4.
In all numerical examples considered in the current work (see the next section), the numerical solution was computed in the time interval $[0, 100]$. Following the idea, proposed in Campillo-Funollet et al. (2019), the time derivative of the solution was evaluated at final time point $T = 100$ by a finite difference scheme. It was checked that for the chosen time interval the L_2-norm of the time derivative was less than $\delta = 10^{-3}$ for all the systems considered. This value was relatively small compared to the values observed during the transient process; therefore it was assumed that the steady state was reached. For several randomly chosen values of control parameters used in numerical experiments, the system was also integrated on the interval $[0, 2T]$ to verify that the difference between the solutions at both times was less than δ.

3.7 Summary

Correlation Integral Likelihood allows for a statistically sound way to determine if a given set of patterns belongs to the same family of patterns as the training data. The Gaussian likelihood can be used as a cost function for parameter identification, which can be done by the methods of statistical optimisation. MCMC sampling methods can be applied to determine the distribution of those parameters of a reaction-diffusion system that produce patterns similar to data.
The construction of a parameter posterior distribution by the Metropolis-Hastings algorithm requires a long enough MCMC chain to be computed. Moreover, the evaluation of the cost function based on the correlation integral vector requires repeated solutions of the underlying model. Running the simulations on GPU allows for an efficient computation of a large number of solutions in parallel. The code for numerical simulations was built using the Nvidia CUDA parallel computing platform. This enables a significant improvement in performance, making the proposed approach more suitable for numerical applications.
The MATLAB/C++ code, which was used for all numerical simulations discussed here, is publicly available on GitHub. Please see the link:
https://github.com/AlexeyKazarnikov/CILNumericalCode

4 Numerical experiments

4.1 Introduction

In this section we study the performance of the CIL approach, which was introduced in the previous section. First, the accuracy is considered. That is, we analyse how well the model parameters are identified by a given training data. We create synthetic training data using a known model parameter vector $\boldsymbol{\theta_0}$ and create the CIL likelihood as described in Section 3. Next, we employ MCMC (Markov Chain Monte Carlo) sampling methods to find out the posterior distribution of model parameters determined by the likelihood. We begin with large data sets and next consider a limited data case. Finally, we demonstrate parameter estimation, i.e. convergence of the method when starting with initial parameter values far away from the correct one. This leads to minimising of a stochastic cost function, solved by an evolutionary optimisation algorithm.

4.2 Numerical construction of the CIL likelihood

For simplicity, we consider only two parameters to be estimated for each equation system, grouped in a vector $\boldsymbol{\theta}$. All other model parameters are fixed, see Table 4.1 for the values. Denote the given "correct" values of the estimated parameters by $\boldsymbol{\theta_0}$. Typical Turing patterns obtained for the chosen parameter values are shown in Fig. 3.1. Where possible, we verified that the patterns we obtained for $\boldsymbol{\theta} = \boldsymbol{\theta_0}$ are similar to those obtained by other authors and available in literature (see Painter et al. (2012) for the case of the Gierer-Meinhardt system (3.2) and Peña and Pérez-García (2001) for the case of the Brusselator reaction-diffusion system (3.3)).
We start by constructing an empirical approximation for the likelihood of the correlation

Table 4.1: Parameter values used for creating the training set for statistics of generalised correlation integral vector $\boldsymbol{y}(\boldsymbol{x}, \boldsymbol{\theta_0})$. FHN, GM and BRS mean the FitzHugh-Nagumo model, Gierer-Meinhardt system and Brusselator reaction-diffusion system respectively.

Parameter	FHN	GM	BRS
$\boldsymbol{\theta}$	(μ, ε)	(μ_v, μ_w)	(A, B)
$\boldsymbol{\theta_0}$	$(1, 10)$	$(0.5, 1)$	$(4.5, 6.96)$
	$\nu_1 = 0.05$,	$\nu_1 = 0.00025$,	$\nu_1 = 0.0016$
	$\nu_2 = 0.00028$,	$\nu_2 = 0.01$	$\nu_2 = 0.0132$
	$\alpha = 1$		
R_0	1.23	6.3	1.9
M	18	18	18
b	1.031	1.050	1.040
N	500	500	500
n_{ens}	46	46	46

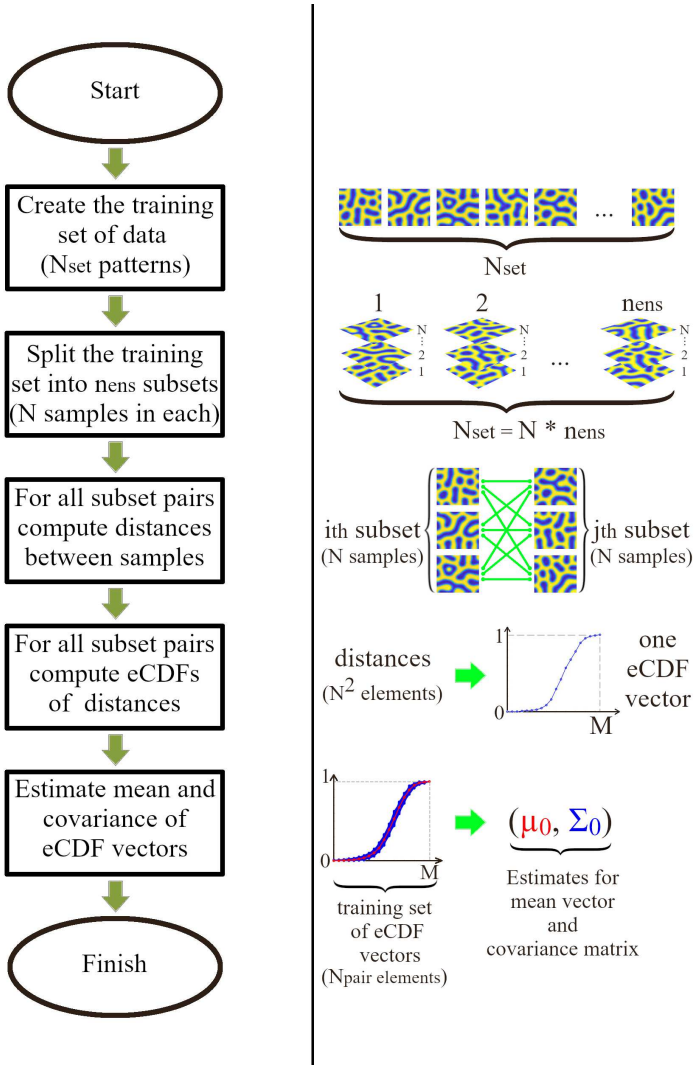

Figure 4.1: Creation of the correlation integral likelihood. The training set is divided into n_{ens} subsets, each containing N samples. Next, for any given subset pair the distances between all respective samples are computed (N^2 values). Next, the empirical cumulative distribution function (eCDF) of the distances is constructed. This gives us $N_{pair} = n_{ens}(n_{ens} - 1)/2$ samples of eCDF vectors, from which the mean and covariance of the eCDF vectors are estimated.

integral vector $\boldsymbol{y}$. To create the statistics of $\boldsymbol{y}$ at $\boldsymbol{\theta} = \boldsymbol{\theta_0}$ we first create ensembles of $N = 500$ samples s_i, repeated $n_{ens} = 46$ times. This yields $N_{pair} = \frac{46(46-1)}{2} = 1035$ different ensemble pairs. For each pair we compute the N^2 distances between the pattern samples and create the respective eCDF vector. The set of ensemble pairs gives us 1035 examples of the eCDF vectors, from which the mean and covariance of $\boldsymbol{y}(\boldsymbol{x}, \boldsymbol{\theta_0})$ are estimated (see Fig. 4.1 for details).

So, altogether we create $N_{set} = n_{ens} \times N = 23000$ patterns for the training set, each by randomising the initial conditions and solving the ODE system (3.5). For the numerical experiments we discretise the spatial terms in a square mesh of 64×64 points and arrive at a set of 8192 equations in the MOL system.

Next, we find the constants used to construct the cumulative distribution functions of the distances. For this we set R_0 as the maximum of all computed distances. As the bin values are given by $R_k = b^{-k} R_0$, $k = 1, ..., M$ some manual tuning is needed to find suitable M, as always with histograms or empirical CDF functions. With R_0 and M given, the value of b can be found by the requirement that the smallest radius $R_M = b^{-M} R_0$ is somewhat larger than the minimum of the distances computed by the training set. A final check for the R_k values is performed to verify that the resulting covariance matrix is not singular, which might happen if some R_k values are too large or too small. All parameter values for the current experiment are listed in Table 4.1.

To numerically verify the Gaussianity of the set of vectors (3.9), we apply the chi-square criterion, which states that if the Gaussian hypothesis is true then:

$$(\boldsymbol{\mu_0} - \boldsymbol{y}) \boldsymbol{\Sigma}_0^{-1} (\boldsymbol{\mu_0} - \boldsymbol{y}) \sim \chi^2_M, \tag{4.1}$$

where $\boldsymbol{\mu_0}$ and $\boldsymbol{\Sigma}_0$ are mean vector and covariance matrix of the training set, χ^2_M is a chi-squared distribution with M degrees of freedom. Examples of the density function of χ^2_M and the corresponding empirical histogram of (4.1) are shown in Fig. 4.2. Individual components $y_m^{k,l}$ of the vectors (3.9) are also normally distributed, which can be verified by any scalar Normality test.

The parameter posterior distribution can now be constructed by MCMC sampling methods. We generate a sequence of parameter values $\boldsymbol{\theta_0^1}, \boldsymbol{\theta_0^2}, \ldots, \boldsymbol{\theta_0^n}$ whose empirical distribution approaches the posterior distribution. A new point $\boldsymbol{\theta_0^{n+1}}$ in the chain is generated by the following rule. First, a new candidate $\boldsymbol{\theta^*}$ is generated by a Gaussian proposal distribution with a prescribed covariance matrix. The reaction-diffusion system (1.1) is simulated N times for the proposed parameter vector $\boldsymbol{\theta^*}$, and a CIL vector $\boldsymbol{y^{k,\theta^*}}$ is calculated using distances between the simulated patterns and those from a randomly chosen ensemble $\boldsymbol{s}^k$ from the training set. The proposed parameter $\boldsymbol{\theta^*}$ is finally accepted or rejected, depending on the value of the likelihood for $\boldsymbol{y^{k,\theta^*}}$. For more details on MCMC methods see Hastings (1970). We use the adaptive Metropolis-Hastings algorithm, which updates the covariance matrix in order to improve the proposal during the sampling (Haario et al. (2001, 2006)).

We sample a parameter chain of length 4000. The results shown in Fig. 4.2 demonstrate that the sampling performs well, producing a strong correlation but clearly limited variability of the parameter values. Fig. 4.3 shows examples of Turing patterns, obtained for

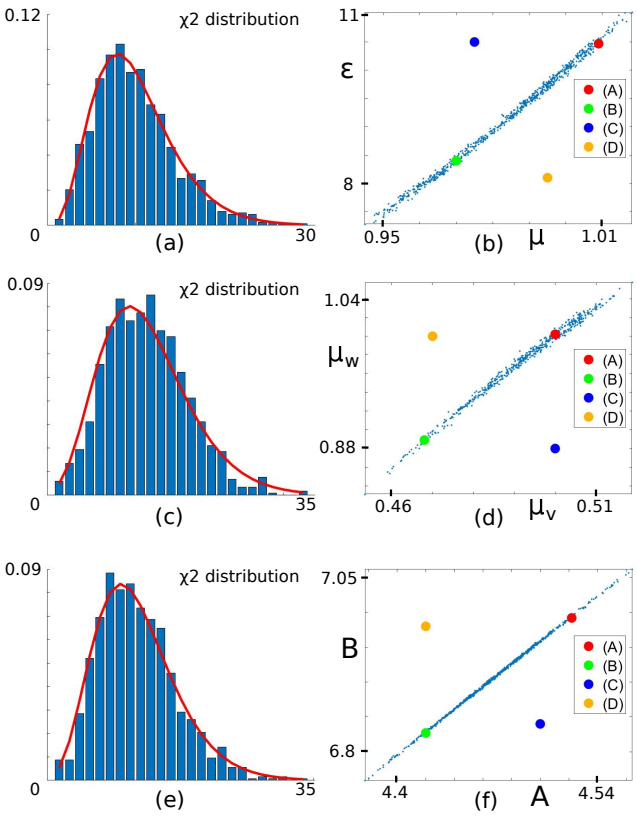

Figure 4.2: Density function χ^2_M with the corresponding empirical histograms and posterior distributions of model parameters with verification values inside and outside the region for the case $N = 500$: (a)-(b) the FitzHugh-Nagumo model (verification values are: (A) $\mu = 1.01$, $\varepsilon = 10.47$, (B) $\mu = 0.97$, $\varepsilon = 8.4$, (C) $\mu = 0.98$, $\varepsilon = 10.5$ and (D) $\mu = 1.0$, $\varepsilon = 8.1$), (c)-(d) the Gierer-Meinhard system (verification values are: (A) $\mu_v = 0.5$, $\mu_w = 1.002$, (B) $\mu_v = 0.47$, $\mu_w = 0.89$, (C) $\mu_v = 0.5$, $\mu_w = 0.88$ and (D) $\mu_v = 0.47$, $\mu_w = 1.0$) and (e)-(f) the Brusselator reaction-diffusion system (verification values are: (A) $A = 4.522$, $B = 6.992$, (B) $A = 4.42$, $B = 6.827$, (C) $A = 4.5$, $B = 6.84$ and (D) $A = 4.44$, $B = 7.0$).

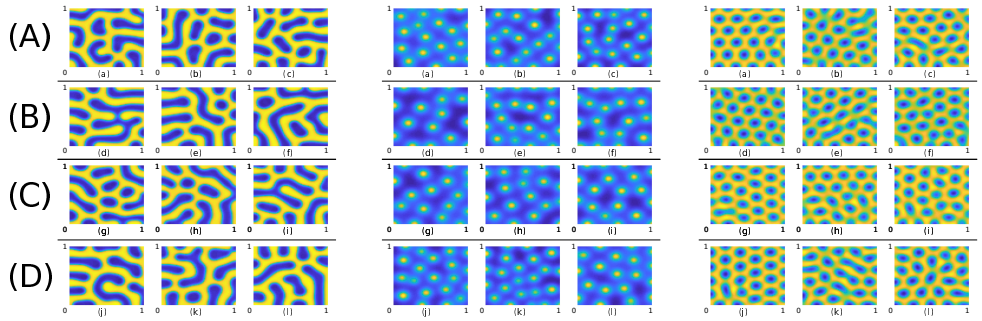

Figure 4.3: Turing patterns, obtained from direct simulations of the equations under study for verification values of control parameters, lying inside the posterior distribution region for the case $N = 500$ (points (A) and (B)) and outside it (points (C) and (D)). Initial conditions are taken as small random perturbations of the homogeneous steady state. Verification values of varying control parameters and posterior distribution regions are shown in Fig. 4.2, while values of fixed model parameters are listed in Table 4.1. Left column: the FitzHugh-Nagumo model (variable w). Central column: the Gierer-Meinhardt system (variable w). Right column: the Brusselator reaction-diffusion system (variable v).

the verification values from inside the parameter posterior and slightly outside it. We can observe that while the algorithm is able to detect structural changes in the patterns due to slightly changed parameter values, it would be practically impossible to distinguish any systematic differences between those pictures with the naked eye. The strong correlation of the parameters might naturally suggest the underlying invariance of the patterns. This does not affect, however, the ability of the approach to properly identify the bounded posterior regions. It can be verified numerically that parameter values, lying on the respective curves outside of the posteriors give bigger values of the likelihood than points inside the sampled regions and as a result can be successfully distinguished by the algorithm.

4.3 Limited data

We have to note that our previous training set contains a large number of Turing pattern examples, of the order 23,000. Such an amount of data allows us to keep the number of patterns for one feature vector, as well as the number of pairs of the vectors, high enough to produce smooth eCDF curves and accurate estimates of $\boldsymbol{\mu_0}$ and $\boldsymbol{\Sigma}_0$. It is, however, most likely an "overkill" for many practical purposes. Let us next consider situations where we possess a limited amount of information. First we assume that we have a limited set $S = \{\boldsymbol{s}_i\}_{i=1}^{N_{set}}$ of patterns available. In this situation it is possible to use a bootstrapping method that allows us to keep the number of trajectory pairs in training set high enough by resampling. However, posterior distributions of model parameters naturally grow larger as the amount of data N decreases. Next we consider the situation when data patterns are scaled by min-max normalisation. This may be considered as switching to the 2D "observations" of patterns, which could be treated as greyscale images of the data. In

Table 4.2: Parameter values used for creating the training set for statistics of generalised correlation integral vector $\boldsymbol{y}(\boldsymbol{x}, \boldsymbol{\theta_0})$ in the case of min-max normalised data. FHN, GM and BRS denote the FitzHugh-Nagumo model, Gierer-Meinhardt system and Brusselator reaction-diffusion system respectively.

Parameter	FHN	GM	BRS
R_0	0.81	0.47	0.7
M	32	32	32
b	1.016	1.05	1.025
N	500	500	500
n_{ens}	46	46	46

this situation the approach performs well; however, the posterior regions become larger as some amount of information has been lost. Finally we test the method in the situation of a sparse mesh when the spatial resolution of the picture decreases.
We split the set S into two equal parts S_1 and S_2, each containing $N = \frac{N_{set}}{2}$ elements. Then, we create the training set for statistics of $\boldsymbol{y}(\boldsymbol{x}, \boldsymbol{\theta_0})$ using the following algorithm:

1. Create a set $\tilde{S_1}$ by sampling N patterns with replacement from data set S_1.
2. Create a set $\tilde{S_2}$ by sampling N patterns with replacement from data set S_2.
3. Use the sets $\tilde{S_1}$ and $\tilde{S_2}$ to compute the correlation integral vector $\boldsymbol{y}(\tilde{S_1}, \tilde{S_2}, \boldsymbol{\theta_0})$.
4. Randomising S_1 and S_2, repeat steps 1-3 until N_{pair} vectors $\boldsymbol{y}$ for the training set have been created.

The vectors $\boldsymbol{y}$ constructed in the above way again follow a multivariate Gaussian distribution, as can be once more verified by the chi-square test. The bootstrapping is able to produce estimates for mean vector $\boldsymbol{\mu}_0$ and covariance matrix $\boldsymbol{\Sigma}_0$, which are needed for the construction of parameter posterior distribution. We tested the impact of decreasing data using training sets containing 1000, 500 and 50 patterns. The results of the MCMC sampling for the model parameters are shown in Fig. 4.4. We see how the decrease in original data samples results in larger parameter posterior distributions. But this is only natural: a decreasing amount of data always results in increasing uncertainty. However, we note that the value $N_{set} = 50$ is at the lower limit where the bootstrapping approach still works in a numerically stable manner, because a smaller set of distances gives too crude an approximation for eCDF (see Fig. 4.5).
Finally, we can again visually verify the patterns created by the model using parameter values at the tails or outside the sampled distribution. As the verification points we selected a few examples as shown in Fig. 4.6, using the least accurate case obtained with $N_{set} = 50$ data patterns. Examples of Turing patterns obtained for these verification values are shown in Fig. 4.7. We might observe that the patterns corresponding to the parameters at the tails of the posterior are yet difficult to distinguish from the reference

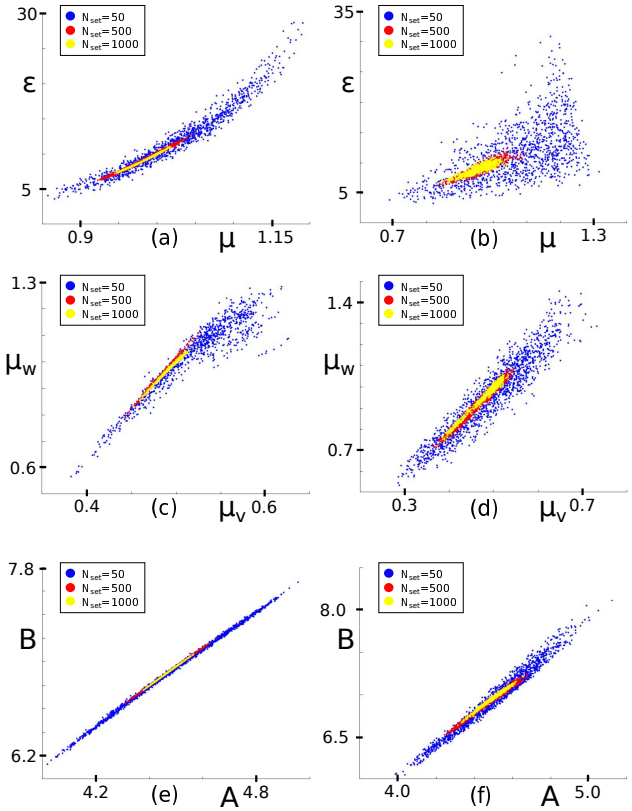

Figure 4.4: Posterior distribution of model parameters for the different number of samples in the training set ($N_{set} = 1000$ (yellow), $N_{set} = 500$ (red) and $N_{set} = 50$ (blue)). Left column: non-normalised case. Right column: min-max normalised case. Values of all model parameters are given in Table 4.1 for non-normalised data and in Table 4.2 for min-max normalised data. The FitzHugh-Nagumo model: (a) and (b), the Gierer-Meinhardt system: (c) and (d) and the Brusselator reaction-diffusion system: (e) and (f).

patterns with the naked eye, while the patterns created using the parameter values outside the distribution now are clearly different.

Recall that the Turing patterns used as data samples are the steady state concentration fields, obtained from points of a square domain Ω, determined by equations (3.5). However, we can also consider the case when the information of the absolute concentration values is removed from the data. This is done by normalisation. We scale all samples s_i by min-max values, i.e. by the transformation:

$$s_i = (v_i(x),\, w_i(x)) \to \tilde{s}_i = (\tilde{v}_i(x),\, \tilde{w}_i(x)),$$
$$\tilde{v}_i(x) = \frac{v_i(x) - v_i^{min}}{v_i^{max} - v_i^{min}},\; \tilde{w}_i(x) = \frac{w_i(x) - w_i^{min}}{w_i^{max} - w_i^{min}},$$

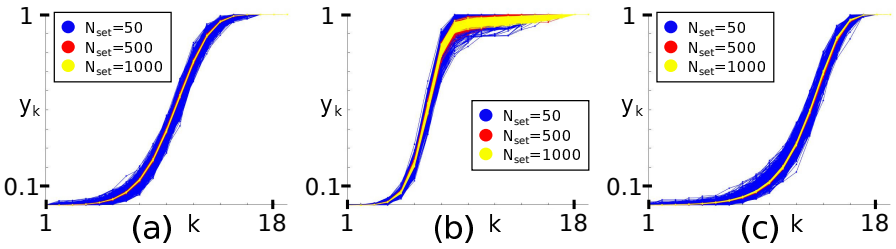

Figure 4.5: The distribution of correlation integral vector components y_k for different number of samples in the training set ($N_{set} = 1000$ (yellow), $N_{set} = 500$ (red) and $N_{set} = 50$ (blue)). The FitzHugh-Nagumo model (a), the Gierer-Meinhardt system (b) and the Brusselator reaction-system (c).

where v_i^{min}, w_i^{min} and v_i^{max}, w_i^{max} are minimum and maximum values of corresponding functions on a squared domain Ω. We may consider this transformation as a replacement of the computed Turing pattern by its greyscale image (Nomura et al. (2011); Ebihara et al. (2003)).

We create the training set in the same way as in the first case, and successfully test the normality of the correlation integral vectors, again by the chi-square criterion. All parameter values used for the construction of the likelihood for the normalised case are listed in Table 4.2.

The sampled parameter distributions for both normalised and non-normalised cases are shown in Fig. 4.4. It can be seen that the posterior distribution region is larger in the latter case. However, if the number of data samples is large enough, the variability of the model parameters remains very low and the overall conclusion remains: with a large enough training set the algorithm finds small systematic changes of pattern formation, far below what one can intuitively see with the naked eye, even if only 2D information of the patterns is employed.

We also tested the robustness of the proposed approach in the situation with larger spatial step h. We repeated all the experiments from this and previous sections in a square mesh of 32×32 points (and spatial step size $h = 1/31 = 0.0322$). Considering less dense meshes may be inappropriate due to the size of spatial step with respect to the domain size. However, we have found that in this case the statistical approach worked in a numerically stable manner, reproducing similar results and conclusions for the spatial mesh of 64×64 points. The posterior distribution of model parameters for the different values of N_{set} and Brusselator reaction-diffusion system (3.3) are shown in Fig. 4.8.

It is naturally possible to sample other model parameters as well, such as the diffusion coefficients ν_1, ν_2. The approach works as expected; however, a higher number of sampled parameters results in longer MCMC chains.

As noted above, the number of $N_{set} = 50$ patterns was observed to be a lower limit for reliable results. While the number n_{ens} of disjoint subsets, of size $N = N_{set}/2$ that can be drawn from the training set, is not a limiting factor, a too small value of N^2 leads to too noisy values for the calculated eCDF vectors. A way around the limitation is to

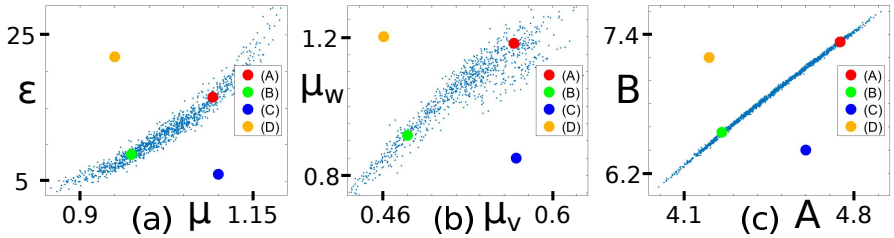

Figure 4.6: Posterior distributions of model parameters with verification values inside and outside the region for the case $N_{set} = 50$: (a) the FitzHugh-Nagumo model (verification values are: (A) $\mu = 1.092$, $\varepsilon = 16.5$, (B) $\mu = 0.97$, $\varepsilon = 8.7$, (C) $\mu = 1.1$, $\varepsilon = 6.0$ and (D) $\mu = 0.95$, $\varepsilon = 22.0$), (b) the Gierer-Meinhard system (verification values are: (A) $\mu_v = 0.57$, $\mu_w = 1.18$, (B) $\mu_v = 0.48$, $\mu_w = 0.91$, (C) $\mu_v = 0.76$, $\mu_w = 0.85$ and (D) $\mu_v = 0.46$, $\mu_w = 1.2$) and (c) the Brusselator reaction-diffusion system (verification values are: (A) $A = 4.742$, $B = 7.335$, (B) $A = 4.253$, $B = 6.554$, (C) $A = 4.6$, $B = 6.4$ and (D) $A = 4.2$, $B = 7.2$).

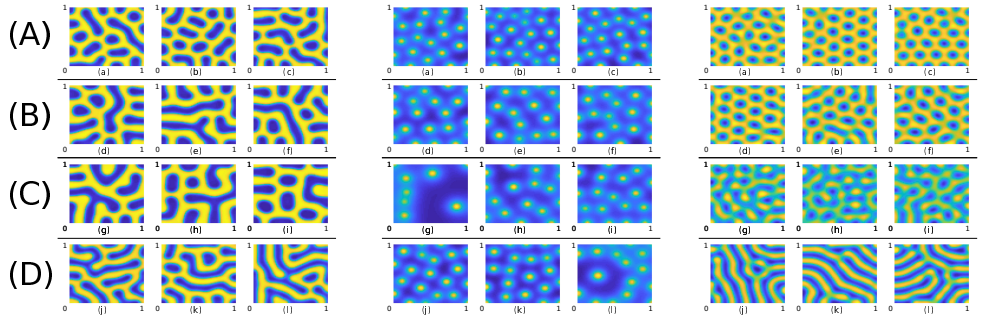

Figure 4.7: Turing patterns, obtained from direct simulations of the equations under study for verification values of control parameters, lying inside the posterior distribution region for the case $N_{set} = 50$ (points (A) and (B)) and outside it (points (C) and (D)). Non-normalised case. Initial conditions are taken as small random perturbations of the homogeneous steady state. Verification values of varying control parameters and posterior distributions are shown in Fig. 4.6, values of fixed model parameters are listed in Table 4.1. Left column: the FitzHugh-Nagumo model (variable w). Central column: the Gierer-Meinhardt system (variable w). Right column: the Brusselator reaction-diffusion system (variable v).

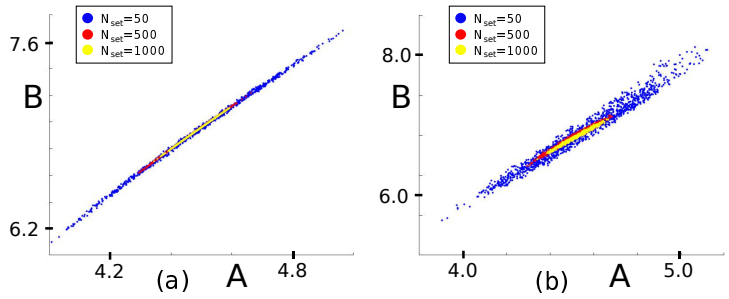

Figure 4.8: Posterior distributions of model parameters for the case of sparse mesh of 32×32 points and different number of samples in the training set ($N_{set} = 1000$ (yellow), $N_{set} = 500$ (red) and $N_{set} = 50$ (blue)). The Brusselator reaction-diffusion system: non-normalised case (a) and min-max normalised case (b). The values of model control parameter vector $\boldsymbol{\theta_0}$ and fixed model parameters are given in Table 4.1.

employ a different strategy, the so-called synthetic likelihood (Price et al. (2018); Wood (2010)). In this approach, the likelihood is computationally re-created for every new parameter value, and the data is tested against the likelihood. In our situation, even the data of one pattern could be used. Naturally, the results remain less accurate with less data. Moreover, the re-creation of the likelihood at every estimation step considerably increases the computational cost. If enough parallel processing power is available, the simulations can be performed, but nevertheless they need more resources than the off-line likelihood construction employed here.

Table 4.3: Parameter values used for creating the training set for statistics of $\boldsymbol{y}(\boldsymbol{x}, \boldsymbol{\theta_0})$ and running the DE algorithm of stochastic optimisation. FHN, GM and BRS mean the FitzHugh-Nagumo model, Gierer-Meinhardt system and Brusselator reaction-diffusion system respectively.

Parameter	FHN	GM	BRS
$\boldsymbol{\theta_0}$	$(1, 10)$	$(0.5, 1)$	$(4.5, 6.96)$
N_{set}	50	50	50
N_{iter}	100	100	100
D_0	$[1, 2] \times [35, 50]$	$[0.5, 1] \times [2.5, 5]$	$[3, 6] \times [10, 15]$
$\tilde{\boldsymbol{\theta}}_{\mathbf{0}}$	$(1.067, 10.27)$	$(0.46, 0.9)$	$(4.47, 6.86)$
R_0	0.81	0.47	0.7
M	32	32	32
b	1.016	1.05	1.025
N	25	25	25

4.4 Parameter identification

In the numerical experiments of the previous sections we started from known values of parameters to study the identifiability of them, by constructing the parameter posterior distributions in different cases. In this section we describe the correlation integral likelihood as a cost function for parameter identification of the same systems (3.1), (3.2) and (3.3). Now we start from creating a training set of $N_{set} = 50$ Turing patterns for the control parameter vector $\boldsymbol{\theta_0}$ and "forget" the true value $\boldsymbol{\theta_0}$. Next we apply CIL approach to estimate the values of control parameters from the data. In all experiments here we use the min-max normalised version of data.

We use the same likelihood construction as above (see Table 4.3 for details) to define the likelihood as a stochastic cost function:

$$f(\boldsymbol{\theta}) = (\boldsymbol{\mu_0} - \boldsymbol{y}(\boldsymbol{\theta}))\boldsymbol{\Sigma}_0^{-1}(\boldsymbol{\mu_0} - \boldsymbol{y}(\boldsymbol{\theta})),$$

and minimise it with respect to $\boldsymbol{\theta}$, starting with initial parameter values far away from $\boldsymbol{\theta_0}$. For the cost function minimisation we employ the method of Differential Evolution (Storn and Price (1997)). We create an initial population of candidate solutions (control

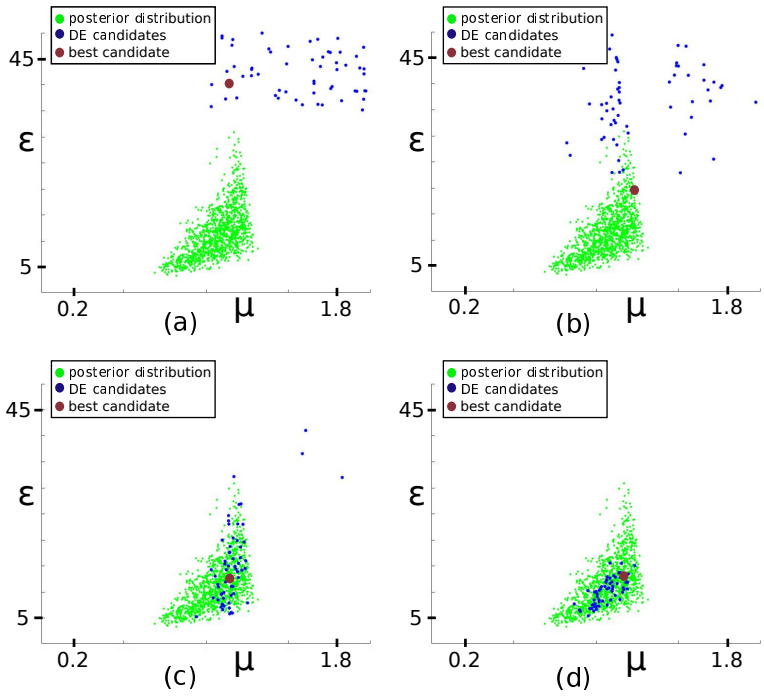

Figure 4.9: Parameter identification for the case of the FitzHugh-Nagumo model. The optimisation of stochastic cost function $f(\boldsymbol{\theta})$ is done by Differential Evolution algorithm: (a) step 0 (initial population), (b) step 3, (c) step 10, (d) step 100 (final population). Parameters values, used for the numerical experiment, are given in Table 4.3.

parameter values), uniformly distributed on a square D_0. Note that in our example case D_0 does not contain the point $\boldsymbol{\theta_0}$ (see Table 4.3). The algorithm optimises the cost function $f(\boldsymbol{\theta})$ by iteratively updating a population of candidate solutions. New candidate solutions are created from existing ones by defined combination rules; points with lowest values for the cost function replace the old ones. However, due to the stochasticity in $f(\boldsymbol{\theta})$, values for all candidate solutions are updated here at each iteration step.
In our example, the algorithm is run for $N_{iter} = 100$ iterations. The behaviour of the optimisation steps is exhibited in Fig. 4.9. It can be observed that after several "generations" the population converges towards $\boldsymbol{\theta_0}$ and remains in the vicinity of it, but the stochasticity of the cost function prevents convergence to a point estimate. After the optimisation we can continue with MCMC sampling to find the posterior distribution of the parameters, as given in Fig. 4.9. Note also that the parameter values of the populations at final iteration steps of DE can be used to create an initial proposal covariance for the adaptive sampling algorithms.
Similar results were observed in other examples, but we omit further details here. We can conclude that the approach provides a robust algorithm to identify the distribution of those model parameters that correspond to a given data set of patterns, without the need for transient data or knowledge of initial values.

4.5 Summary

In this section the Correlation Integral Likelihood was tested using the well-known FitzHugh-Nagumo, Gierer-Meinhardt and Brusselator reaction-diffusion systems. The amount of training data was varied from 23000 to 50 patterns. For a large data set the proposed approach shows a strong sensitivity with respect to even small changes in pattern formation, which are practically impossible to detect visually. The method was used as a tool for estimating parameters of the reaction-diffusion systems, only using a collection of steady-state solutions as data, without the knowledge of initial state values. The performance of the method was satisfactory in all cases: a large amount of data leads to an extremely accurate detection of model parameters, while a modest amount of training patterns leads to the same level of detection as, roughly speaking, might be observed by the naked eye.

5 Discussion

In this thesis the problem of parameter identification of reaction-diffusion systems by Turing patterns was studied. By applying the concept of Correlation Integral Likelihood, a statistical feature vector following a multinomial Gaussian distribution was introduced. With a large enough set of pattern data, this allowed a statistically sound way to determine if a given set of patterns belongs to the same family of patterns as the training data. The parameter identification can then be done by the methods of statistical optimization, while Markov Chain Monte Carlo (MCMC) sampling methods can be used to determine the distribution of those parameters of a reaction-diffusion system that produce patterns similar to data.

The method was tested using the well-known FitzHugh-Nagumo, Gierer-Meinhardt and Brusselator reaction-diffusion systems. The amount of training data was varied from 23000 to 50 patterns. The performance of the method was satisfactory in all cases: a large amount of data leads to an extremely accurate detection of changes in model parameters, practically impossible to detect visually, while a modest amount of training patterns leads to the same level of detection as, roughly speaking, might be observed with the naked eye. It is possible to further minimize the amount of data needed, all the way to one pattern only, by combining the correlation integral likelihood (CIL) feature vectors with the idea of synthetic likelihoods. This, however, will come at the cost of considerably increased computational demands.

The efficiency of numerical simulations is crucial for the successful run of the algorithm. That results from the fact that numerical simulation of the model is repeated many times to construct parameter posterior distribution by MCMC methods or to run DE stochastic optimization. To resolve this issue, an efficient parallel algorithm for solving the equations under study by the explicit Runge-Kutta ”RK4” method was implemented. The computations were done on GPU by using Nvidia CUDA computing platform. All experiments, discussed in the current work, were performed by using a single laptop with two Nvidia GTX 980 graphic cards.

Possible future applications of the approach include model identification in developmental biology based on patterns obtained from experimental data and comparing the performance of different models suggested to explain various pattern formation processes. The presented technique can also be applied to the case of dynamic spatio-temporal patterns, with some necessary modifications.

References

Agladze, K., Dulos, E., and De Kepper, P. (1992). Turing patterns in confined gel and gel-free media. *The Journal of Physical Chemistry*, 96(6), pp. 2400–2403. doi: 10.1021/j100185a002.

Asai, R., et al. (1999). Zebrafish Leopard gene as a component of the putative reaction-diffusion system. *Mechanisms of Development*, 89(1), pp. 87 – 92. ISSN 0925-4773, doi:https://doi.org/10.1016/S0925-4773(99)00211-7.

Bailleul, R., Manceau, M., and Touboul, J. (2020). A Numerical Evo-Devo Synthesis for the Identification of Pattern-Forming Factors. *Cells*, 9(8). ISSN 2073-4409, doi:10.3390/cells9081840, url: https://www.mdpi.com/2073-4409/9/8/1840.

Barrass, I., Crampin, E.J., and Maini, P.K. (2006). Mode Transitions in a Model Reaction–Diffusion System Driven by Domain Growth and Noise. *Bulletin of Mathematical Biology*, 68(5), pp. 981–995. ISSN 1522-9602, doi:10.1007/s11538-006-9106-8, url: https://doi.org/10.1007/s11538-006-9106-8.

Belousov, B.P. (1959). A periodic reaction and its mechanism [In Russian]. *Collection of short papers on radiation medicine for 1958*, p. 76.

Borovkova, S., Burton, R., and Dehling, H. (2001). Limit Theorems for Functionals of Mixing Processes with Applications to U-Statistics and Dimension Estimation. *Transactions of the American Mathematical Society*, 353(11), pp. 4261–4318. ISSN 00029947, url: http://www.jstor.org/stable/2693737.

Brinkmann, F., Mercker, M., Richter, T., and Marciniak-Czochra, A. (2018). Post-Turing tissue pattern formation: Advent of mechanochemistry. *PLOS Computational Biology*, 14(7), pp. 1–21. doi:10.1371/journal.pcbi.1006259, url: https://doi.org/10.1371/journal.pcbi.1006259.

Butcher, J.C. (1987). *The Numerical Analysis of Ordinary Differential Equations: Runge-Kutta and General Linear Methods*. Wiley-Interscience. ISBN 0471910465.

Campillo-Funollet, E., Venkataraman, C., and Madzvamuse, A. (2019). Bayesian Parameter Identification for Turing Systems on Stationary and Evolving Domains. *Bulletin of Mathematical Biology*, 81(1), pp. 81–104. ISSN 1522-9602, doi:10.1007/s11538-018-0518-z, url: https://doi.org/10.1007/s11538-018-0518-z.

Carpenter, G.A. (1977). A geometric approach to singular perturbation problems with applications to nerve impulse equations. *Journal of Differential Equations*, 23(3), pp. 335 – 367. ISSN 0022-0396, doi:https://doi.org/10.1016/0022-0396(77)90116-4.

Cartwright, M.L. (1960). Balthazar Van Der Pol. *Journal of the London Mathematical Society*, s1-35(3), pp. 367–376. doi:10.1112/jlms/s1-35.3.367.

Cartwright, M.L. and Littlewood, J.E. (1945). On Non-Linear Differential Equations of the Second Order: I. The Equation $y'' + k(1 - y^2)y' + y = b\lambda kcos(\lambda l + \alpha)$, k — large. *Annals of Mathematics Second Series*, 48(2), pp. 472–494. doi:10.2307/1969181.

Castets, V., Dulos, E., Boissonade, J., and De Kepper, P. (1990). Experimental evidence of a sustained standing Turing-type nonequilibrium chemical pattern. *Phys. Rev. Lett.*, 64, pp. 2953–2956. doi:10.1103/PhysRevLett.64.2953.

Cencini, M., Cecconi, F., and Vulpiani, A. (2009). *Chaos: From Simple Models To Complex Systems*. World Scientific Publishing Co. 480 p.

Chakravarti, S., Marek, M., and Ray, W.H. (1995). Reaction-diffusion system with Brusselator kinetics: Control of a quasiperiodic route to chaos. *Phys. Rev. E*, 52, pp. 2407–2423. doi:10.1103/PhysRevE.52.2407, url: `https://link.aps.org/doi/10.1103/PhysRevE.52.2407`.

Chunbiao, G., Qishao, L., and Kelei, H. (1999). Strongly resonant bifurcations of nonlinearly coupled van der Pol-Duffing Oscillator. *Applied Mathematics and Mechanics*, 20(1), pp. 68–75. doi:10.1007/BF02459275.

Cross, M.C. and Greenside, H. (2009). *Pattern formation and dynamics in nonequilibrium systems*. Cambridge University Press. ISBN 9780521770507, 553 p.

Cross, M.C. and Hohenberg, P.C. (1993). Pattern formation outside of equilibrium. *Reviews of Modern Physics*, 65(3), pp. 851–1112. doi:10.1103/RevModPhys.65.851.

Cveticanin, L. (2015). Lord Rayleigh and Rayleigh Oscillator: An Overview. *Proceedings of the 14th IFToMM World Congress*, pp. 93–100. doi: 10.6567/IFToMM.14TH.WC.OS20.012.

Doelman, A., Eckhaus, W., and Kaper, T.J. (2000). Slowly modulated two-pulse solutions in the Gray–Scott model I: asymptotic construction and stability. *SIAM J. Appl. Math.*, 61(3), pp. 1080–1102.

Doelman, A., Gardner, R., and Kaper, T. (2001a). Large stable pulse solutions in reaction-diffusion equations. *Indiana University Mathematics Journal*, 50, pp. 443–507.

Doelman, A., Heijster, P.V., and Kaper, T. (2009). Pulse Dynamics in a Three-Component System: Existence Analysis. *Journal of Dynamics and Differential Equations*, 21, pp. 73–115.

Doelman, A., Kaper, T., and Ploeg, H.V.D. (2001b). Spatially periodic and aperiodic multi-pulse patterns in the one-dimensional Gierer-Meinhardt equation. *Methods and applications of analysis*, 8, pp. 387–414.

Doelman, A., Kaper, T., and Promislow, K. (2007). Nonlinear Asymptotic Stability of the Semistrong Pulse Dynamics in a Regularized Gierer-Meinhardt Model. *SIAM J. Math. Anal.*, 38, pp. 1760–1787.

Doelman, A. and Veerman, F. (2015). An Explicit Theory for Pulses in Two Component, Singularly Perturbed, Reaction–Diffusion Equations. *Journal of Dynamics and Differential Equations*, 27, pp. 555–595.

Doelman, A., Eckhaus, W., and Kaper, T.J. (2001c). Slowly Modulated Two-Pulse Solutions in the Gray–Scott Model II: Geometric Theory, Bifurcations, and Splitting Dynamics. *SIAM Journal on Applied Mathematics*, 61(6), pp. 2036–2062. doi: 10.1137/S0036139900372429.

Doelman, A., Gardner, R.A., and Kaper, T.J. (1997a). Stability analysis of singular patterns in the 1-D Gray-Scott model I: A matched asymptotics approach. *Physica D*, 122, pp. 1–36.

Doelman, A., Kaper, T.J., and Zegeling, P.A. (1997b). Pattern formation in the one-dimensional Gray - Scott model. *Nonlinearity*, 10(2), pp. 523–563. doi:10.1088/0951-7715/10/2/013.

Dong, T., Xu, W., and Liao, X. (2017). Hopf bifurcation analysis of reaction–diffusion neural oscillator system with excitatory-to-inhibitory connection and time delay. *Nonlinear Dynamics*, 89(4), pp. 2329–2345. ISSN 1573-269X, doi:10.1007/s11071-017-3589-8, url: `https://doi.org/10.1007/s11071-017-3589-8`.

Donsker, M. (1951). *An Invariance Principle for Certain Probability Limit Theorems*, American Mathematical Society. Memoirs.

Donsker, M.D. (1952). Justification and Extension of Doob's Heuristic Approach to the Kolmogorov- Smirnov Theorems. *Ann. Math. Statist.*, 23(2), pp. 277–281. doi:10.1214/aoms/1177729445, url: `https://doi.org/10.1214/aoms/1177729445`.

Ebihara, M., et al. (2003). Image processing by a discrete reaction-diffusion system. *Proceeding of Visualization, Imaging, and Image Processing*, 396.

Erneux, T., Hiernaux, J., and Nicolis, G. (1978). Turing's theory in morphogenesis. *Bulletin of Mathematical Biology*, 40(6), pp. 771 – 789. doi:https://doi.org/10.1016/S0092-8240(78)80008-1.

Escala, D.M., Guiu-Souto, J., and Munuzuri, A.P. (2015). Externally controlled anisotropy in pattern-forming reaction-diffusion systems. *Chaos*, 25(6), p. 064309. doi: 10.1063/1.4922303.

Facchini, A., Rossi, F., and Mocenni, C. (2009). Spatial recurrence strategies reveal different routes to Turing pattern formation in chemical systems. *Physics Letters, Section A: General, Atomic and Solid State Physics*, 373(46), pp. 4266–4272. doi: 10.1016/j.physleta.2009.09.049.

Field, R.J. and Burger, M., eds, (1985). *Oscillations and traveling waves in chemical systems*. Wiley, New York. 720 p.

Filho, A.C.d.P., Dutra, M.S., and Raptopoulos, L.S.C. (2005). Modeling of a bipedal robot using mutually coupled Rayleigh oscillators. *Biological Cybernetics*, 92(1), pp. 1–7. doi:10.1007/s00422-004-0531-1.

Fisher, R.A. (1937). The wave of advance of advantageous genes. *The Annals of Eugenics*, 7, pp. 355–369.

FitzHugh, R. (1955). Mathematical models of threshold phenomena in the nerve membrane. *The bulletin of mathematical biophysics*, 17(4), pp. 257–278. doi: 10.1007/BF02477753.

FitzHugh, R. (1961). Impulses and Physiological States in Theoretical Models of Nerve Membrane. *Biophysical Journal*, 1(6), pp. 445–466. doi:10.1016/S0006-3495(61)86902-6.

Garvie, M.R., Maini, P.K., and Trenchea, C. (2010). An efficient and robust numerical algorithm for estimating parameters in Turing systems. *Journal of Computational Physics*, 229(19), pp. 7058 – 7071. ISSN 0021-9991, doi: https://doi.org/10.1016/j.jcp.2010.05.040.

Gerstner, W. and Kistler, W.M. (2002). *Spiking Neuron Models: Single Neurons, Populations, Plasticity*. Cambridge University Press. 480 p.

Ghorai, S. and Poria, S. (2016). Pattern formation and control of spatiotemporal chaos in a reaction diffusion prey-predator system supplying additional food. *Chaos, Solitons and Fractals*, 85, pp. 57–67. doi:10.1016/j.chaos.2016.01.013.

Gierer, A. and Meinhardt, H. (1972). A theory of biological pattern formation. *Kybernetik*, 12(1), pp. 30–39. doi:10.1007/BF00289234.

Glansdorff, P. and Prigogine, I. (1971a). *Thermodynamic Theory of Structure, Stability and Fluctuations*. Wiley-Interscience, London. 306 p.

Glansdorff, P. and Prigogine, I. (1971b). *Thermodynamic Theory of Structure, Stability and Fluctuations*. John Wiley & Sons. 232 p.

Gmitro, J.I. and Scriven, L.E. (1966). A physicochemical basis for pattern and rhythm. *Intracellular Transport*, 5, pp. 221 – 255. doi:https://doi.org/10.1016/B978-1-4831-9872-9.50016-0.

Gray, P. and Scott, S.K. (1983). Autocatalytic reactions in the isothermal, continuous stirred tank reactor. *Journal of Chemical Engineering Science*, 38(1), pp. 29–43.

Gray, P. and Scott, S.K. (1985). Sustained oscillations and other exotic patterns of behavior in isothermal reactions. *The Journal of Physical Chemistry*, 89(1), pp. 22–32. doi:10.1021/j100247a009.

Gray, P. and Scott, S. (1984). Autocatalytic reactions in the isothermal, continuous stirred tank reactor: Oscillations and instabilities in the system A + 2B ¿ 3B; B ¿ C. *Chemical Engineering Science*, 39(6), pp. 1087 – 1097. doi:https://doi.org/10.1016/0009-2509(84)87017-7.

Grossmann, C., Gorg, H.R., and Stynes, M. (2007). *Numerical Treatment of Partial Differential Equations*. Berlin, Heidelberg: Springer Berlin Heidelberg. ISBN 978-3-540-71584-9, 591 p.

Haario, H., Kalachev, L., and Hakkarainen, J. (2015). Generalized correlation integral vectors: A distance concept for chaotic dynamical systems. *Chaos*, 25(6). doi: 10.1063/1.4921939.

Haario, H., Laine, M., Mira, A., and Saksman, E. (2006). DRAM: Efficient adaptive MCMC. *Statistics and Computing*, 16(4), pp. 339–354. ISSN 1573-1375, doi:10.1007/s11222-006-9438-0, url: https://doi.org/10.1007/s11222-006-9438-0.

Haario, H., Saksman, E., and Tamminen, J. (2001). An adaptive Metropolis algorithm. *Bernoulli*, 7(2), pp. 223–242. url: https://projecteuclid.org:443/euclid.bj/1080222083.

Han, X., Xia, F., Zhang, C., and Yu, Y. (2017). Origin of mixed-mode oscillations through speed escape of attractors in a Rayleigh equation with multiple-frequency excitations. *Nonlinear Dynamics*, 88(4), pp. 2693–2703. doi:10.1007/s11071-017-3403-7.

Härting, S., Marciniak-Czochra, A., and Takagi, I. (2017). Stable patterns with jump discontinuity in systems with Turing instability and hysteresis. *Discrete & Continuous Dynamical Systems — A*, 37(2), pp. 757–800. ISSN 1078-0947, doi: 10.3934/dcds.2017032.

Hasegawa, H. (2011). Jarzynski equality in Van der Pol and Rayleigh oscillators. *Physical Review E*, 84, p. 061112. doi:10.1103/PhysRevE.84.061112.

Hastings, S.P. (1976). On the existence of homoclinic and periodic orbits for the FitzHugh-Nagumo equations. *The Quarterly Journal of Mathematics*, 27(1), pp. 123–134. ISSN 0033-5606, doi:10.1093/qmath/27.1.123, url: https://doi.org/10.1093/qmath/27.1.123.

Hastings, S.P. (1974). The existence of periodic solutions to Nagumo's equation. *The Quarterly Journal of Mathematics*, 25(1), pp. 369–378. ISSN 0033-5606, doi:10.1093/qmath/25.1.369, url: https://doi.org/10.1093/qmath/25.1.369.

Hastings, W.K. (1970). Monte Carlo sampling methods using Markov chains and their applications. *Biometrika*, 57(1), pp. 97–109. ISSN 0006-3444, doi: 10.1093/biomet/57.1.97.

Hek, G. (2009). Geometric Singular Perturbation Theory in Biological Practice. *Journal of mathematical biology*, 60, pp. 347–386. doi:10.1007/s00285-009-0266-7.

Hodgkin, A. and Huxley, A. (1952). A quantitative description of membrane current and its application to conduction and excitation in nerve. *The Journal of Physiology*, 117(4), pp. 500–44. doi:10.1113/jphysiol.1952.sp004764.

Horváth, A.K., et al. (1999). Control of Turing Structures by Periodic Illumination. *Phys. Rev. Lett.*, 83, pp. 2950–2952. doi:10.1103/PhysRevLett.83.2950, url: `https://link.aps.org/doi/10.1103/PhysRevLett.83.2950`.

Hupkes, H.J. and Van Vleck, E.S. (2016). Travelling Waves for Complete Discretizations of Reaction Diffusion Systems. *Journal of Dynamics and Differential Equations*, 28(3), pp. 955–1006. doi:10.1007/s10884-014-9423-9.

Inaba, N. and Mori, S. (1992). Folded torus in the forced Rayleigh oscillator with a diode pair. *IEEE Transactions on Circuits and Systems I: Fundamental Theory and Applications*, 39(5), pp. 402–411. doi:10.1109/81.139290.

Jaeger, D. and Jung, R. (2015). *Encyclopedia of Computational Neuroscience*. New York, NY: Springer New York. ISBN 978-1-4614-7320-6, 3180 p.

Jones, C.K.R.T. (1984). Stability of the Travelling Wave Solution of the Fitzhugh-Nagumo System. *Transactions of the American Mathematical Society*, 286(2), pp. 431–469. ISSN 00029947.

Jung, H.S., et al. (1998). Local Inhibitory Action of BMPs and Their Relationships with Activators in Feather Formation: Implications for Periodic Patterning. *Developmental Biology*, 196(1), pp. 11 – 23. ISSN 0012-1606, doi: https://doi.org/10.1006/dbio.1998.8850.

Kaper, T.J. (1999). An introduction to geometric methods and dynamical systems theory for singular perturbation problems. In: Cronin, J. and O'Malley, R.E., eds, *Analyzing multiscale phenomena using singular perturbation methods, Proceedings of Symposia in Applied Mathematics*, vol. 56, p. 85–131. American Mathematical Society.

Kazarnikov, A. (2018). *The formation of spatio-temporal patterns in the FitzHugh-Nagumo reaction-diffusion system and its limit cases [in Russian]*. Ph.D. thesis. Southern Federal University, Rostov-on-Don, Russia.

Kazarnikov, A. and Haario, H. (2020). Statistical approach for parameter identification by Turing patterns. *Journal of Theoretical Biology*, 501, p. 110319. ISSN 0022-5193, doi:https://doi.org/10.1016/j.jtbi.2020.110319.

Kazarnikov, A.V. and Revina, S.V. (2016a). Asimptotika statsionarnykh reshenii sistemy Releya s diffusiei [Asymptotics of stationary solutions of Rayleigh reaction-diffusion system]. *Izvestiya VUZov. Severo-Kavkazskii region. Estestvennye nauki [Bulletin of*

higher education institutes. North Caucasus region. Natural sciences], (191), pp. 13–19. doi:10/18522/0321-3005-2016-3-13-19.

Kazarnikov, A.V. and Revina, S.V. (2016b). Vozniknovenie avtokolebanii v sisteme Releya s diffusiei [The onset of auto-oscillations in Rayleigh system with diffusion]. *Bulletin of the South Ural State University. Ser. Mathematical Modeling, Programming & Computer Software*, 9(2), pp. 16–28. doi:10/14529/mmp160202.

Kazarnikov, A.V. and Revina, S.V. (2017). Bifurcations in the Rayleigh reaction-diffusion system [in Russian]. *Vestnik Udmurtskogo Universiteta. Matematika. Mekhanika. Komp'yuternye Nauki [The Bulletin of Udmurt University. Mathematics. Mechanics. Computer Science]*, 27(4), pp. 499–514. doi:10.20537/vm170402.

Kazarnikov, A.V. and Revina, S.V. (2018). Monotonous Instability in FitzHugh-Nagumo Reaction-Diffusion System [in Russian]. *Izvestiya Vuzov. Severo-Kavkazskii Region. Estestvennye nauki [Bulletin of higher education institutes. North Caucasus region. Natural sciences]*, (4), pp. 18–24.

Koch, A.J. and Meinhardt, H. (1994). Biological pattern formation: from basic mechanisms to complex structures. *Rev. Mod. Phys.*, 66, pp. 1481–1507. doi:10.1103/RevModPhys.66.1481, url: `https://link.aps.org/doi/10.1103/RevModPhys.66.1481`.

Kolmogorov, A.N., Petrovskii, I.G., and Piskunov, N.S. (1937). A study of the diffusion equation with increase in the amount of substance and its application to a biological problem. *Bull. Moscow Univ., Math. Mech.*, 1, pp. 1–25.

Kolmogorov, A.N., Petrovskii, I.G., and Piskunov, N.S. (1991). A study of the diffusion equation with increase in the amount of substance and its application to a biological problem. *Selected Works of A. N. Kolmogorov*, 1, pp. 248–270.

Kondo, S. and Asai, R. (1995). A reaction-diffusion wave on the skin of the marine angelfish Pomacanthus. *Nature*, 376, p. 765?768.

Kondo, S. and Miura, T. (2010a). Reaction-Diffusion Model as a Framework for Understanding Biological Pattern Formation. *Science*, 329(5999), pp. 1616–1620. ISSN 0036-8075, doi:10.1126/science.1179047, url: `https://science.sciencemag.org/content/329/5999/1616`.

Kondo, S. and Miura, T. (2010b). Reaction-Diffusion Model as a Framework for Understanding Biological Pattern Formation. *Science*, 329(5999), pp. 1616–1620. doi:10.1126/science.1179047.

Kramer, S. and Bollt, E.M. (2013). Spatially dependent parameter estimation and nonlinear data assimilation by autosynchronization of a system of partial differential equations. *Chaos*, 23(3). doi:10.1063/1.4812722.

Krupa, M., Sandstede, B., and Szmolyan, P. (1997). Fast and Slow Waves in the FitzHugh–Nagumo Equation. *Journal of Differential Equations*, 133(1), pp. 49 – 97. ISSN 0022-0396, doi:https://doi.org/10.1006/jdeq.1996.3198.

Kuehn, C. (2015). *Multiple Time Scale Dynamics*. Springer International Publishing. ISBN 978-3-319-12316-5, 814 p.

Kuznetsov, A.P., Paksyutov, V.I., and Roman, Y.P. (2007). Features of the synchronization of coupled van der Pol oscillators with nonidentical control parameters. *Technical Physics Letters*, 33(8), pp. 636–638. doi:10.1134/S1063785007080032.

Lee, K.J., McCormick, W.D., Ouyang, Q., and Swinney, H.L. (1993a). Pattern Formation by Interacting Chemical Fronts. *Science*, 261(5118), pp. 192–194. doi:10.1126/science.261.5118.192.

Lee, K.J., McCormick, W.D., Ouyang, Q., and Swinney, H.L. (1993b). Pattern Formation by Interacting Chemical Fronts. *Science*, 261(5118), pp. 192–194. doi:10.1126/science.261.5118.192.

Lengyel, I. and Epstein, I.R. (1991). Modeling of Turing Structures in the Chlorite—Iodide—Malonic Acid—Starch Reaction System. *Science*, 251(4994), pp. 650–652. doi:10.1126/science.251.4994.650.

Li, A.W. (2011). Impact of noise on pattern formation in a predator–prey model. *Nonlinear Dynamics*, 66(4), pp. 689–694. doi:10.1007/s11071-010-9941-x.

Li, Y., Marciniak-Czochra, A., Takagi, I., and Wu, B. (2019). Steady states of FitzHugh-Nagumo system with non-diffusive activator and diffusive inhibitor. *Tohoku Math. J. (2)*, 71(2), pp. 243–279. doi:10.2748/tmj/1561082598.

Madzvamuse, A., Thomas, R.D.K., Maini, P.K., and Wathen, A.J. (2002). A numerical approach to the study of spatial pattern formation in the ligaments of arcoid bivalves. *Bulletin of Mathematical Biology*, 64(3), pp. 501–530. doi:10.1006/bulm.2002.0283.

Maini, P.K., Painter, K.J., and Nguyen Phong Chau, H. (1997). Spatial pattern formation in chemical and biological systems. *J. Chem. Soc., Faraday Trans.*, 93, pp. 3601–3610. doi:10.1039/A702602A.

Meinhardt, H. (1995). *The Algorithmic Beauty of Sea Shells*. Springer:Heidelberg. 253 p.

Mercker, M., Hartmann, D., and Marciniak-Czochra, A. (2013). A Mechanochemical Model for Embryonic Pattern Formation: Coupling Tissue Mechanics and Morphogen Expression. *PLOS ONE*, 8(12), pp. 1–6. doi:10.1371/journal.pone.0082617, url: `https://doi.org/10.1371/journal.pone.0082617`.

Mercker, M., Köthe, A., and Marciniak-Czochra, A. (2015). Mechanochemical Symmetry Breaking in Hydra Aggregates. *Biophysical Journal*, 108(9), pp. 2396–2407. doi:10.1016/j.bpj.2015.03.033.

Miura, T., Komori, M., and Shiota, K. (2000). A novel method for analysis of the periodicity of chondrogenic patterns in limb bud cell culture: correlation of in vitro pattern formation with theoretical models. *Anatomy and Embryology*, 201(5), pp. 419–428. ISSN 1432-0568, doi:10.1007/s004290050329, url: https://doi.org/10.1007/s004290050329.

Mocenni, C., Facchini, A., and Vicino, A. (2010). Identifying the dynamics of complex spatio-temporal systems by spatial recurrence properties. *Proceedings of the National Academy of Sciences of the United States of America*, 107(18), pp. 8097–102. doi: 10.1073/pnas.0910414107.

Morgan, D.S. and Kaper, T.J. (2004). Axisymmetric ring solutions of the 2D Gray–Scott model and their destabilization into spots. *Physica D: Nonlinear Phenomena*, 192(1), pp. 33 – 62. ISSN 0167-2789, doi:https://doi.org/10.1016/j.physd.2003.12.012.

Müller, S.C., Plesser, T., and Hess, B. (1985). The Structure of the Core of the Spiral Wave in the Belousov-Zhabotinskii Reaction. *Science*, 230(4726), pp. 661–663. ISSN 0036-8075, doi:10.1126/science.230.4726.661, url: https://science.sciencemag.org/content/230/4726/661.

Müller, S.C., Plesser, T., and Hess, B. (1987). Distinctive sites in chemical waves: The spiral core and the collision area of two annuli. *Journal of Statistical Physics*, 48(5), pp. 991–1004. doi:10.1007/BF01009528.

Murray, J.D. (1993). *Mathematical biology II: Spatial models and biomedical applications*. Springer-Verlag. 838 p.

Nagumo, J., Arimoto, S., and Yoshizawa, S. (1962). An Active Pulse Transmission Line Simulating Nerve Axon. *Proceedings of the IRE*, 50(10), pp. 2061–2070. doi: 10.1109/JRPROC.1962.288235.

Neumeyer, N. (2004). A central limit theorem for two-sample U-processes. *Statistics & Probability Letters*, 67(1), pp. 73 – 85. doi:doi.org/10.1016/j.spl.2002.12.001.

Nomura, A., et al. (2011). Edge detection algorithm inspired by pattern formation processes of reaction-diffusion systems. *International Journal of Circuits, Systems and Signal Processing*, 5, pp. 105–115.

Owen, M.R. and Lewis, M.A. (2001). How predation can slow, stop or reverse a prey invasion. *Bulletin of Mathematical Biology*, 63(4), p. 655. doi:10.1006/bulm.2001.0239.

Painter, K.J., et al. (2012). Towards an integrated experimental-theoretical approach for assessing the mechanistic basis of hair and feather morphogenesis. *Interface Focus*, 2(4), pp. 433–50. doi:10.1098/rsfs.2011.0122.

Peña, B. and Pérez-García, C. (2001). Stability of Turing patterns in the Brusselator model. *Phys. Rev. E*, 64, p. 056213. doi:10.1103/PhysRevE.64.056213, url: https://link.aps.org/doi/10.1103/PhysRevE.64.056213.

Pearson, J.E. and Horsthemke, W. (1989). Turing instabilities with nearly equal diffusion coefficients. *The Journal of Chemical Physics*, 90(3), pp. 1588–1599. doi: 10.1063/1.456051.

Pearson, J.K. (1993). Complex Patterns in a Simple System. *Science*, 261(5118), pp. 189–192. doi:10.1126/science.261.5118.189.

Perthame, B. (2015). *Parabolic Equations in Biology: Growth, reaction, movement and diffusion*. Springer International Publishing. ISBN 978-3-319-19500-1, 201 p.

Van der Pol, B. (1920). A theory of the amplitude of free and forced triode vibrations. *Radio Review*, (1), pp. 701–710.

Van der Pol, B. (1926). On relaxation-oscillations. *The London, Edinburgh, and Dublin Philosophical Magazine and Journal of Science*, 2(7), pp. 978–992.

Van der Pol, B. and Van der Mark, J. (1927). Frequency demultiplication. *Nature*, 120, pp. 363–364.

Price, L.F., Drovandi, C.C., Lee, A., and Nott, D.J. (2018). Bayesian Synthetic Likelihood. *Journal of Computational and Graphical Statistics*, 27(1), pp. 1–11. doi: 10.1080/10618600.2017.1302882.

Prigogine, I. and Nicolis, G. (1967). On Symmetry Breaking Instabilities in Dissipative Systems. *The Journal of Chemical Physics*, 46(9), pp. 3542–3550. doi: 10.1063/1.1841255.

Rovinskii, A.B. (1987). Turing bifurcation and stationary patterns in the ferroin-catalyzed Belousov-Zhabotinskii reaction. *The Journal of Physical Chemistry*, 91(17), pp. 4606–4613. doi:10.1021/j100301a036.

Salazar-Ciudad, I. and Jernvall, J. (2002). A gene network model accounting for development and evolution of mammalian teeth. *Proceedings of the National Academy of Sciences*, 99(12), pp. 8116–8120. ISSN 0027-8424, doi:10.1073/pnas.132069499, url: `https://www.pnas.org/content/99/12/8116`.

Sandstede, B. (1998). Stability of N-Fronts Bifurcating from a Twisted Heteroclinic Loop and an Application to the FitzHugh-Nagumo Equation. *SIAM J. Math. Anal.*, 29(1), p. 183–207. ISSN 0036-1410, doi:10.1137/S0036141096297388.

Schnakenberg, J. (1979). Simple chemical reaction systems with limit cycle behaviour. *Journal of Theoretical Biology*, 81(3), pp. 389 – 400. doi:https://doi.org/10.1016/0022-5193(79)90042-0.

Segel, L.A. and Jackson, J.L. (1972). Dissipative structure: An explanation and an ecological example. *Journal of Theoretical Biology*, 37(3), pp. 545 – 559. doi: https://doi.org/10.1016/0022-5193(72)90090-2.

Selkov, E.E. (1968). Self-Oscillations in Glycolysis. *European Journal of Biochemistry*, 4(1), pp. 79–86. doi:10.1111/j.1432-1033.1968.tb00175.x.

Storn, R. and Price, K. (1997). Differential Evolution – A Simple and Efficient Heuristic for global Optimization over Continuous Spaces. *Journal of Global Optimization*, 11(4), pp. 341–359. ISSN 1573-2916, doi:10.1023/A:1008202821328, url: https://doi.org/10.1023/A:1008202821328.

Strutt (Lord Rayleigh), J.W. (1883). On maintained vibrations. *The London, Edinburgh, and Dublin Philosophical Magazine and Journal of Science*, 15(94), pp. 229–235. doi: 10.1080/14786448308627342.

Strutt (Lord Rayleigh), J.W. (1899). *Scientific Papers*, vol. 1. Cambridge University Press. 596 p.

Suzuki, K. (2011). Mechanism Generating Spatial Patterns in Reaction-Diffusion Systems. *Interdisciplinary Information Sciences*, 17(3), pp. 131–153. doi: 10.4036/iis.2011.131.

Szalai, I. and De Kepper, P. (2008). Pattern formation in the ferrocyanide-iodate-sulfite reaction: The control of space scale separation. *Chaos*, 18(2), pp. 0–9. doi: 10.1063/1.2912719.

Tang, X., Song, Y., and Zhang, T. (2016). Turing–Hopf bifurcation analysis of a predator–prey model with herd behavior and cross-diffusion. *Nonlinear Dynamics*, 86(1), pp. 73–89. doi:10.1007/s11071-016-2873-3.

Turing, A.M. (1952). The Chemical Basis of Morphogenesis. *Philosophical Transactions of the Royal Society of London. Series B, Biological Sciences*, 237(641), pp. 37–72.

Upadhyay, R.K., Roy, P., and Datta, J. (2014). Complex dynamics of ecological systems under nonlinear harvesting: Hopf bifurcation and Turing instability. *Nonlinear Dynamics*, 79, pp. 2251–2270. doi:10.1007/s11071-014-1808-0.

van der Vaart, A.W. (1998). *Asymptotic Statistics*, Cambridge Series in Statistical and Probabilistic Mathematics. Cambridge University Press.

Vanag, V.K. (2004). Waves and patterns in reaction–diffusion systems. Belousov–Zhabotinsky reaction in water-in-oil microemulsions. *Physics-Uspekhi*, 47(9), pp. 923–941. doi:10.1070/pu2004v047n09abeh001742.

Vanag, V.K. and Epstein, I.R. (2008). Design and control of patterns in reaction-diffusion systems. *Chaos*, 18(2). doi:10.1063/1.2900555.

Veerman, F. and Doelman, A. (2013). Pulses in a Gierer–Meinhardt Equation with a Slow Nonlinearity. *SIAM Journal on Applied Dynamical Systems*, 12(1), pp. 28–60. doi:10.1137/120878574.

Vilas, C., Balsa-Canto, E., and Garcia, M.G. (2012). Dynamic optimization of distributed biological systems using robust and efficient numerical techniques. *BMC Systems Biology*, 6(79).

Ward, M.J. and Wei, J. (2003). Hopf Bifurcations and Oscillatory Instabilities of Spike Solutions for the One-Dimensional Gierer-Meinhardt Model. *Journal of Nonlinear Science*, 13, pp. 209–264.

Wei, J. and Winter, M. (2001). Spikes for the Two-Dimensional Gierer-Meinhardt System: The Weak Coupling Case. *Journal of Nonlinear Science*, 11, pp. 415–458.

Wei, J. and Winter, M. (2002). Spikes for the Gierer-Meinhardt system in two dimensions: The strong coupling case. *Journal of Differential Equations*, 178, pp. 478–518.

Wei, J. (1999). Existence, stability and metastability of point condensation patterns generated by the Gray-Scott system. *Nonlinearity*, 12(3), pp. 593–616. doi:10.1088/0951-7715/12/3/011.

Wei, J. (2001). Pattern formations in two-dimensional Gray–Scott model: existence of single-spot solutions and their stability. *Physica D: Nonlinear Phenomena*, 148(1), pp. 20 – 48. ISSN 0167-2789, doi:https://doi.org/10.1016/S0167-2789(00)00183-4.

Wei, J. and Winter, M. (1999). On the Two-Dimensional Gierer–Meinhardt System with Strong Coupling. *SIAM Journal on Mathematical Analysis*, 30(6), pp. 1241–1263. doi:10.1137/S0036141098347237.

Wei, J. and Winter, M. (2003). Asymmetric Spotty Patterns for the Gray–Scott Model in R2. *Studies in Applied Mathematics*, 110(1), pp. 63–102. doi:https://doi.org/10.1111/1467-9590.00231.

Welsh, B.J. and Gomatam, J. (1990). Diversity of three-dimensional chemical waves. *Physica D: Nonlinear Phenomena*, 43(2), pp. 304 – 317. ISSN 0167-2789, doi:https://doi.org/10.1016/0167-2789(90)90139-G.

Welsh, B.J., Gomatam, J., and Burgess, A.E. (1983). Three-dimensional chemical waves in the Belousov-Zhabotinskii reaction. *Nature*, 304(5927), pp. 611–614. doi:10.1038/304611a0.

Winfree, A.T. (1973). Scroll-Shaped Waves of Chemical Activity in Three Dimensions. *Science*, 181(4103), pp. 937–939. ISSN 0036-8075, doi:10.1126/science.181.4103.937, url: https://science.sciencemag.org/content/181/4103/937.

Wood, S.N. (2010). Statistical inference for noisy nonlinear ecological dynamic systems. *Nature*, 466(7310), pp. 1102–1104. doi:10.1038/nature09319.

Xu, J., Yang, G., Xi, H., and Su, J. (2015). Pattern dynamics of a predator-prey reaction-diffusion model with spatiotemporal delay. *Nonlinear Dynamics*, 81(4), pp. 2155–2163. doi:10.1007/s11071-015-2132-z.

Yudovich, V.I. (1971). The onset of auto-oscillations in a fluid. *Applied Mathematics and Mechanics*, 35(4), pp. 587–603.

Yudovich, V.I. (1972). Investigation of auto-oscillations of a continuous medium, occuring at loss of stability of a stationary mode. *Applied Mathematics and Mechanics*, 36(3), pp. 587–603.

Zaikin, A.N. and Zhabotinsky, A.M. (1970). Concentration wave propagation in two-dimensional liquid-phase self-oscillating system. *Nature*, 225, pp. 535–537.

Zhabotinsky, A.M. (1974). *Concentration oscillations [in Russian]*. Nauka, Moscow. 179 p.

Zhang, Q. and Tian, C. (2014). Pattern dynamics in a diffusive Rössler model. *Nonlinear Dynamics*, 78(2), pp. 1489–1501. doi:10.1007/s11071-014-1530-y.

Zhang, Y.L. and Li, C.Q. (2017). Fractional modified Duffing–Rayleigh system and its synchronization. *Nonlinear Dynamics*, 88(4), pp. 3023–3041. doi:10.1007/s11071-017-3430-4.

Zhao, H. and Huang, X. (2014). Turing instability and pattern formation of neural networks with reaction– diffusion terms. *Nonlinear Dynamics*, 76(1), pp. 115–124. doi: 10.1007/s11071-013-1114-2.

ACTA UNIVERSITATIS LAPPEENRANTAENSIS

903. AROLA, KIMMO. Enhanced micropollutant removal and nutrient recovery in municipal wastewater treatment. 2020. Diss.

904. RAHIMPOUR GOLROUDBARY, SAEED. Sustainable recycling of critical materials. 2020. Diss.

905. BURGOS CASTILLO, RUTELY CONCEPCION. Fenton chemistry beyond remediating wastewater and producing cleaner water. 2020. Diss.

906. JOHN, MIIA. Separation efficiencies of freeze crystallization in wastewater purification. 2020. Diss.

907. VUOJOLAINEN, JOUNI. Identification of magnetically levitated machines. 2020. Diss.

908. KC, RAGHU. The role of efficient forest biomass logistics on optimisation of environmental sustainability of bioenergy. 2020. Diss.

909. NEISI, NEDA. Dynamic and thermal modeling of touch-down bearings considering bearing non-idealities. 2020. Diss.

910. YAN, FANGPING. The deposition and light absorption property of carbonaceous matter in the Himalayas and Tibetan Plateau. 2020. Diss.

911. NJOCK BAYOCK, FRANCOIS MITERAND. Thermal analysis of dissimilar weld joints of high-strength and ultra-high-strength steels. 2020. Diss.

912. KINNUNEN, SINI-KAISU. Modelling the value of fleet data in the ecosystems of asset management. 2020. Diss.

913. MUSIKKA, TATU. Usability and limitations of behavioural component models in IGBT short-circuit modelling. 2020. Diss.

914. SHNAI, IULIIA. The technology of flipped classroom: assessments, resources and systematic design. 2020. Diss.

915. SAFAEI, ZAHRA. Application of differential ion mobility spectrometry for detection of water pollutants. 2020. Diss.

916. FILIMONOV, ROMAN. Computational fluid dynamics as a tool for process engineering. 2020. Diss.

917. VIRTANEN, TIINA. Real-time monitoring of membrane fouling caused by phenolic compounds. 2020. Diss.

918. AZZUNI, ABDELRAHMAN. Energy security evaluation for the present and the future on a global level. 2020. Diss.

919. NOKELAINEN, JOHANNES. Interplay of local moments and itinerant electrons. 2020. Diss.

920. HONKANEN, JARI. Control design issues in grid-connected single-phase converters, with the focus on power factor correction. 2020. Diss.

921. KEMPPINEN, JUHA. The development and implementation of the clinical decision support system for integrated mental and addiction care. 2020. Diss.

922. KORHONEN, SATU. The journeys of becoming ang being an international entrepreneur: A narrative inquiry of the "I" in international entrepreneurship. 2020. Diss.

923. SIRKIÄ, JUKKA. Leveraging digitalization opportunities to improve the business model. 2020. Diss.

924. SHEMYAKIN, VLADIMIR. Parameter estimation of large-scale chaotic systems. 2020. Diss.

925. AALTONEN, PÄIVI. Exploring novelty in the internationalization process - understanding disruptive events. 2020. Diss.

926. VADANA, IUSTIN. Internationalization of born-digital companies. 2020. Diss.

927. FARFAN OROZCO, FRANCISCO JAVIER. In-depth analysis of the global power infrastructure - Opportunities for sustainable evolution of the power sector. 2020. Diss.

928. KRAINOV, IGOR. Properties of exchange interactions in magnetic semiconductors. 2020. Diss.

929. KARPPANEN, JANNE. Assessing the applicability of low voltage direct current in electricity distribution - Key factors and design aspects. 2020. Diss.

930. NIEMINEN, HARRI. Power-to-methanol via membrane contactor-based CO2 capture and low-temperature chemical synthesis. 2020. Diss.

931. CALDERA, UPEKSHA. The role of renewable energy based seawater reverse osmosis (SWRO) in meeting the global water challenges in the decades to come. 2020. Diss.

932. KIVISTÖ, TIMO. Processes and tools to promote community benefits in public procurement. 2020. Diss.

933. NAQVI, BILAL. Towards aligning security and usability during the system development lifecycle. 2020. Diss.

934. XIN, YAN. Knowledge sharing and reuse in product-service systems with a product lifecycle perspective. 2020. Diss.

935. PALACIN SILVA, VICTORIA. Participation in digital citizen science. 2020. Diss.

936. PUOLAKKA, TIINA. Managing operations in professional organisations – interplay between professionals and managers in court workflow control. 2020. Diss.

937. AHOLA, ANTTI. Stress components and local effects in the fatigue strength assessment of fillet weld joints made of ultra-high-strength steels. 2020. Diss.

938. METSOLA, JAAKKO. Good for wealth or bad for health? Socioemotional wealth in the internationalisation process of family SMEs from a network perspective. 2020. Diss.

939. VELT, HANNES. Entrepreneurial ecosystems and born global start-ups. 2020. Diss.

940. JI, HAIBIAO. Study of key techniques in the vacuum vessel assembly for the future fusion reactor. 2020. Diss.

LUT University

ISBN 978-952-335-602-3
ISBN 978-952-335-603-0 (PDF)
ISSN-L 1456-4491
ISSN 1456-4491
Lappeenranta 2020